SANDIA REPORT
SAND201X-XXXX
Unlimited Release
Printed Month and Year

Oil and gas flow through fractures and along interfaces in well cement

John C. Stormont[1], Mahmoud Reda Taha[1], Ishtiaque Anwar[1], Mahya Hatambeigi[1]
Kirsten N. Chojnicki[2], Giorgia Bettin[2]

[1] Department of Civil Engineering, University of New Mexico
[2] Sandia National Laboratories

Prepared by
Sandia National Laboratories
Albuquerque, New Mexico 87185 and Livermore, California 94550

Sandia National Laboratories is a multimission laboratory managed and operated by National Technology and Engineering Solutions of Sandia, LLC, a wholly owned subsidiary of Honeywell International, Inc., for the U.S. Department of Energy's National Nuclear Security Administration under contract DE-NA0003525.

Sandia National Laboratories

Issued by Sandia National Laboratories, operated for the United States Department of Energy by National Technology and Engineering Solutions of Sandia, LLC.

Available to DOE and DOE contractors from
U.S. Department of Energy
Office of Scientific and Technical Information
P.O. Box 62
Oak Ridge, TN 37831

Telephone: (865) 576-8401
Facsimile: (865) 576-5728
E-Mail: reports@osti.gov
Online ordering: http://www.osti.gov/scitech

Available to the public from
U.S. Department of Commerce
National Technical Information Service
5301 Shawnee Rd
Alexandria, VA 22312

Telephone: (800) 553-6847
Facsimile: (703) 605-6900
E-Mail: orders@ntis.gov
Online order: https://classic.ntis.gov/help/order-methods/

SAND201X-XXXX
Printed Month Year
Unlimited Release

Oil and gas flow through fractures and along interfaces in well cement

John C. Stormont
Mahmoud Reda Taha
Ishtiaque Anwar
Mahya Hatambeigi
Department of Civil Engineering
MSC01 1070
University of New Mexico
Albuquerque, New Mexico 87131

Kirsten N. Chojnicki
Department of Geotechnologies and Engineering
Sandia National Laboratories
P. O. Box 5800
Albuquerque, New Mexico 87185-MS0735

Giorgia Bettin
Department of Geothermal Research
Sandia National Laboratories
P. O. Box 5800
Albuquerque, New Mexico 87185-MS1033

Abstract

A number of wells at the Strategic Petroleum Reserve (SPR) have shown sustained, positive pressure (referred to as sustained casing pressure or SCP) in the cemented annulus behind the production casing. To better understand how SCP may develop for SPR conditions, we conducted gas and oil flow tests on cement specimens with flaws including cement fractures and discrete interfaces along a cement-steel contact. Many specimens were tested initially with gas, followed by oil, and finally with gas again to identify how the fluid type may affect the flow through flaws in the well cement. Nitrogen was used as the gas, and silicone oil with properties similar to typical crude oil was used in most tests. One set of measurements were made with crude oil. Composite steel-cement specimen with corroded steel were also tested. For both gas and oil tests, the measured flow test data were used to interpret permeability and, assuming the cubic law for flow between parallel plates, the corresponding hydraulic aperture of the flaw. The hydraulic apertures for the flawed specimens ranged from about 20 to >100 μm, which corresponds to permeabilities

of about 10^{-14} to 10^{-12} m^2, respectively; these hydraulic apertures are consistent with the range of values interpreted from field measurements on leaky wells. Observed differences between the flow of gas and oil were attributed to a number of factors, including non-linear flow of gas, possible blocking of flow paths by solids within the crude oil, two-phase gas and oil flow and the presence of residual oil in the cement flaw. Furthermore, we determined that corroded steel itself is permeable. Using input values consistent with the gas and oil flow measurements, we conducted one-dimensional simulations of gas and oil flow through cemented annulus systems to investigate the role of flaw size and fluid type on the expected response (i.e., pressure build-up) in the annular cement.

ACKNOWLEDGMENTS

TABLE OF CONTENTS

FIGURES

TABLES

EXECUTIVE SUMMARY

A number of wells at the Strategic Petroleum Reserve (SPR) have shown sustained, positive pressure in the cemented annulus behind the production casing. The cemented annulus pressure, also known as sustained casing pressure (SCP), may result from small casing, thread or shoe defects or flaws and the subsequent establishment of flow paths through the cement. SCP management usually involves remediation of the wells to stop flow through cement channels, fractures and annuli but those types of remediations have proven to be extremely difficult for the oil and gas industry. To better understand SCP for SPR, we initiated an experimental program to investigate fluid movement through flow paths in cement under SPR conditions. The measurements are part of a larger effort to improve the interpretation of measured of SCP at SPR. In this report we describe how the characteristics of the pathway and the fluid type may contribute to the flow rate through the cement, a factor which ultimately influences the SCP value and its evolution.

We have conducted gas and oil flow tests on cement specimens with flaws including cement fractures and interfaces along the cement-steel contact. Many specimens were tested initially with gas, followed by oil, and finally with gas again. Nitrogen was used as the gas, and silicone oil with properties similar to typical crude oil was used in most tests. One set of measurements were made with crude oil. Steel-cement specimens with corroded steel also tested. We also injected one fractured cement sample with epoxy to preserve the pore structure, sliced the sample and used image analysis techniques to measure the mechanical (actual) aperture along the fracture. An intact cement sample was also tested to provide a baseline response. For both gas and oil tests, we used the measured flow test data to interpret permeability and, assuming the cubic law for flow between parallel plates, the corresponding hydraulic aperture of the flaw. Larger hydraulic apertures correlate with higher flow rates and increased permeability.

The initial gas flow tests yield hydraulic apertures that ranged from about 20 to > 100 μm, which corresponds to permeabilities of about 10^{-14} to 10^{-12} m^2, respectively. The intact cement sample had a gas permeability of $1x10^{-17}$ m^2. Thus, the flawed specimens typically had permeabilities that were many orders of magnitude greater than that of the intact cement, and flow in the experiments was principally through the fractures and interfaces. The measured hydraulic apertures of flawed samples are consistent with a common range of values (5-100 μm) interpreted from field measurements for cement in leaky wells (Checkai et al.; 2013). Because the flows were large enough to permit rapid flow during measurements with gas, non-linear flow developed and had to be corrected for in order to obtain hydraulic apertures and permeabilities. Flow tests using silicone oil were consistent with the initial gas flow tests, but often resulted in slightly smaller hydraulic aperture than the initial gas tests. The single test with crude oil resulted in plugging of the experimental system with small solids from within the crude oil.

Gas flow was significantly reduced when gas flow measurements were made after oil flow measurements. Initially, the gas had to overcome a “displacement pressure” in order to begin to displace oil in the fracture. This effect was difficult to measure in these experiments, but it is expected that the smaller the size of the flow path filled with oil, the greater the gas pressure will be required to displace the oil. Once the gas began to displace oil, both gas and oil flows within the flow path. Under these conditions of two-phase flow, the resulting flow rate of gas and oil will

be different from one another and depend on how much of each fluid type is present. After the gas pressure reached a certain value, no additional oil was displaced from the flaw and only gas moved through the flaw. The interpreted hydraulic aperture (or permeability) from the measured gas flow under these conditions was significantly less that interpreted from the initial gas and oil flow measurements. This result is consistent with residual oil remaining in the flaw and limiting the open space for gas to move through.

The measurements on cement-steel interfaces (often called microannuli) produced similar results and trends to those for fractured cement. Furthermore, we determined that corroded steel itself is permeable, and implies that corroded steel casing can be a continuous flow path in a cemented annulus system.

The larger the hydraulic aperture, the more sensitive it was to changes in the applied confining stresses and fluid (pore) pressures. Increased confining stresses tended to reduce the hydraulic aperture and increased fluid pressures tended to increase the hydraulic aperture. The cement-corroded steel samples were especially sensitive to changes in confining stress, consistent with the corrosion product being very compressible.

To provide insight into the response at the cemented annulus pressure at the surface to different conditions and properties, we conducted some simple calculations that used observations and knowledge derived from the experimental results described previously. In these simulations, we use hydraulic apertures (or permeabilities) for fractures that are consistent with the values we measured. These calculations simulate one-dimensional flow of either nitrogen or crude oil from depth to the surface through the cemented annulus. These calculations are not intended to match a particular well response as they include numerous simplifying assumptions, including single-phase flow, constant crude oil compressibility, no gas solubility in crude oil, and constant permeability or hydraulic aperture of the flow path. Nonetheless, these calculations can provide some useful trends of approximate responses that may be expected. The simulation results highlight that a single fracture, with a size on the order of those measured in the experiments described in this report, can have a dramatic impact on the cemented annulus pressure build-up. Further, the rate of pressure build-up will be different for gas and oil. Even a small amount of gas in the cemented annulus system will affect the pressure build-up response.

NOMENCLATURE

Abbreviation	Definition
Abbreviation	Definition
SPR	Strategic Petroleum Reserve
SCP	Sustained Casing Pressure
MIT	Mechanical Integrity Test
SCCS	Standard cubic centimeters per second

1. INTRODUCTION

The work in this report aims to increase the understanding of how a specific subsurface fluid pathway (flaws in the casing cement), or combination of pathways, may lead to a particular cemented annulus pressure value at surface or as often defined in the literature, Sustained Casing Pressure (SCP).We use laboratory experiments to elucidate the relationship between SCP values (or trends) and the pathway of the fluid, focusing on flow through fractured cement and flow in the microannuli between the cement and casing. We pay particular attention to how the flow in those pathways is impacted by the presence of gas and liquids, such as nitrogen and oil. Although the caverns store oil, wellbores are exposed to nitrogen during Mechanical Integrity Tests (MITs). This report discusses the initial results from an experimental program investigating gas and oil flow through cement cracks and micro annuli.

1.1. Cemented Annulus Pressure at the Strategic Petroleum Reserve

A number of wells at the Strategic Petroleum Reserve (SPR) have shown positive pressure in the cemented annulus behind the production casing (Bettin and Lord 2015, Bettin and Hart 2016). Ideally, the behind casing pressure should read zero and remain independent of wellbore pressures. If the well is not at steady-state, positive pressure may be caused by thermal expansion effects associated with the rapid movement of fluids in the wellbore. However, once the well returns to steady-state and a small volume of fluid is bled off in order to reduce any lingering behind casing pressure to atmospheric, the casing pressure should remain at atmospheric. If the behind casing pressure rises and remains positive, even after bleed off, then the casing exhibits sustained casing pressure (SCP), an indicator that pressure and fluid is moving through the casing into the cemented annulus (Bourgoyne et al., 2000).

In general, the main risk for O&G production wells with SCP is a blowout through the outer casing and secondary containment. The production casing is designed to withstand greater pressure than the outer casing and if the pressure on the production casing causes a failure, the outer casing could also fail because it is not designed to withstand the resultant pressure. At SPR, the main concerns for behind casing pressure is different and consist of product loss, failure of the intermediate casing and failure of Mechanical Integrity Tests (MITs). MITs are designed to measure any unwanted change in pressure in the wellbore while under nitrogen. Unacceptably large pressure changes may occur during this test time for wells with SCP because subsurface pathways may be established for fluid that allows the pressure at the surface to continue to change over time (Bourgoyne et al., 2000).

Although potentially hazardous, behind casing pressure is currently not regulated in onshore wells like those at SPR but may be regulated in the near future. If behind casing pressure becomes regulated, SPR operations will require effective behind casing pressure management and, in turn, a better understanding of behind casing pressure.

1.1.1. Origin of Annular Pressure

SCP can result from small casing, thread, and shoe leaks and the establishment of flow paths through the cemented annulus, although it can be difficult to determine the precise cause of SCP in any specific well. Small casing leaks can be caused by many factors including poor thread connection, corrosion, thermal stress cracking, mechanical rupture and well head seal failures. However, thread and shoe leaks are thought to be the most likely pathways for SPR type wells. Subsequent flow paths through the cement can result from poor primary cementing practices or

subsequent damage to the cement. Primary cement integrity is influenced by a number of factors including the quality of the cementing material, the process by which the cement is cured, and the quality of the bonds between the cement and the steel casing and the cement and the rock formation. Channels are often formed by gas or water flow in the unset cement during poor primary cementing that allow fluids to reach the surface and maintain SCP. Once set, the cement used in wells may be damaged because it is a brittle material and susceptible to cracking when exposed to temperature or pressure induced tensile loads. The cement may also de-bond from the casing if the casing contracts under thermal stress forming a gap at the cement-casing interface, often called a micro annulus, through which fluid can move relatively easily and therefore quickly (Bourgoyne et al., 2000).

1.1.2. Remediation of Annular Pressure

In the oil and gas industry, the primary repair method for SCP is a workover designed to block the leak path causing the problem. This can be relatively straight forward, although expensive, for solutions within the production casing (tubing leak, packer failure, well head failure). Remediation of flow outside the production casing, often requires cutting the casing to squeeze cement or other product into leak paths within the surrounding cement sheath. It is more technically difficult and often has a high cost with a limited rate of success. Remediation of flow through cement channels, cracks and annuli have proven to be extremely difficult (Bourgoyne et al., 2000).

1.1.3. Annular Pressure Study

Additional research is needed to support SCP management at SPR, particularly for understanding flow through cement outside the casing since remedial procedures are often ineffective for that situation. Although we measure behind casing pressure at SPR, we do not understand what controls the pressure value measured at the surface or its evolution over time. We know that behind casing pressure is generated by a fluid driven by a force to move through a pathway. Thus the measured pressure value depends on the type of fluid, the characteristics of the pathway the fluid flowing through and the character of the force driving the flow. However, we lack an understanding of how the fluid is getting to the surface to generate the pressure and consequently cannot reliably choose a behind casing pressure management strategy to slow or stop that flow to reduce or eliminate the resultant pressure. With our current understanding, we may not be able to reduce SCP at SPR and prevent loss of product or failed MITs. This program aims to address SCP at the SPR, and will focus on how the characteristics of the pathway and the fluid type may contribute to the fluid flowrate (leak rate), a factor which ultimately influences the SCP value and its evolution.

[Blank page following section.]

2. CEMENTED ANNULUS FLOW EXPERIMENTS

2.1. EXPERIMENT DESIGN

The experiments are directed at investigating potential gas and oil leakage along cement-steel interfaces and cement fractures associated with SPR wells. To the extent practical, the experimental conditions and parameters are intended to be relevant to conditions expected for SPR wells. Specific objectives of the experiments are:

1. Create samples to represent a variety of potential leakage paths in the cemented annulus (fractured cement, de-bonded cement-steel interface, corroded steel surface).
2. Measure flow of gas and/or oil through these samples with particular attention to identifying conditions when the nature of the gas and oil flow deviates from one another.
3. Interpret and correlate the flow results in terms of the fluid properties, pressures and flow path geometry.

Two types of samples were tested to account for two important potential flow paths in leaky wells: microannuli and cement fractures. The microannuli were created to simulate thermally or mechanically de-bonded contacts as well as cement-steel contacts formed with contaminants (corrosion) that inhibits cement to steel bonding. The size of the microannuli includes the likely range of large microannuli (on the order of 100 μm) and small microannuli (on the order of 50 μm and smaller). Cement used in producing samples was consistent with cements used in SPR wells (type G wellbore cement or equivalent). Steel was standard carbon steel typical of most well casing.

The confining or external stress used in the flow experiments was nominally 13.8 MPa which approximately corresponds to the expected geostatic stress at a depth of about 700 m. This depth is the top of the storage cavern of some of the SPR storage facilities. Because the stresses acting on a cemented well are not well known and can potentially vary widely, larger (up to 20 MPa) and smaller (down to <1 MPa) values of confining stress were applied during some tests to investigate the sensitivity of the flow to the external stress acting on the cement.

The testing sequence for some specimens included alternating flow testing with gas and oil to simulate testing done on SPR wells. The gas used will be nitrogen, which is commonly used for mechanical integrity testing of storage caverns. The oil used had properties similar to a representative crude oil stored in the SPR. Target properties were those of a medium density crude: API gravity 25, density 900 kg/m^3, kinematic viscosity of 10 mm^2/sec, and surface tension of 30 dynes/cm.

The fluid pressures used in the flow tests covers the range from nearly 0 to 7 MPa; 7 MPa is approximately the hydrostatic head at a depth of 700 m. Testing under a range of pressures provides an indication if increased fluid pressures will tend to further prop open the fractures. In addition, testing under different fluid pressures will provide information about the progressive displacement of one fluid by another (e.g., oil displacement by gas). In addition, testing under a range of pressures with gas allows for determining the gas slip or Klinkenberg correction, and also can be used to account for non-linear flow. Further, testing under different pore pressures can

indicate the role of effective stress (confining stress minus pore pressure) on the deformation of the leakage pathway.

In addition to hydraulic aperture data derived from flow testing, some data were collected on the aperture distributions. To accomplish this, a low viscosity epoxy was injected into the flow paths to preserve the pore geometry for subsequent image analysis.

2.1.1. Sample Preparation

A summary of tested samples is given in Table 2.1.1. The sample labeling indicates the type of sample: C for fractured cement, CS for cement-steel interface, or ICZ for intact cement.

Table 2.1.1 Summary of flow tests.

Sample	Test initiation date	Performed tests			
		Gas (Nitrogen)	Silicone Oil	Crude (SPR) Oil	Gas Displacement
C01	1/23/17	✓			
C02	3/24/17	✓	✓		✓
C05	2/23/17	✓	✓		✓
C07	5/1/17	✓	✓		✓
CS01	4/13/17	✓	✓		✓
CS02	5/17/17	✓	✓	✓	✓
CS04	6/27/17	✓	✓		✓
C09	7/6/17	✓	✓		
C12	7/14/17	✓			
C10	11/13/17	✓			
C13	12/21/17	✓			
CSC02	8/10/17	✓	✓		✓
ICZ01	8/16/17	✓			
CSC03	11/5/17	✓			
CSC04		In progress			

Samples were created with two types of cement: type G portland cement and type I-II based on availability of materials. The samples made with type G Portland cement all used the same mix design comprised of Portland cement, silica fume (BASF Rheomac SF100), plasticizer (BASF Glenium 3030) and distilled water. The mix design for the cement used in these samples is given in Table 2.1.2. The abbreviations in the table are: S and C are silica fume and cement, W is the water, and P is for plasticizer.

Table 2.1.2 Mix proportions of the Type G cement samples

S/C ratio	W/(S+C) ratio	P/W ratio
0.1	0.3	0.02

The samples made with type I-II cement all used the same mix deign comprised of Zia type I-II cement, silica fume (BASF Rheomac SF100), plasticizer (BASF Glenium 3030) and distilled water. The mix proportion used to create the cement specimens made with Zia cement type I-II are presented in Table 2.1.3.

Table 2.1.3 Mix proportions of the Type I-II cement samples

S/C ratio	W/(S+C) ratio	P/W ratio
0.1	0.4	0.02

Cement was mixed in accordance with ASTM C305-14. To batch the mixes, the amount of each material to achieve the desired mix design was measured and then mixed together in a bowl using a high-speed laboratory mixer until a smooth and homogenous slurry was achieved. After mixing, the obtained mixture was poured in 76 mm (3 in) diameter by 152 mm (6 in.) long plastic cylinder molds. The samples were then placed on a flat surface for the 24 hours of initial setting time. On the second day, the specimens are removed carefully from the molds and kept in water for a minimum of 28 days at ambient temperature (23 °C) as shown in Fig. 2.1.1, or 7 days under elevated temperature (65 °C) in a heated water bath.

Fig. 2.1.1: Curing of various cement samples in water tank.

To create flaws in the samples, an axial fracture was created in the cement samples making use of the Brazilian tensile test. The setup for creating the tensile fracture is shown in Fig. 2.1.2 The loading rate during the tensile splitting was 13.8 MPa/min. The fracture divided each cement sample longitudinally into two almost equal parts (Fig. 2.1.3).

Fig. 2.1.2: Tensile splitting (Brazilian test) equipment. Cylindrical cement sample is in load frame on left, control system is on right.

For the Type 1 samples, a semi-circular, perforated steel sheet 0.75mm thick (Fig. 2.1.4) was placed on the opposite ends of each half of the cement sample to create an “offset” of the fracture

surfaces and prevent perfect mating of fracture surfaces under confining stress. For one sample (C09), the two pieces were inverted to create a mismatch of the fracture.

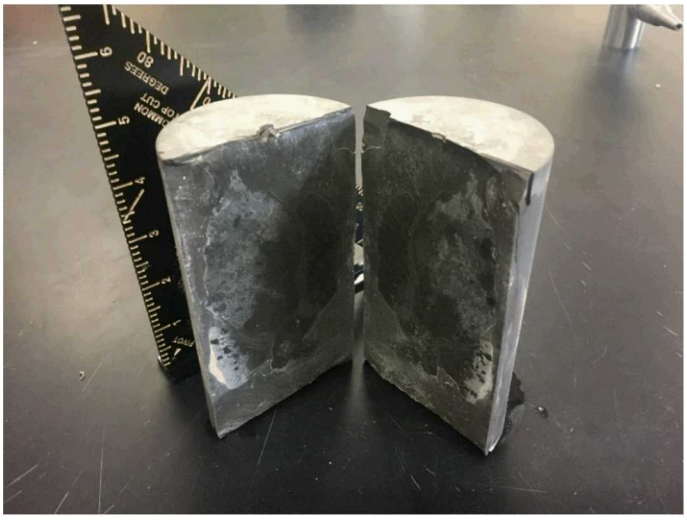

Fig. 2.1.3: Sample after tensile splitting.

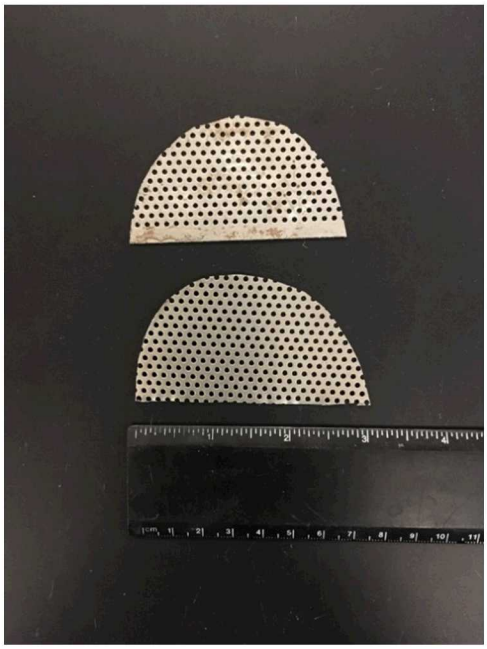

Fig. 2.1.4: Perforated thin steel sheets used to create offset of fractured cement samples.

The sample is then cast in a molding epoxy (PMC-770 from Reynolds Advanced Materials) to produce samples that are 102 mm in diameter to fit in the pressure vessel (Fig. 2.1.5). Finally, the samples are covered with a plastic sheet to ease the process of putting in and removing the sample from the pressure vessel.

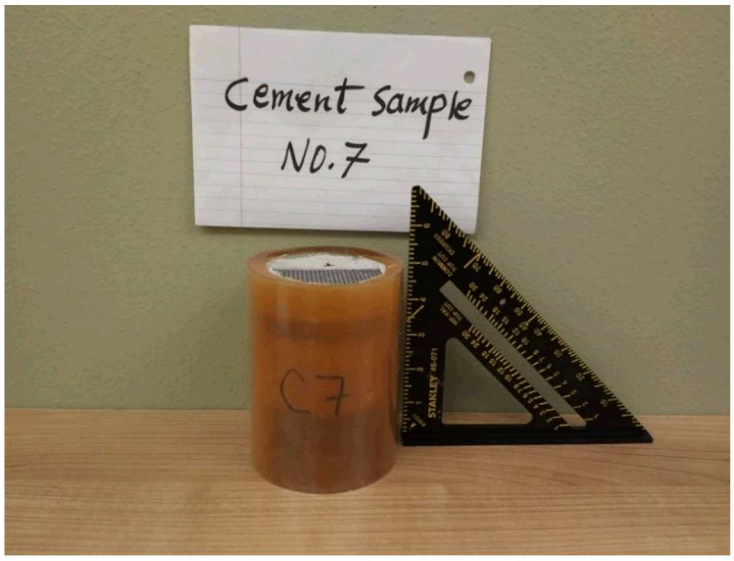

Fig. 2.1.5: Type 1 sample after casting in molding epoxy.

A number of different methods were attempted for creating Type 2 cement-steel samples. The preferred method has been to create them from fractured cement samples. A 3 mm thick cold rolled mild steel sheet is affixed with a glue (silicon or epoxy-based) to one of the cement surfaces. The sample is then reassembled so that an "open" cement-steel interface is produced. A photograph of the components of a Type 2 sample is given in Fig. 2.1.6a. These samples are also cast in molding epoxy to create samples with a 102 mm diameter (Fig. 2.1.6b).

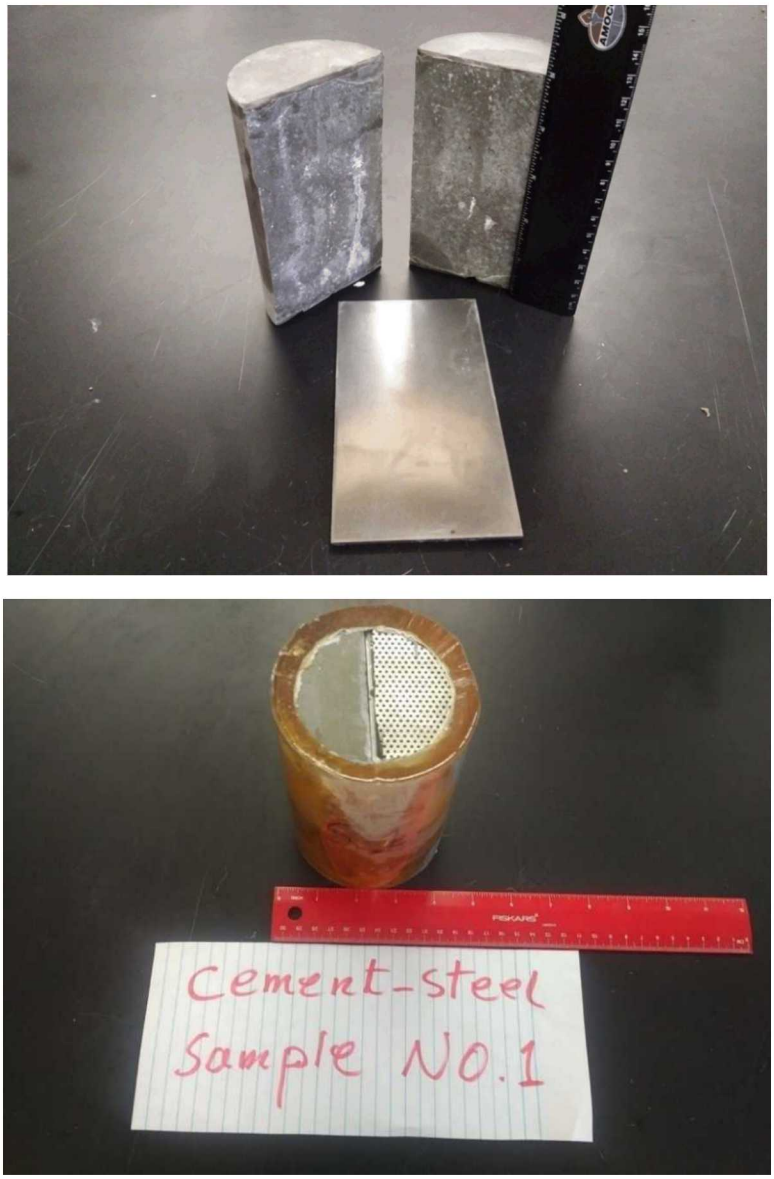

Fig. 2.1.6: (a) Top, split cement sample with steel plate prior to affixing to one cement face, and (b) bottom, completed Type 2 sample.

We also created samples with a cement-corroded steel interface that represents the interface between corroded steel casing and the surrounding cement material. The specimens were prepared from the same mix design (Table 1) using cement type class G, silica fume, plasticizer and distilled water.

To batch the mixes, the amount of each material to achieve the desired mix design is measured and then mixed together in a bowl. After mixing, the obtained mixture was poured in 76 mm (3 in) diameter by 152 mm (6 in.) long plastic cylinder molds. A 3.175 mm (11GA) thick cold rolled steel plate was placed in the middle of the mold. As described previously, the sample was then placed on a flat surface for the 24 hours of initial setting time. After 24 hours, the specimen was removed carefully from the molds and the steel plate was uncoupled cautiously from the hardened

cement paste. The steel plate divided the sample longitudinally into two identical parts. Cement samples were cured accordingly (similar to Type 1 sample).

One side of the cold rolled steel plate was protected by waterproof plastic tape (using rubber based adhesive) and the other side of the plate remains unprotected. The unprotected interface was cleaned using diluted acetic acid (CH_3COOH) and 30% peroxide (H_2O_2) solution in order to get rid of rust prevention layer (if any). The plate was then placed in a humid room (with a continuous supply of mist/humidity at controlled temperature) for three weeks to expedite the environmental corrosion. A corroded plate is shown in Fig. 2.1.7.

Fig. 2.1.7: Corroded steel plate

The plastic tape was carefully removed from the steel plate and the uncorroded interface was affixed with a glue (Polyurethane Rubber Compounds PMC 770) to one of the cement surfaces. The sample is then reassembled so that an “open” cement-corroded steel interface is produced (Fig 2.1.8).

Fig. 2.1.8: Split cement sample with steel plate affixed to one cement face

The sample is then cast in a molding epoxy to produce samples that are 102 mm in diameter to fit in the pressure vessel (Fig. 2.1.9). Finally, the samples are covered with a thin plastic sheet to ease the process of putting in and removing the sample from the pressure vessel.

Fig. 2.1.9: (a) Left, a mold for Polyurethane Rubber Compounds PMC 770, and (b) right, completed Type 3 sample (CSC 02).

To understand more about the influence of corrosion product on the permeability, we created samples with cement, corroded steel (one face) and molded alloy sandwiched in a cylindrical assembly (140 mm long, 76 mm diameter) that represents the flow through corroded steel casing.

The cement specimens were prepared from the same mix design (Table 1) using cement type class G, silica fume, plasticizer and distilled water. A schematic diagram of the prepared sample is presented in fig 2.1.10.

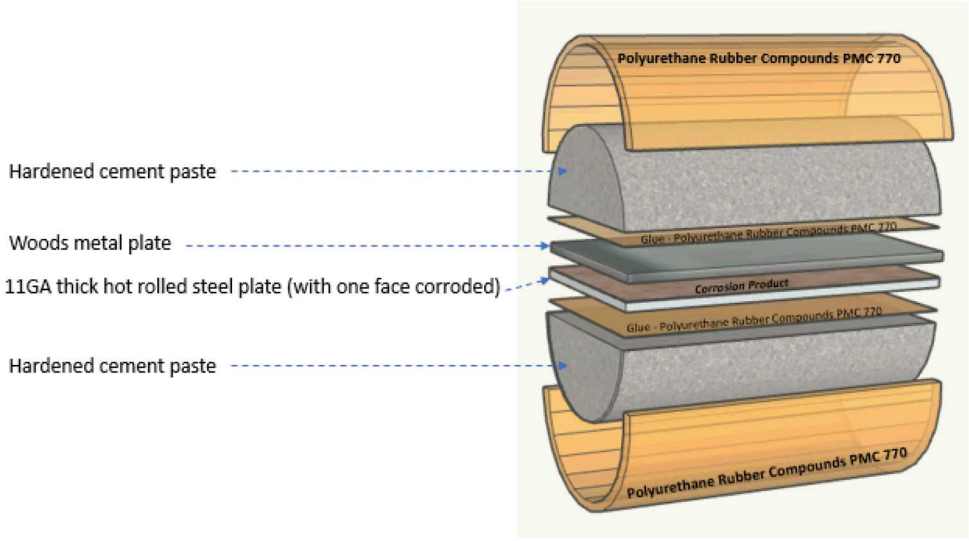

Fig. 2.1.10: Schematic diagram of sample prepared for measuring permeability of corrosion product

For sample preparation, the quantity of each material to achieve the desired mix design is measured and then mixed in a bowl. After mixing, the mix was poured in 76 mm (3 in) diameter by 152 mm (6 in.) long plastic cylinder molds with the separator (two 3.175 mm thick steel plate) in the middle of the mold to obtain two half-cylindrical hardened cement paste sample. After an initial setting time of 24 hours, the specimen was removed carefully from the molds, and the steel plates were uncoupled cautiously from the hardened cement paste. The steel plates divided the sample longitudinally into two identical parts. Cement samples were then cured accordingly (similar to Type 1 sample).

For sample CSC 04, first, the one-face protected hot rolled steel plate was then casted along with comparatively porous identical half cylindrical hardened cement sample (prepared from Zia Portland cement with water cement ratio = 0.40) and immersed in an electrolysis cell (with $NaHCO_3$ solution acting as electrolyte solution) together with parallelly connected stainless steel plates (as less active or cathodic material). The hot rolled steel plate and the stainless steel plates assembly were and linked to an external power supply (12 volt DC) for approximately 48 hours to expedite the representative galvanic corrosion occurs in the wellbore casing. A photograph of hardened cement paste with corroded steel sample (galvanic corrosion) after electrolysis is presented in fig 2.1.11.

Fig. 2.1.11: Hardened cement paste (prepared from Zia Portland cement) with one-face protected hot rolled steel plate, after electrolysis (for sample CSC 04)

Then the corroded steel plate was uncoupled cautiously from the hardened cement paste and placed with molded fusible alloy (wood's metal) and hardened cement paste (previously prepared from type G cement, and of comparatively lower permeability) sandwiched in a cylindrical assembly (140 mm long, 76 mm diameter), as shown in fig 2.1.10. For sample CSC 03, the steel plate was corroded electrochemically without any hardened cement paste. A corroded plate with molded fusible alloy (Wood's metal) is shown in Fig. 2.1.12.

Fig. 2.1.12: Corroded plate with molded fusible alloy (Wood's metal) – sample CSC 03

The sample is then cast in a molding epoxy to produce samples that are 102 mm in diameter to fit in the pressure vessel. Summary of corrosion mechanisms used for sample preparation is presented in Table 2.1.4.

Table 2.1.4 Summary of corrosion mechanisms used for sample preparation

	Sample No	Method of corrosion
1	CSC 02	The plate was then placed in a humid room (with a continuous supply of mist/humidity at controlled temperature) for three weeks to represent atmospheric corrosion
2	CSC 03	One face protected steel plate corroded electrochemically for 24 hrs to represent galvanic corrosion of unprotected steel casing
3	CSC 04	Cylindrical hardened cement paste with a steel plate (one face protected) placed in the middle - corroded electrochemically for 48 hrs to represent galvanic corrosion of protected steel casing

Samples have been created in separate 9 batches to date. Many samples were discarded as we developed the sample preparation method described above. Modes of sample failure include poor tensile fractures (either too smooth or not a single fracture). Samples that are used for testing are assigned a label which includes a designation of the type of sample: C for Type 1 (cement) samples, and CS for Type 2 samples (cement – steel).

2.1.2. Flow Testing Equipment and Methods

Cement (intact and fractured) and cement-steel (not corroded and corroded) samples were placed in a pressure vessel and subjected to a constant hydrostatic confining stress while measuring gas and liquid (oil) flow through the samples. A schematic representing the sample subjected to these stresses and pressure is shown in Figure 2.1.13. The confining or external stress is applied equally to all surfaces of the sample; this stress simulates the confinement on the cement due to the presence of the surrounding earth. The fluid (gas or oil) pressure is applied to the top and bottom of the sample. If these pressures are different, a pressure gradient across the sample develops and results in flow from the higher pressure (referred to as the upstream pressure) to the lower pressure (referred to as the downstream or back pressure). In many tests, the downstream pressure is simply vented to atmosphere, that is, the downstream pressure is zero. The fluid pressure in the sample is also referred to as the pore pressure. The effective stress is taken as the difference between the confining stress and the pore (fluid) pressure. The confining stress tends to close fractures, whereas an increased pore pressure tends to open the fracture. Thus, the effective stress is often used to represent the net stress accounting for both external stress and fluid pressures.

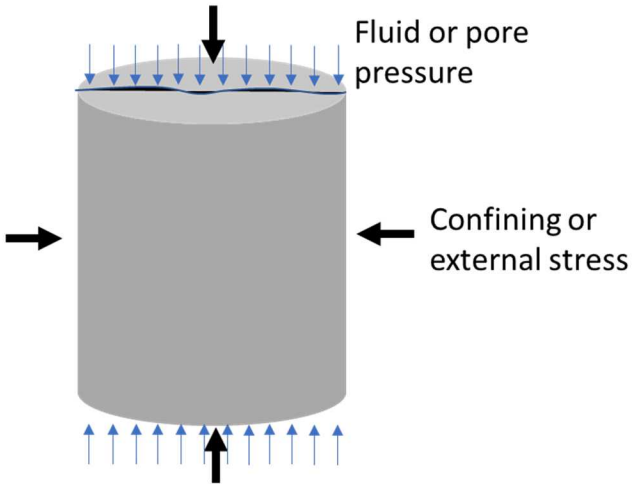

Fig. 2.1.13: Schematic of confining stress and fluid pressures applied to samples during testing.

The schematic diagram of the testing system is shown in Fig. 2.1.14.

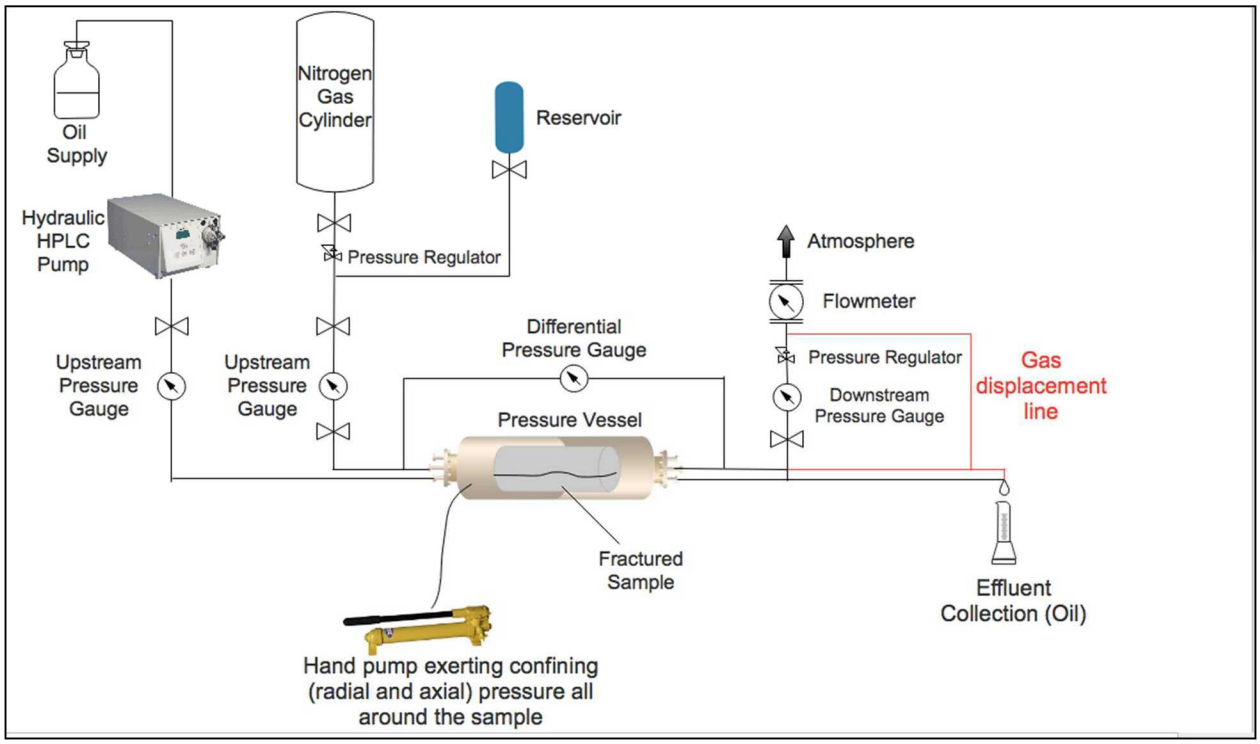

Fig. 2.1.14: Schematic of flow test configuration.

A hydrostatic (equal in all directions) confining stress was applied to the samples after they were placed in the pressure vessel, which was controlled by a hydraulic hand pump. In these experiments, the confining stress was in the range of 0.9-19.7 MPa (125-2850 psi) which approximately corresponds to the overburden pressure at the top of a typical salt cavern at a depth of about 700 m and shallower.

The experimental system is capable of measuring gas or liquid flow, which are largely two different systems. For the gas flow tests, nitrogen gas cylinders were used to supply the upstream side of the sample. The gas pressure at upstream side of the sample was controlled and measured using a pressure regulator and a digital pressure gauge, respectively. At the downstream side of the sample, pressure was controlled with a regulator and measured with digital pressure gauge. In some tests, the downstream side was set to atmospheric pressure. A differential pressure transducer measured the pressure difference between the upstream and downstream pressures. The transducers are connected to a computer via a signal conversion system that enables display and recording pressures as a function of time using LABVIEW software. Volumetric gas flow was measured at the downstream outlet with a rotameter in which interchangeable flow tubes could accommodate flows ranging up to CS01 (cement steel sample) and C05 (cement sample with fracture) 60,000 cc/min. Nitrogen was used for all tests. The gas flow tests were steady-state, constant pressure tests. Pore pressures were varied during tests by either varying the upstream pressure, downstream pressure, or both.

Liquid flow tests were conducted using a metering pump capable of applying flowrate ranging from 0.01 to 10 ml/min to the upstream side of the sample at pressures to 17 MPa. The upstream pressure was measured with a digital pressure gage, and downstream outflow was collected in a 100ml graduated cylinder at the atmospheric pressure. These tests were intended to be continued until steady-state could be observed by comparing the flow rate of the pump with the liquid collected on the downstream side.

Two liquids have been used: silicone oil and crude oil. The silicone oil was PMX-200 and was purchased from Krayden, Inc. The crude oil was supplied by Sandia personnel. Properties for the two liquids are given in Table 2.1.5 below. The contact angles reported in the table are described in Appendix B. The crude oil was filtered to remove particulate matter to limit clogging of the pump and permeameter lines (Fig. 2.1.15).

Table 2.1.5 Summary of properties for oils used in flow tests.

	Viscosity (mm^2/s)	Specific gravity		Surface tension (dynes/cm)	Contact angle
		API	(g/cc)		
Silicone oil	10.0[1]	20	0.935[1]	20.1[1]	13[3]
Crude oil	6.496[2]	33[2]	0.860	30.5[4]	21[3]

[1]Xiameter data sheet
[2]From Kirsten Chojnicki, May 11, 2017
[3]Measurements described in Appendix B
[4]http://petrowiki.org/Interfacial_tension, Equation 17

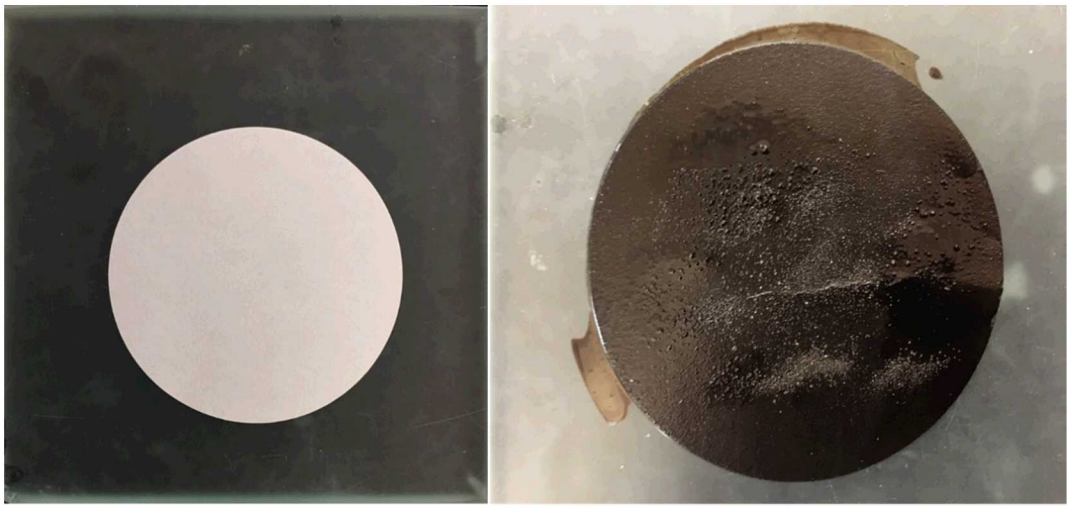

Fig. 2.1.15: Filter paper before (on left) and after (on right) filtering crude oil.

At the conclusion of the oil flow testing, many samples were subjected to an additional gas flow test referred to as the gas displacement test. Gas was supplied to the upstream and oil displacement from the sample was measured as a function of the gas pressure. The gas pressure at which the gas appeared at the downstream is known as the gas breakthrough or gas displacement pressure. Detection of gas flow through the oil-wet sample is done by making use of either the flowmeter measurement, or observation of gas bubble formation in the cylinder containing oil at the downstream side. In some other cases, when the downstream is saturated with oil, the gas breakthrough is detected by observing the first drop of oil at the downstream. After gas broke-through, the gas flowrate was measured in some tests. Liquid flow produced during the gas displacement and flow test was simultaneously measured in a graduated cylinder.

2.1.3. Flow Data Interpretation

2.1.3.1. Gas flow data interpretation

The measured gas flowrates through the specimens with flaws were interpreted using the Forchheimer equation (Forchheimer, 1901), which includes both viscous (Darcy) and inertial (non-linear) flow terms,

$$-\nabla P = \frac{\mu}{kA}Q + \frac{\beta\rho}{A^2}Q^2 \qquad (2.1)$$

where ∇P is the gradient, Q is the volumetric flowrate, k is the permeability, β is the inertial coefficient, A is the cross sectional area involved in the flow, μ is viscosity, and ρ is density. For steady-state flow of a real gas, Eqn (2.1) can be rewritten as (Zeng and Grigg, 2006)

$$\frac{MA(P_u^2 - P_d^2)}{2zRT\mu L\rho Q} = \frac{1}{k} + (\frac{\rho Q}{\mu A})\beta \qquad (2.2)$$

where M is the molecular weight of the gas, L is the is the sample length, z is the gas compressibility factor, R is the universal gas constant, and T is temperature. This equation can be rewritten as y =

(1/k) + xβ, where *y* is the left-side of Eqn (2.2) and *x* is the term in parentheses on the right-hand side of Eqn. (2). Flow measurements made at different pressures will generate (*x,y*) pairs, which can be plotted. The plotted data should produce a straight line with a slope that is a function of the inertial coefficient β and an intercept proportional to permeability. In the absence of non-linear flow, the slope will be zero and Eqn. (2.1) reduces to Darcy's Law.

The specimens with flaws are expected to yield flow rates more than 3 orders of magnitude greater than that for intact cement specimens under comparable conditions. If flow was assumed to occur only through the flaws, the calculated permeability can be interpreted as a hydraulic aperture (*h*) using the so-called cubic law (Witherspoon et al., 1980)

$$h^3 = \frac{12kA}{w} \qquad (2.3)$$

where *w* is the flaw width. From uncertainties in measured quantities, the error in the reported hydraulic aperture is +/- 5%. In the tests reported here, gas slip effects (i.e., Klinkenberg effects) were not observed.

In Figure 2.1.16., the hydraulic aperture and effective cement permeability are plotted for the geometry of the samples used in these tests. This figure reflects the one-to-one relationship between the hydraulic aperture and the effective cement permeability that is a consequence of the cubic law.

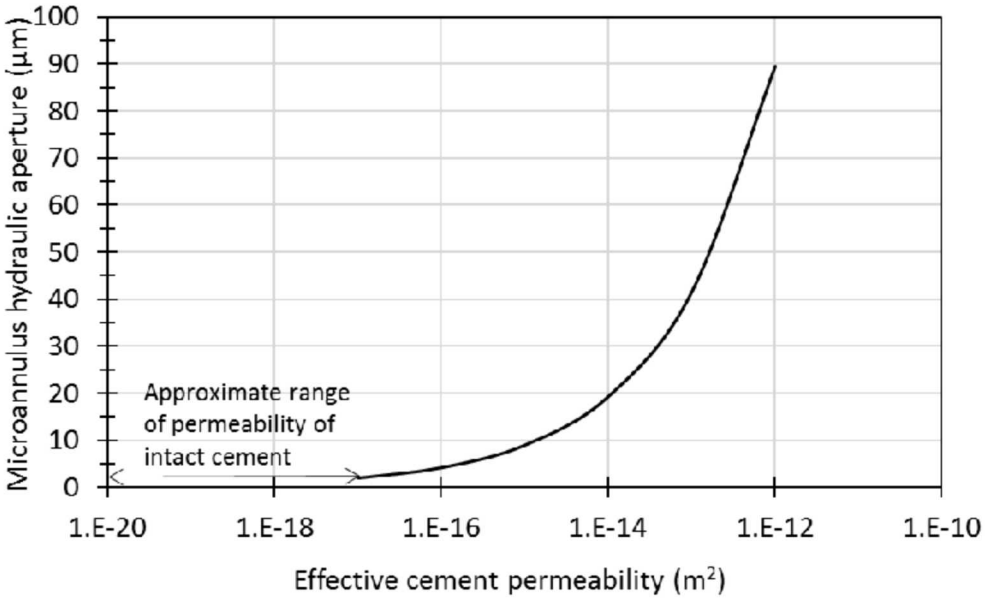

Fig. 2.1.16: Relationship between hydraulic aperture and effective cement permeability for geometry of samples used in these experiments.

2.1.3.2. Liquid flow data interpretation

The liquid flow rates were many orders of magnitude less than that for gas, and non-linear flow was not considered. The permeability to liquid can be found directly from Darcy's law using measured flow rates and pressures. The liquid permeability can be interpreted as a hydraulic aperture using the cubic law (Eqn. 2.3). From uncertainties in measured quantities, the error in the reported hydraulic aperture is +/- 5%.

2.1.3.3. Gas displacement data interpretation

The pressure at which gas displaces oil from a fracture is a function of the properties of the oil as well as the aperture of the fracture as given by

$$p = 2 \gamma \cos \theta / h \qquad (2.4)$$

where p is differential gas pressure across the wetting liquid in the pore, γ is surface tension of the wetting liquid, θ is the contact angle of the liquid on pore surface, and h is the aperture of the fracture. Because fracture apertures are not expected to be constant across a real fracture, the pressure at which gas first appears is associated with the smallest aperture along the continuous gas flow path through the sample.

2.1.4. Post-test measurement of flow path dimensions

To further characterize the flow geometry of cement samples with flaws, epoxy was injected into the sample after flow testing in the pressure vessel to allow the flow path geometry to be measured. The samples were first cast into a test fixture, and then gas permeability measurements were made. The samples were then injected with epoxy. In this way, the gas permeability measurement and the epoxy injection were conducted under the same stress condition. The samples were then sliced and microphotographs were taken, and the fracture size was measured using image analysis methods. To date, two samples have been prepared for this characterization: CS01 (Cement Steel sample) and C05 (Cement sample with fracture). Detailed methodology of both is presented below,

The sample was placed in a PVC fixture with glue (Polyurethane Rubber Compounds and hot melt adhesive or HMA) in between the sample (with molding epoxy) and the enclosure wall (Fig. 2.1.17). After curing the sample for approximately 16 hours, gas permeability tests were undertaken.

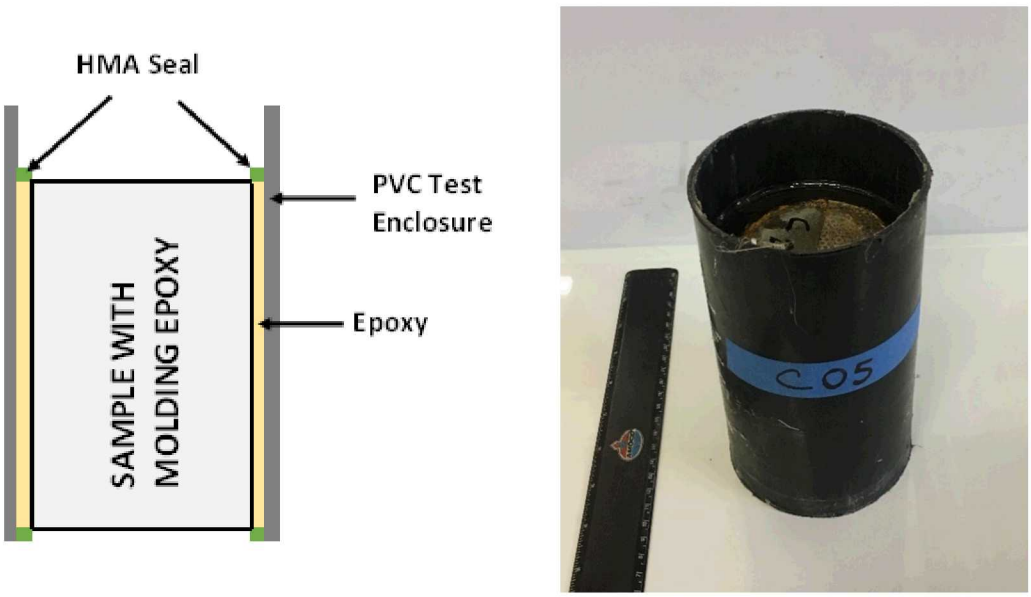

Fig. 2.1.17: a) Left, Schematic section of sample in enclosure, b) Right, Sample C05 in PVC enclosure.

Specially designed end caps were fabricated of polyurethane rubber with Swagelok connections were used to carry out the low-pressure permeability test at the same test configuration presented in Fig 2.1.18.

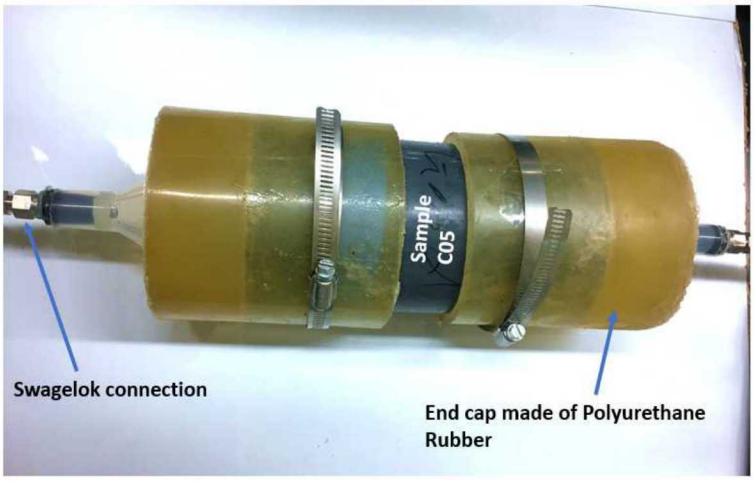

Fig. 2.1.18: Sample C05 for Gas permeability test (before epoxy intrusion).

After the permeability test, we injected dyed epoxy (2-part HCR Saturant Clear Resin manufactured by Epoxy Chemicals Inc.) to fill the sample's flow path (Fig. 2.1.19). Rhodamine B ($C_{28}H_{31}ClN_2O_3$) was mixed into the epoxy as a tracer dye (color: brilliant pink) so that it can be easily detected during image analysis. To push the epoxy into the flow path, compressed air

(<15 kPa) was placed on the upstream side of the sample. During the epoxy injection, we had closely monitored the pressure exertion and epoxy flow at the downstream to ensure that the whole flow path was filled with epoxy.

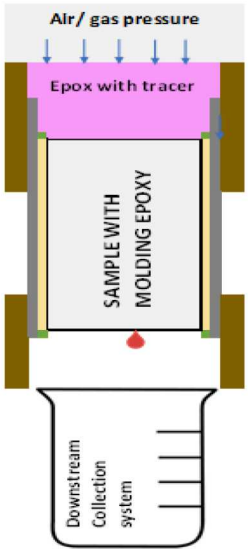

Fig. 2.1.19: Schematic diagram for epoxy intrusion

The sample was then cured for 24 hours and sectioned (Fig. 2.1.20) for high resolution image analysis to determine the aperture size.

Fig. 2.1.20: a) Left, Sample CS01 after sectioning b) Right, circumferential section

Photographs of the fractured cement specimen were taken with a 5MP resolution camera with a magnification of x220, where one pixel represents an area of 0.47 μm^2. The photographs had a certain overlap between them to allow the use of the built-in function "photomerge" in Photoshop. This function recognizes the common pixels between photographs and merge them in a larger file. ImageJ is used for the rest of the process. The merged photograph is split in as

many measurements as desired. To obtain the aperture size in every split section, the area of the fracture is measured, and divided over the length of the fracture (which was set constant at 250 μm). Since the aperture is continuous and there were no drastic changes observed, a measurement every 250 μm was used.

2.2. EXPERIMENT RESULTS

Eleven samples have been subjected to flow testing; six cement fractures, four were cement-steel interfaces (one corroded) and one intact cement core. A summary of the flow tests conducted on these samples is given in Table 2.1.1. Most samples were subjected to testing with gas and oil to discern differences in the flow response as a function of the fluid type. Fluid pressure conditions were varied in these tests to provide data to correct for non-linear flow as well as to investigate whether flow paths will become more permeable with increased fluid pressure. Confining stress was varied in some tests to determine the sensitivity of the flow path response to external stresses acting on the cement.

2.2.1. Flow through fractures in cement

2.2.1.1. Sample C01

The testing of sample C01 involved gas testing at different pore pressures, summarized in Table 2.2.2. All stresses and pressures in this table are "gauge" pressures, that is, atmospheric pressure is taken as the reference (zero) pressure. Each "test" identified in this table involves conducting a series of gas flow measurements (typically 7 or more) so that non-linear flow can be corrected for using the approach described previously in Section 2.1.3. As a typical example, data from Test 5 on this sample are given in Fig. 2.2.1. Each data point represents a separate steady-state flow test. The intercept is used to interpret the permeability as implied by Eqn. 2.2. As is the case with the data given in Fig. 2.2.1, an R^2 greater than 0.99 was often obtained when fitting the data to a straight line, especially when the flow rates are above about 5 SCCS.

Table 2.2.1 Gas flow tests conducted on C01.

Test No.	Confining stress	Back Pressure	Effective Stress
1	13.79 MPa (2000 psi)	0	13.79 MPa (2000 psi)
2	13.79 MPa (2000 psi)	0.69 MPa (100 psi)	13.1 MPa (1900 psi)
3	13.79 MPa (2000 psi)	2.07 MPa (300 psi)	11.72 MPa (1700 psi)
4	13.79 MPa (2000 psi)	3.45 MPa (500 psi)	10.34 MPa (1500 psi)
5	13.79 MPa (2000 psi)	4.84MPa (700 psi)	8.95 MPa (1300 psi)

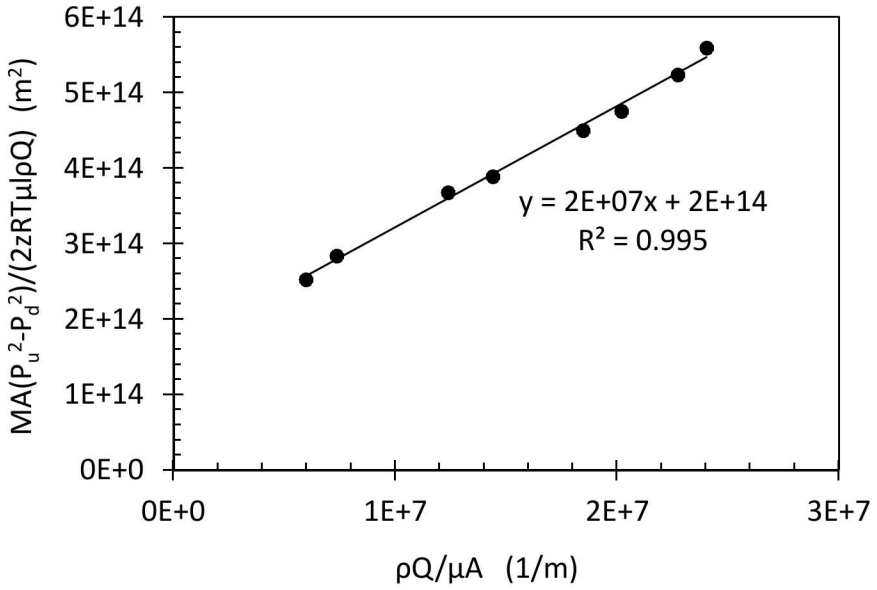

Fig 2.2.1: Forchheimer data from Test 5 of gas flow measurements made on C01.

Results from these tests are given in Fig. 2.2.2 as hydraulic aperture as a function of the average gas pore pressure (Pavg) during each of the tests. The hydraulic aperture is the size of the equivalent smooth-walled fracture that would produce these results. The hydraulic aperture and the effective permeability of the sample are directly related to one another by the so-called cubic law given by Eqn. 2.3 The hydraulic aperture is a single value for the entire fracture, whereas the actual or mechanical aperture of the fracture varies along the fracture. The hydraulic aperture and the mean mechanical aperture can be related to one another if detailed information about the fracture roughness is known. Note that each data point given in Fig. 2.2.2 involved a series of measurements to correct for non-linear flow as explained previously.

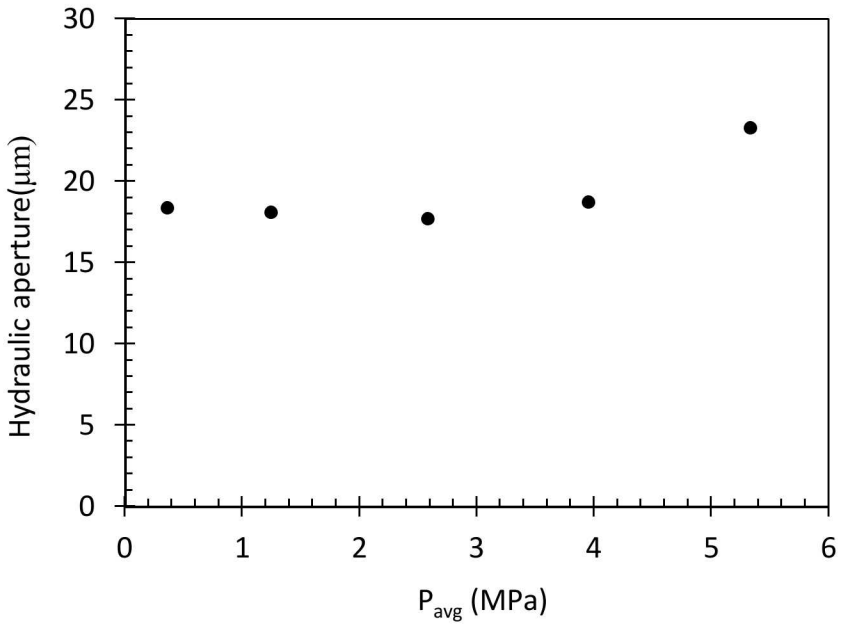

Fig 2.2.2: Results from series of gas flow measurements made on C01. Results are given as hydraulic aperture vs. average gas pore pressure during tests.

2.2.1.2. Sample C02

Sample C02 was tested first with gas, then silicone oil, and finally with gas again. The initial gas flow tests are summarized in Table 2.2.2 below.

Table 2.2.2– Initial gas flow tests conducted on C02.

Test No.	Confining stress	Back Pressure	Effective Stress
1	13.79 MPa (2000 psi)	0	13.79 MPa (2000 psi)
2	13.79 MPa (2000 psi)	1.03 MPa (150 psi)	12.76 MPa (1850 psi)
3	13.79 MPa (2000 psi)	4 MPa (580 psi)	9.79 MPa (1420 psi)

In these tests, low flow rates were achieved and the data was not corrected for non-linear flow. Results from these tests are given in Fig. 2.2.3 as hydraulic aperture as a function of the average pore pressure during each of the tests. If these data are interpreted as permeability, they are in the 10^{-18} m^2 range, well below that which was expected for a relatively open fracture.

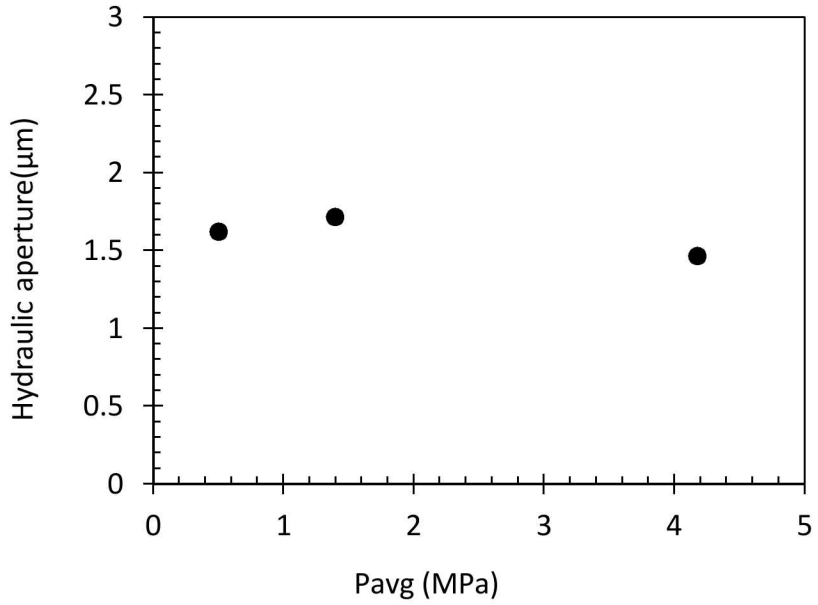

Fig 2.2.3: Results from series of gas flow measurements made on C02. Results are given as hydraulic aperture vs. average gas pore pressure during tests.

Silicone oil testing was conducted at the end of the gas flow testing. Consistent with the gas flow results, these measurements resulted in relatively small permeabilities and hydraulic apertures as given in Fig. 2.2.4. It is noted that the oil data were interpreted only with the imposed flow rate and pressure on the upstream side. Normally, we collect effluent at the downstream side to confirm steady-state has been reached. Due to the low flows, oil did not arrive at the downstream and thus steady-state flow was not confirmed.

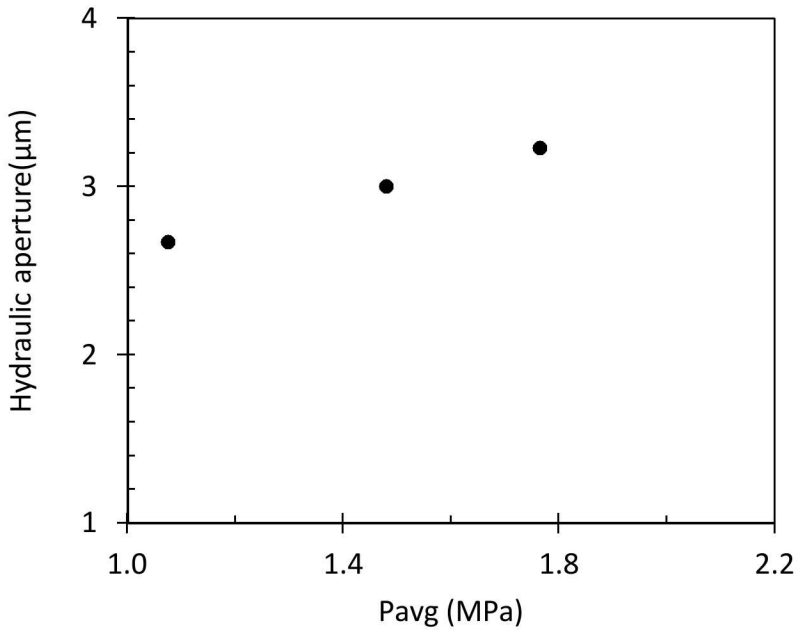

Fig 2.2.4: Results from silicone oil measurements made on C02. Results are given as hydraulic aperture vs. average oil pore pressure during tests.

The hydraulic apertures from the oil measurements are about two time larger than the gas values (Fig. 2.2.5). One reason may be that steady-state flow had not been established through the sample. There may be a trend of increased aperture with pore pressure, which could be from oil pressure propping open the fracture. Regardless, the hydraulic apertures from the oil measurements are much smaller than expected for a relatively open fracture.

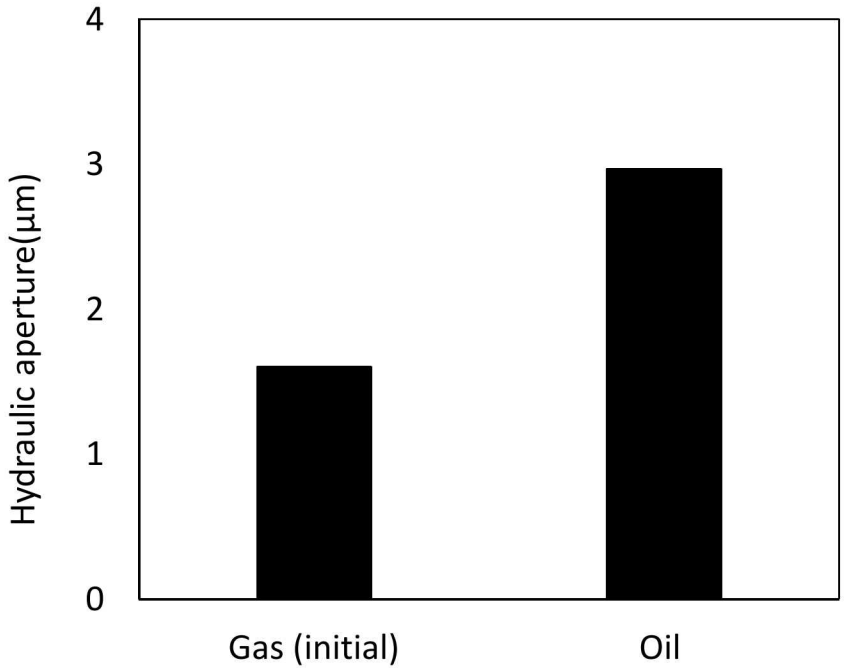

Fig 2.2.5: Comparison of average hydraulic aperture measured with gas and silicone oil for C02.

Following the oil measurements, the gas displacement pressure of 0.95 MPa (138 psi) was measured. This value corresponds to an aperture much less than 1 μm (Eqn 2.4). No gas flow measurements were made after the gas displacement pressure was achieved.

Taken together, these results suggest the fracture was very tight. It was believed that the initial fracture was very smooth, so even with the fracture offset during the sample construction, the fracture surfaces mate together very tightly under 13.8 MPa (2000 psi) confining stress. In response to these results, subsequent tensile splitting of samples was changed to produce rougher, more undulating fractures.

2.2.1.3. Sample C05

Sample C05 was tested first with gas, then silicone oil, and finally with gas again. The initial gas flow tests are summarized in Table 2.2.3 below.

Table 2.2.3 Initial gas flow tests conducted on C05.

Test No.	Confining stress	Back Pressure	Effective Stress
1	13.79 MPa (2000 psi)	1.03 MPa (150 psi)	12.76 MPa (1850 psi)
2	13.79 MPa (2000 psi)	4 MPa (580 psi)	9.79 MPa (1420 psi)

3	13.79 MPa (2000 psi)	7.24 MPa (1050 psi)	6.55 MPa (950 psi)

Results from the initial gas flow tests are given in Fig. 2.2.6 as hydraulic aperture as a function of the average pore pressure during each of the tests. Interpreted as permeability, they are in the 10^{-14} m^2 range, consistent with that which was expected for a relatively open fracture.

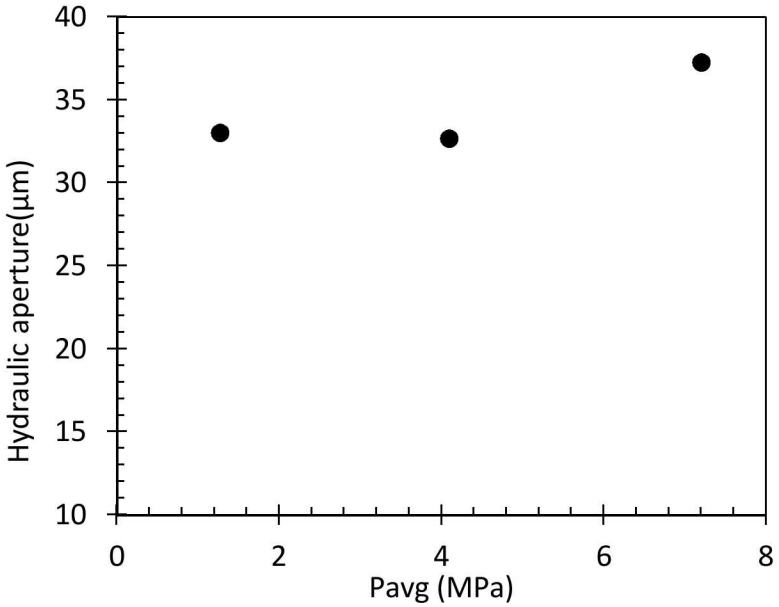

Fig 2.2.6: Results from series of gas flow measurements made on C05. Results are given as hydraulic aperture vs. average gas pore pressure during tests.

Silicone oil tests were conducted at 5 different upstream pressures in order to determine if increasing the pore pressure further props open the fracture. Results are given in Fig. 2.2.7. There is an indication that the hydraulic aperture increases with increasing oil pore pressure. The values are similar to those found in the initial gas testing.

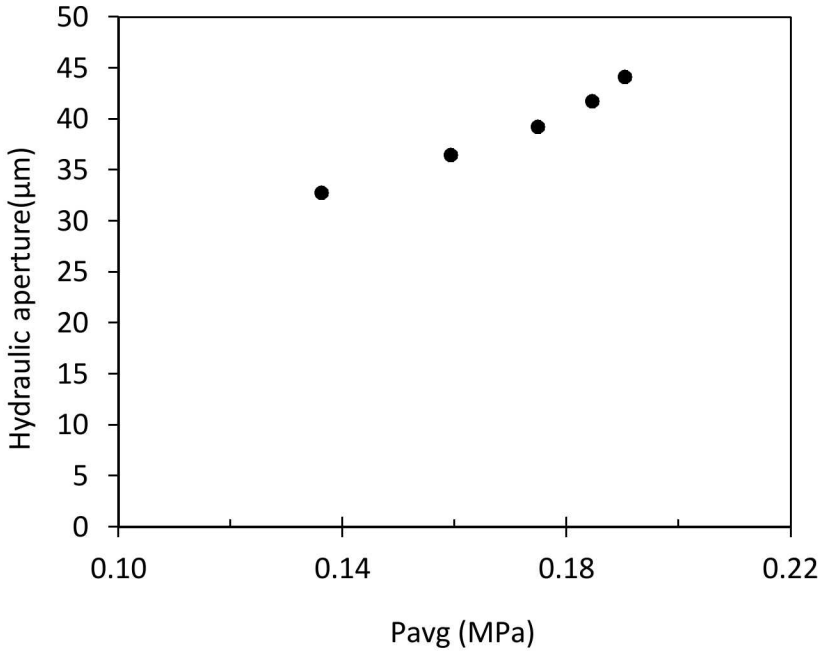

Fig 2.2.7: Results from silicone oil measurements made on C05. Results are given as hydraulic aperture vs. average oil pore pressure during tests.

In the subsequent gas displacement test, the gas displacement pressure was about 100 kPa (15 psi). The subsequent gas flow was interpreted after gas displacement is shown in Fig. 2.2.8 along with the average hydraulic aperture from the initial gas flow results and the silicone oil results. The results are also given as permeabilities in Fig. 2.2.9.

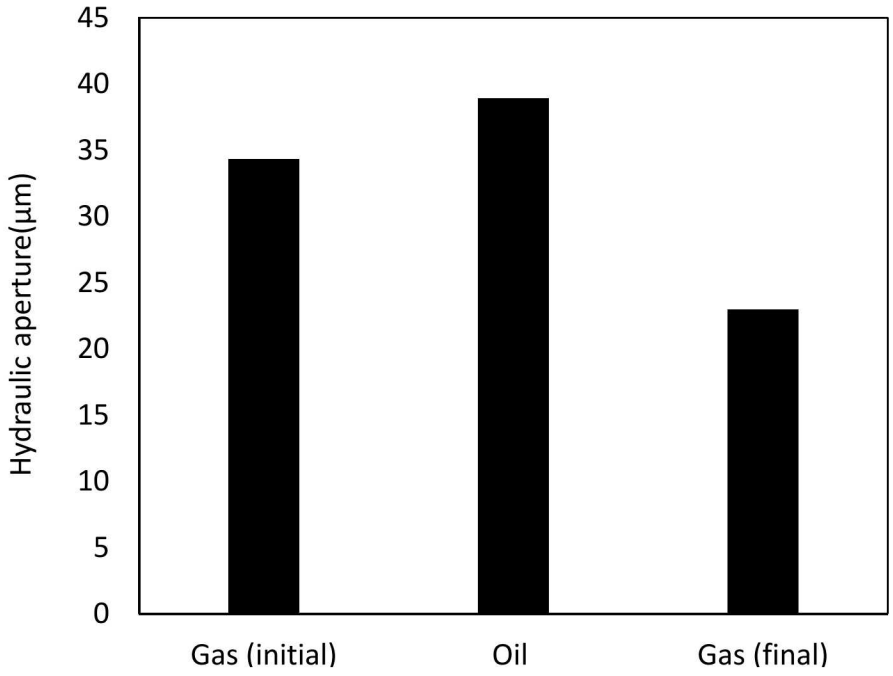

Fig 2.2.8: Comparison of average hydraulic aperture measured with initial gas, silicone oil and after gas displacement for C05.

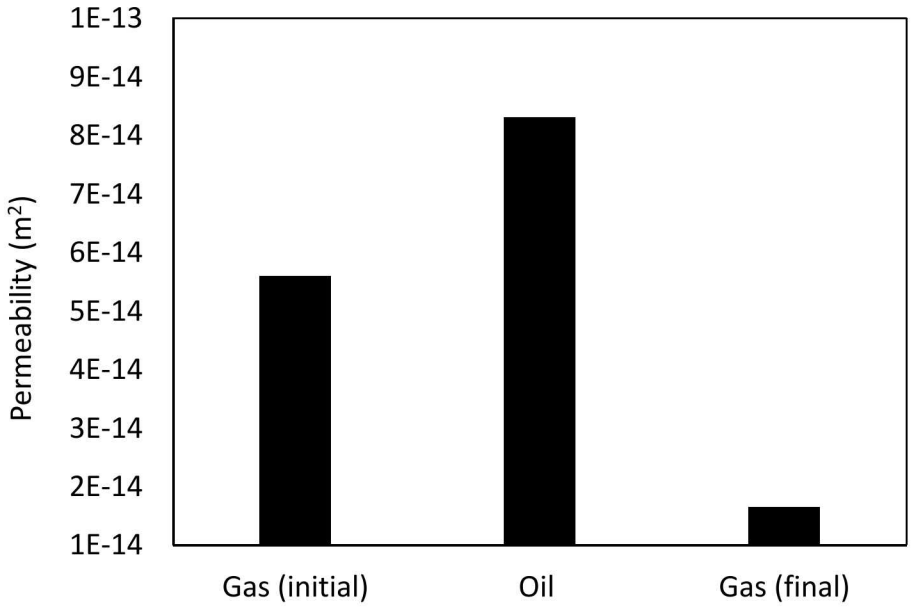

Fig 2.2.9: Comparison of average permeability measured with initial gas, silicone oil and after gas displacement for C05.

These results indicate that the final gas hydraulic aperture and permeability is less than either the initial gas or subsequent oil values. These results are consistent with some residual oil remaining along the fracture, limiting the amount of the fracture available for gas flow. This response is seen from gas tests following oil tests on other samples: C07 (Section 2.2.1.4); CS02 (Section 2.2.2.2): CSC04 (Section 2.2.2.3): and CSC02 (Section 2.2.2.4).

2.2.1.4. Sample C07

Sample C07 was tested first with gas, then silicone oil, and finally with gas again. The initial gas flow tests are summarized in Table 2.2.4 below.

Table 2.2.4 Initial gas flow tests conducted on C07.

Test No.	Confining stress	Back Pressure	Effective stress
1	13.79 MPa (2000 psi)	0	13.79 MPa (2000 psi)
2	13.79 MPa (2000 psi)	1.03 MPa (150 psi)	12.76 MPa (1850 psi)
3	13.79 MPa (2000 psi)	4.14 MPa (600 psi)	9.65 MPa (1400 psi)
4	16.89 MPa (2450 psi)	4.14 MPa (600 psi)	12.76 MPa (1850 psi)
5	13.79 MPa (2000 psi)	6.89 MPa (1000 psi)	6.90 MPa (1000 psi)
6	19.65 MPa (2850 psi)	6.89 MPa (1000 psi)	12.76 MPa (1850 psi)

In some of these gas flow measurements (test series no. 1), very low flow rates were obtained by maintaining very small pressure gradients across the samples. The purpose of these measurements was to detect the flow rates that were sufficiently small so that there was no appreciable non-linear flow. Results are given in Fig. 2.2.10 and 2.2.11 in terms of the non-linear flow correction analysis. In Fig. 2.2.10, data with low flow rates (less than 0.5 SCCS, shown in solid circles) have an essentially zero slope indicative of the absence of non-linear flow. Data with slightly greater flow rates shown in open circles are labelled as “transitional” and appear to begin to depart from a zero slope. In Fig. 2.2.11, data with high flow rates (greater than 2 SCCS, shown in solid circles) have a well-defined linear slope consistent with a significant non-linear flow component. The open circles are the same transitional data identified in Fig. 2.2.10. From these measurements, we conclude that flows must be less an about 0.5 SCCS through the cement fracture to not have significant non-linear flow.

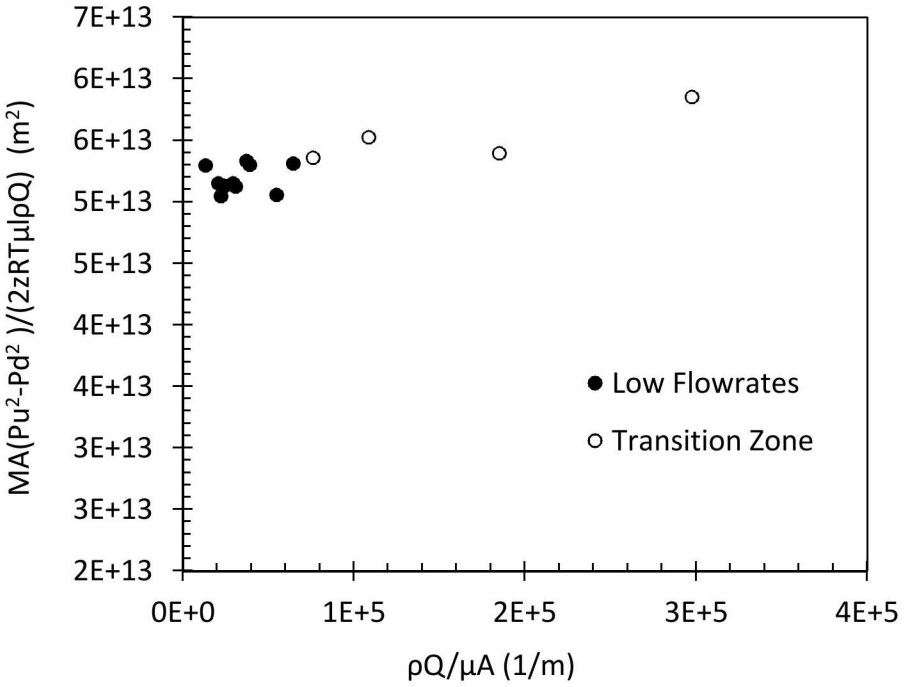

Fig 2.2.10: Forchheimer data from test number 1 of gas flow measurements made on C07 at relatively low flow rates. Solid circles are data with no appreciable non-linear flow component.

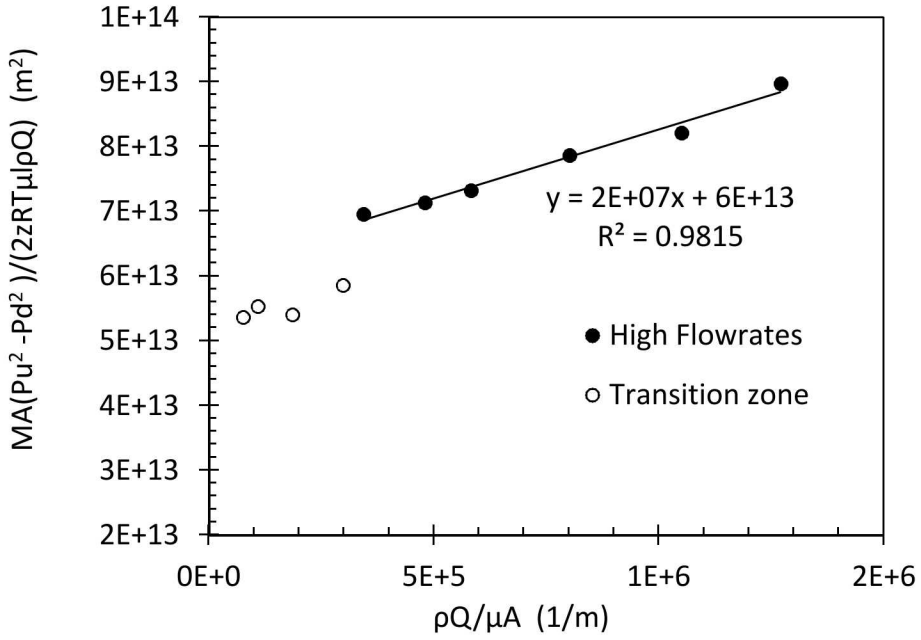

Fig 2.2.11: Forchheimer data from test number 1 of gas flow measurements made on C07 at relatively high flow rates. Solid circles are data with appreciable non-linear flow component.

Results from the initial gas flow tests are summarized in Fig. 2.2.12 as hydraulic aperture as a function of the average pore pressure during each of the tests. Interpreted as permeability, they are in the 10^{-15} m^2 range, in line with that which was expected for a relatively open fracture. Some of the tests were conducted at different confining stresses; there is no obvious trend of hydraulic aperture with pore pressure or confining stress.

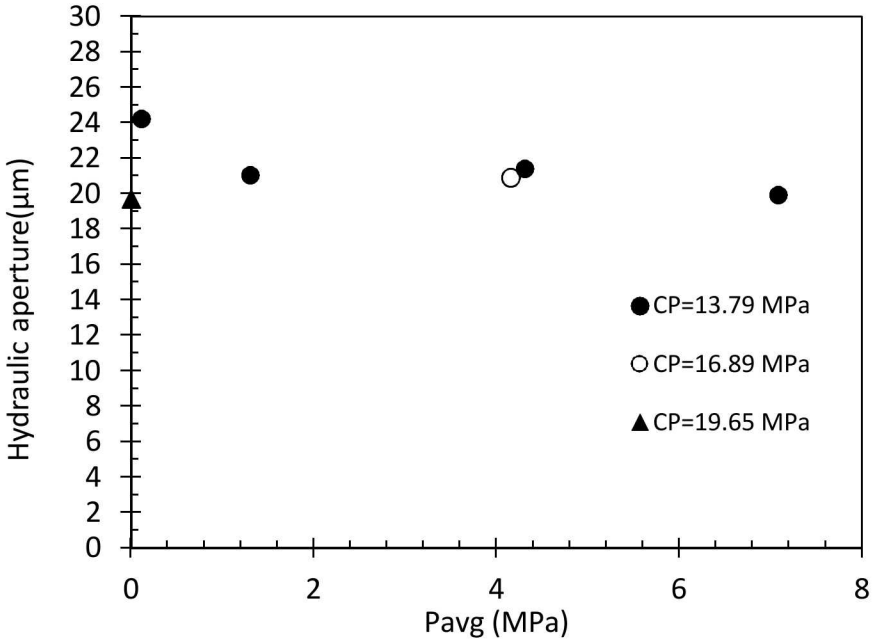

Fig 2.2.12: Results from series of gas flow measurements made on C07. Results are given as hydraulic aperture vs. average gas pore pressure during tests as a function of confining stress.

Silicone oil tests were conducted at 6 different flow rates and consequently slightly different pore pressures. Results are given in Fig. 2.2.13. The hydraulic aperture does not vary systematically with oil pore pressure. The values are similar to those found in the initial gas testing.

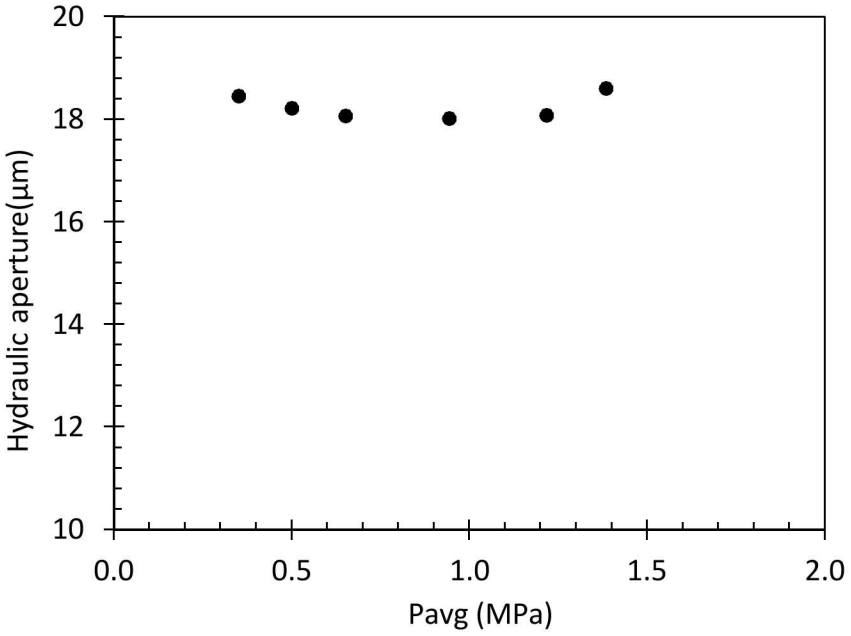

Fig 2.2.13: Results from silicone oil measurements made on C07. Results are given as hydraulic aperture vs. average oil pore pressure during tests.

The gas displacement pressure was about 70 kPa (10 psi). After the gas displacement pressure was reached, the flow rate was measured and the gas pressure was progressively increased. In response, oil continued to be produced and the gas flow rate was periodically measured. Results from these measurements are shown in Fig. 2.2.14 as oil volume produced and gas permeability as a function of gas pressure. After 300 kPa (43.5 psi), no additional oil was produced. Gas flow measurements continued to 2.7 MPa.

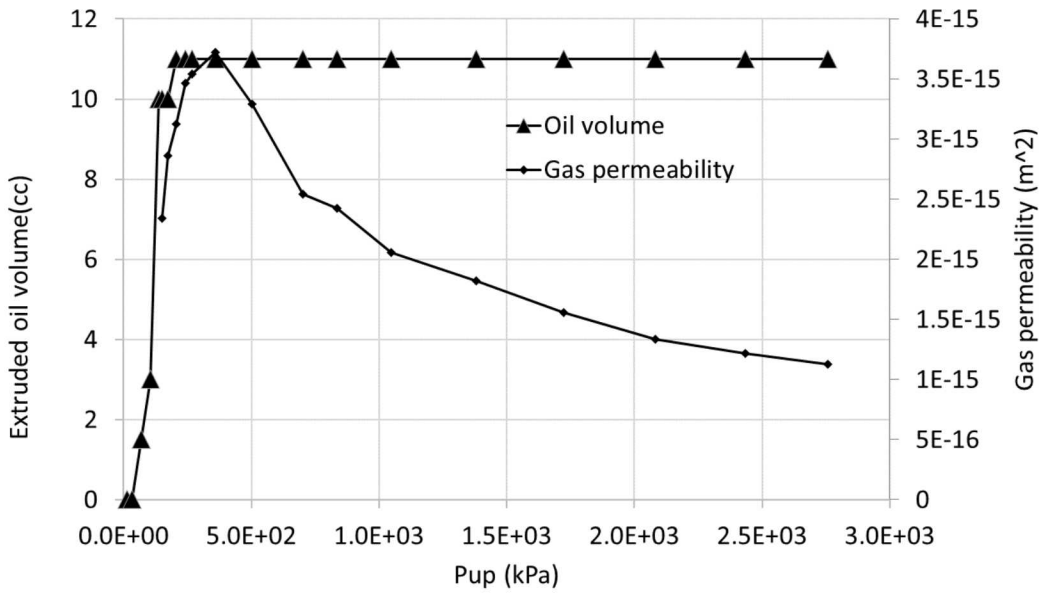

Fig 2.2.14: Silicone oil collected from downstream and gas permeabilty during gas displacement testing of sample C07.

The gas permeabilities indicate an increasing gas permeability as oil is displaced from the sample (between 70 and 300 kPa (10-43.5 psi)). These results are consistent with the gas permeability increasing while the oil saturation decreases (two-phase flow). These results are not possible to interpret as saturation due to the volume of oil in the "dead space" downstream of the end of the sample. Also, the permeability data are interpreted without being corrected for non-linear flow. The decrease in gas permeability with gas pressures above 300 kPa (43.5 psi) is a consequence of non-linear flow.

The average hydraulic aperture from the initial gas flow tests, the silicone oil tests, and the gas displacement tests are given in Fig. 2.2.15. Again, the final hydraulic aperture from the final gas flow tests are less than the previous measurements, possibly due to residual oil in the specimen reducing the gas-accessible pore spaces.

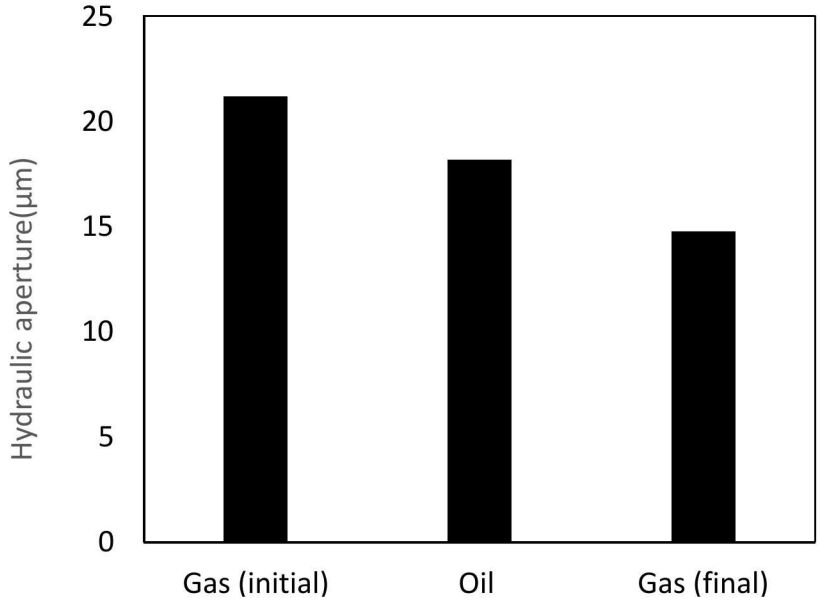

Fig 2.2.15: Comparison of average hydraulic aperture measured with initial gas, silicone oil and after gas displacement for C07.

2.2.1.5. Sample C09

This sample was tested first with gas and then silicone oil. The sample had a very large aperture while under pressure with both gas and silicone oil, and it was believed that the gas displacement pressure would be very low and difficult to measure. Consequently, there was no gas displacement test.

The conditions for the single initial gas test are given in Table 2.2.5.

Table 2.2.5 Conditions for initial gas flow measurements on sample C09.

TEST NO.	Confining stress	Back Pressure	Effective stress
1	13.79 MPa (2000 psi)	0	13.79 MPa (2000 psi)

The interpreted hydraulic aperture from the gas flow test was about 130 μm.

Subsequent silicone oil tests, conducted at a number of different oil pressures, yielded interpreted hydraulic apertures of 110 to 116 μm (Fig. 2.2.16).

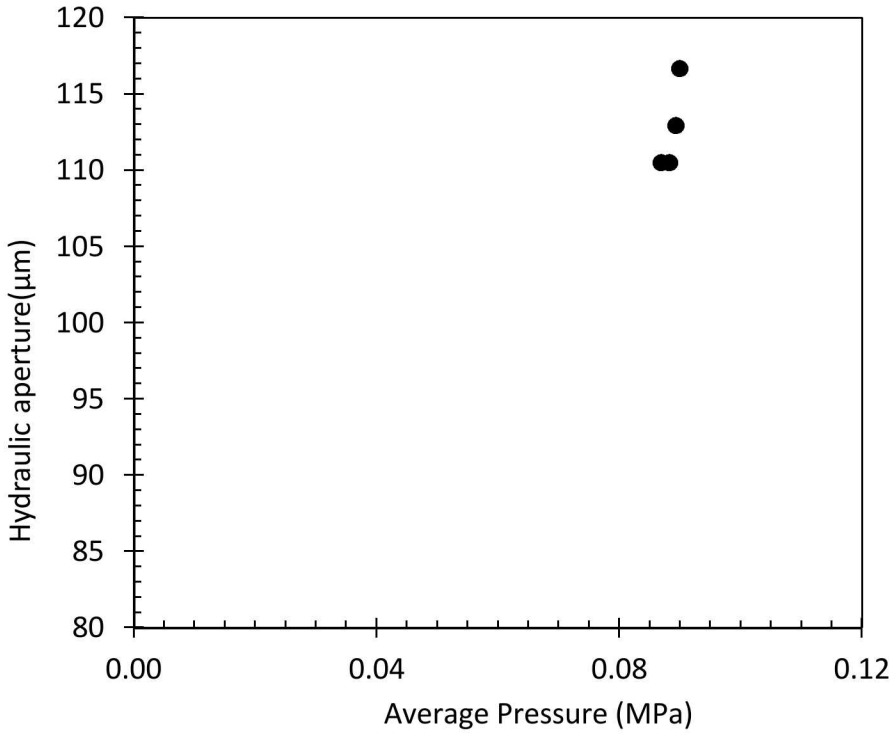

Fig 2.2.16: Results from first silicone oil measurements made on C09. Results are given as hydraulic aperture vs. average oil pore pressure during tests.

The average hydraulic aperture from the initial gas flow tests and the subsequent silicone oil tests are given in Fig. 2.2.17. The hydraulic aperture from the initial gas flow tests is somewhat greater than that from the silicone oil test. One possible reasons for this result is gas may move through pores in the cement adjacent to the flaws that are too small to permit entry of oil

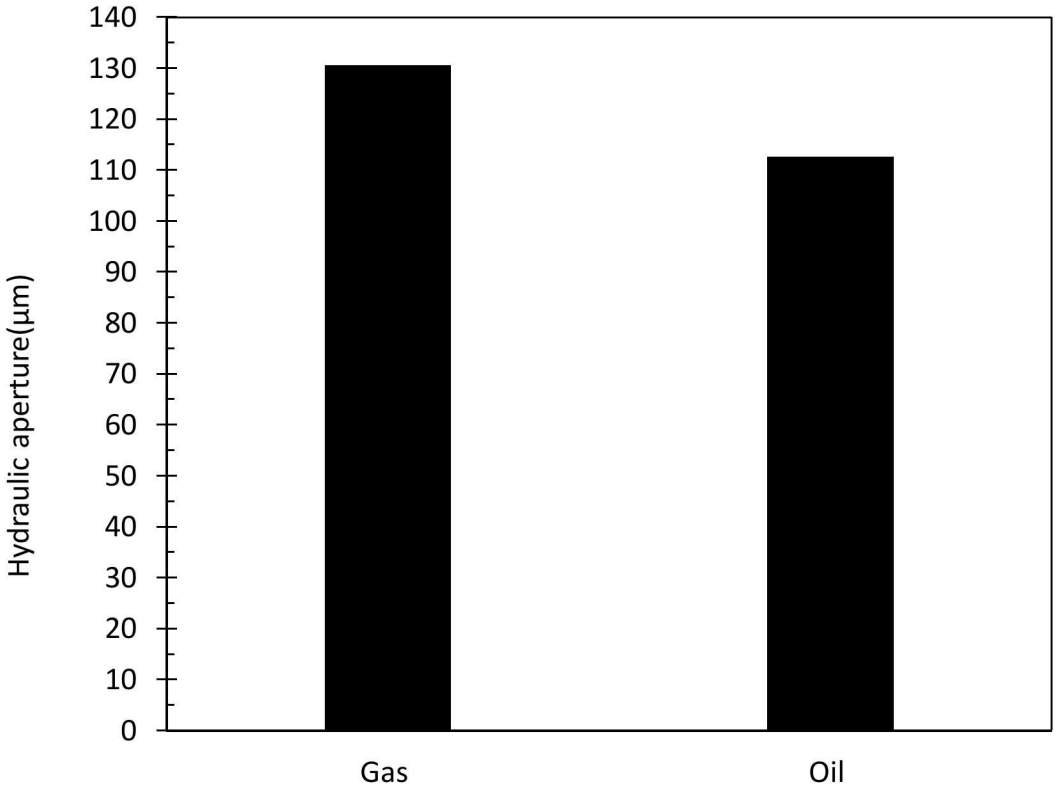

Fig 2.2.17: Comparison of average hydraulic aperture measured with initial gas and subsequent silicone oil tests for C09.

2.2.1.6. Sample C12

The objective of the testing on sample C12 was to determine the transition from linear to non-linear flow as a function of confining stress. To achieve this objective, a series of gas flow measurements were made on under a range of confining stresss as described in Table 2.2.6.

Table 2.2.6 Gas flow measurements made on sample C12.

TEST No.	Confining stress	Back Pressure	Effective stress
1	13.79 MPa (2000 psi)	0	13.79 MPa (2000 psi)
2	11.03 MPa (1600 psi)	0	11.03 MPa (1600 psi)
3	8.27 MPa (1200 psi)	0	8.27 MPa (1200 psi)
4	16.55 MPa (2400 psi)	0	16.55 MPa (2400 psi)

5	5.52 MPa (800 psi)	0	5.52 MPa (800 psi)
6	2.76 MPa (400 psi)	0	2.76 MPa (400 psi)

After correcting for non-linear flow, the hydraulic aperture as a function of effective stress is shown in Fig. 2.2.18. Because the pore pressure was kept nearly constant between tests, the change in effective stress is due solely to changes in confining stress. These results indicate that the hydraulic aperture and permeability of this sample was not a clear function of confining stress, and suggests this fracture will not readily close under increased external or confining stress. Increased pore pressures might, however, prop the fracture open more.

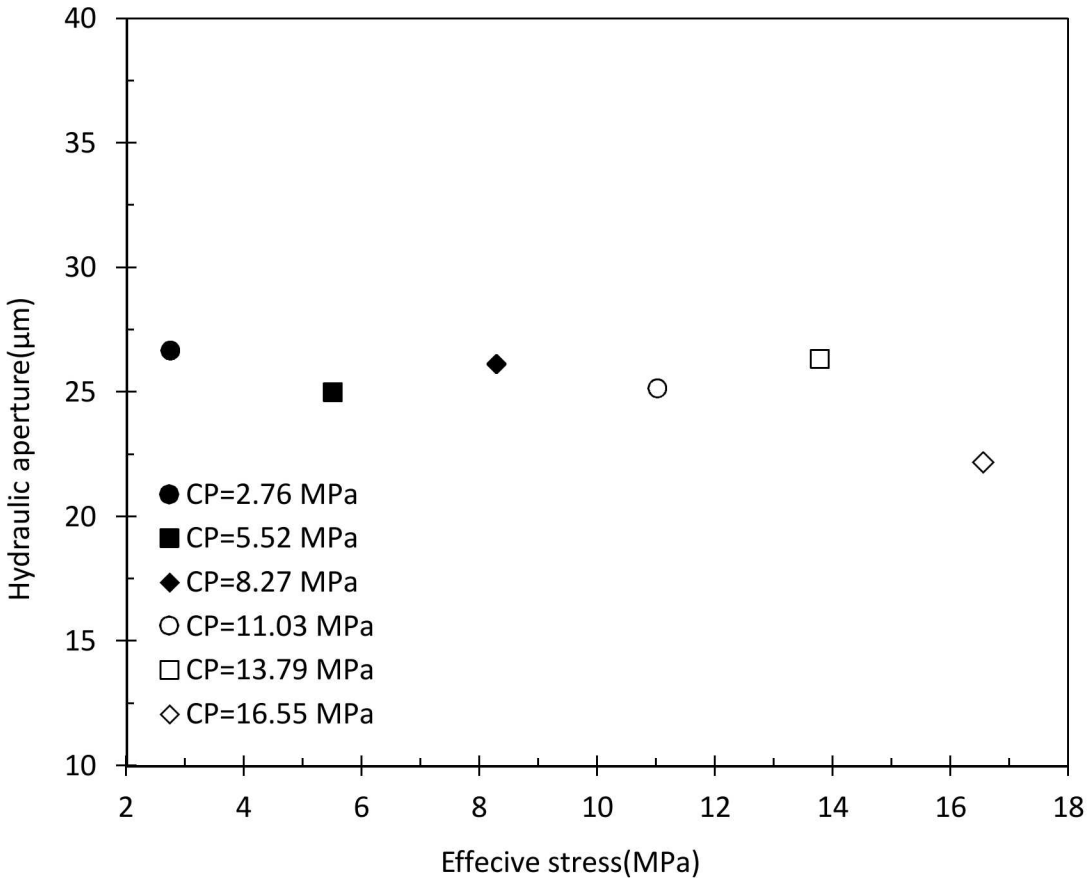

Fig 2.2.18: Hydraulic aperture determined from gas flow measurements as a function of effective stress for sample C12.

The flow rate as a function of the fluid (gas) pressure squared difference ($P_{up}^2 - P_{down}^2$, where P_{up} is the upstream pressure and P_{down} is the downstream) across the sample is shown in Fig. 2.2.19 for test 1 (conducted at 13.79 MPa confining stress). For gas flow, a linear relationship between

the flow rate and the pressure squared difference is indicative of linear flow which can be described by Darcy's law. These results clearly show that the flow is linear at low flow rates and becomes increasingly non-linear with increasing flow rates. Interpreting the measurements assuming linear (Darcy) flow will lead to an erroneous estimation of permeability and hydraulic aperture.

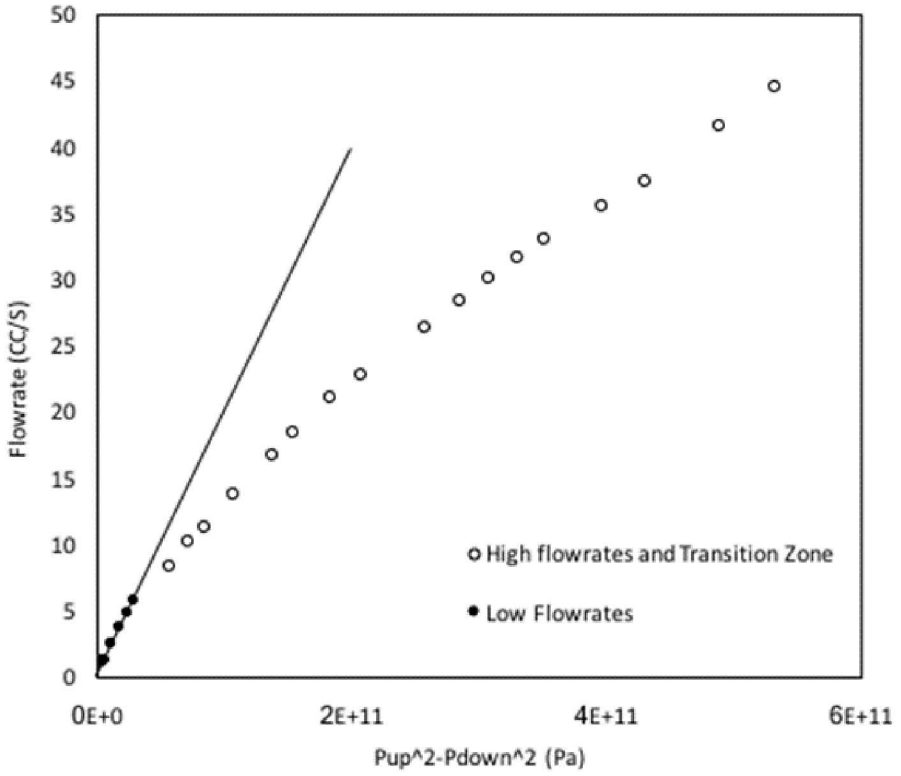

Fig 2.2.19: Flow rate as a function of the pressure squared difference ($P_{up}^2 - P_{down}^2$) during test 1 on sample C12.

The Reynolds number has been used in the past for identifying the beginning of non-Darcy (non-linear) flow. Reynolds number for flow between two parallel plates, idealized case of fracture flow, can be expressed in the following form (Fox et al., 2004):

$$Re = \frac{\rho Q}{\mu w} \quad (2.5)$$

where ρ and μ are the density and viscosity of the fluid, respectively. Q is the mean volumetric flowrate and w is the fracture's width. The transmissivity ratio (equivalent to the permeability at the current test condition divided by the permeability at very low flow rate) is given in Fig. 2.2.20 as a function of the Reynolds number. The transmissivity ratio is 1 if only linear flow occurs, and thus the conditions at which this value deviates from 1 can be used to reveal the transition between linear and non-linear flow. For this test, the critical Reynolds number associated with transition is Re= 5.3, which corresponds to a flow rate of about 6 standard cubic centimeters per second (SCCS). It should be mentioned that based on the Forchheimer's correction graphs (not shown for this test), the estimated transition point was calculated at the flowrate of 6.3 CC/S. Therefore,

there is a very good agreement between the results from these two analyses. Moreover, this Reynolds number agrees well with the critical Reynolds number of 3–10 obtained by Ma and Ruth (1993) in porous media as well as the critical Reynolds number of 1.8-22.0 in fractured rocks with small-scale unevenness proposed by Wang et al. (2016).

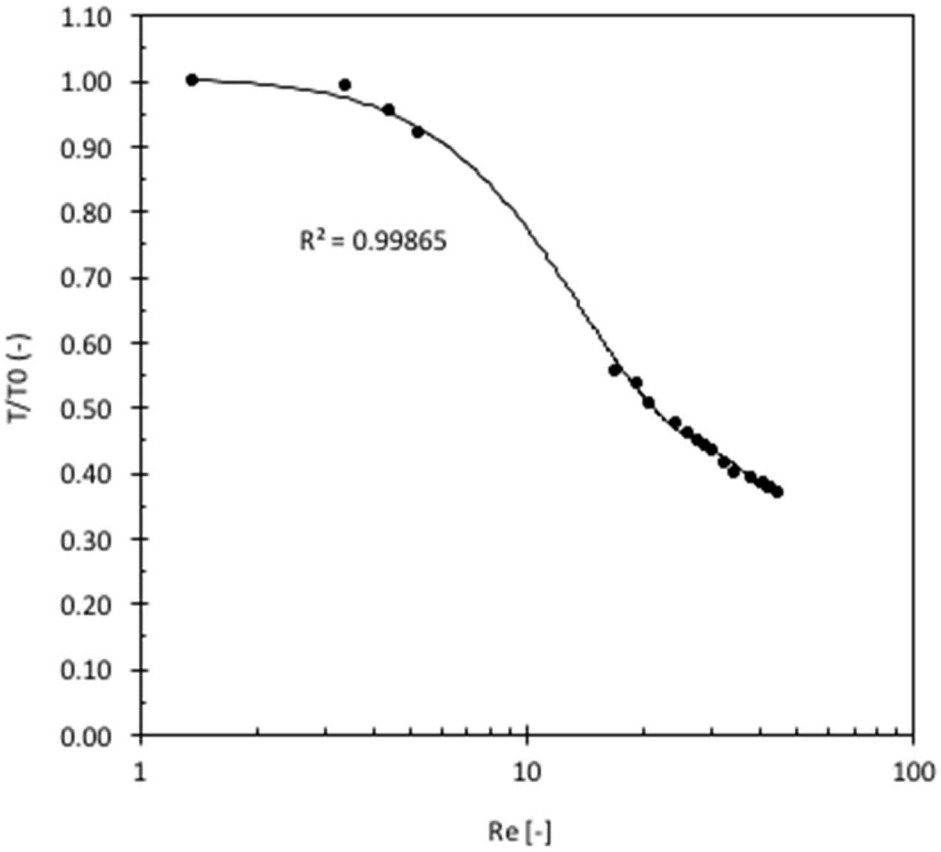

Fig 2.2.20: Normalized transmissivity as a function of Reynolds number for test 1 on sample C12.

The correction for non-linear flow yields the non-linear coefficient (β) as well as the permeability or hydraulic aperture. From the correction developed at each confining stress, the non-linear coefficient (β) given as a function of confining stress in Fig. 2.2.21. There is an apparent trend of increasing β with increasing confining stress. This result is consistent with the results of Tiss and Evans (1989) on consolidated porous media. One explanation for this result is that at greater confining stresses, the fracture is forced together more and results in narrower and more tortuous flow paths. It is expected that non-linear flow will increase with increasing tortuosity of the flow paths.

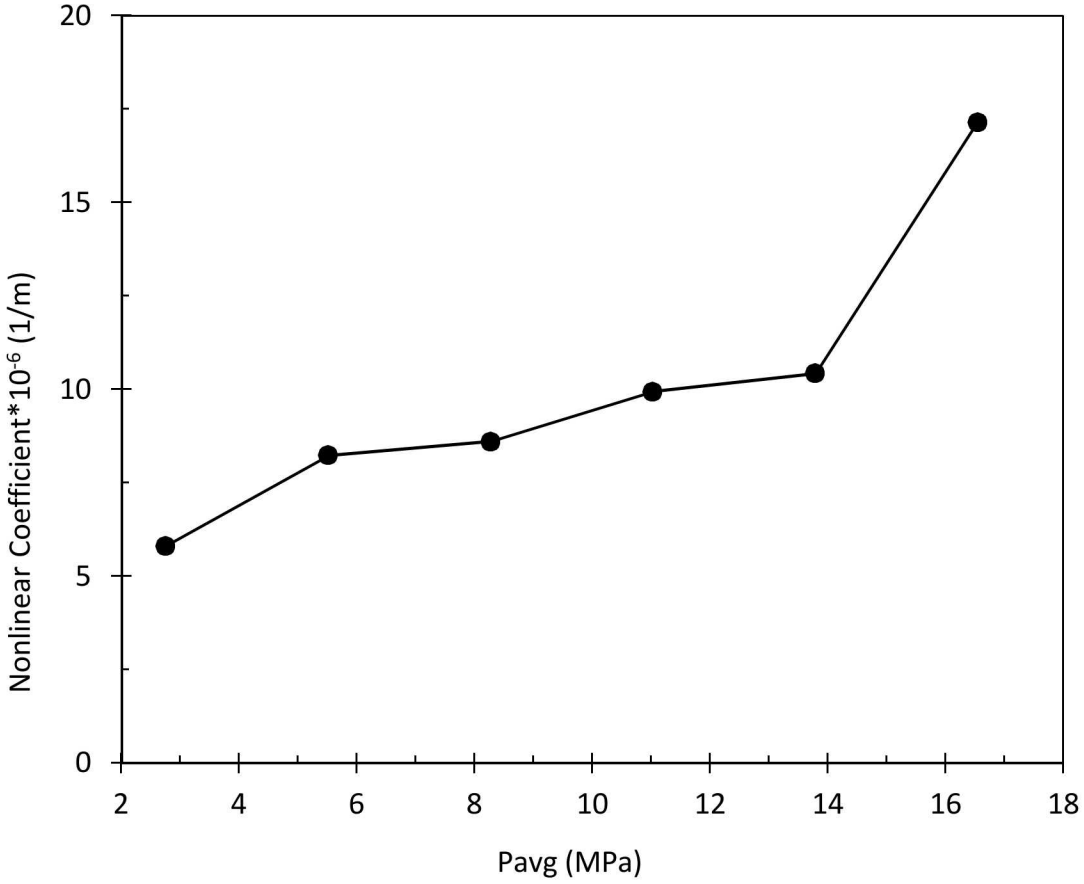

Fig 2.2.21: Nonlinear coefficient β as a function of the confining stress.

2.2.1.7. ICZ01

The purpose of this test was to obtain the hydraulic properties of the intact cement as the baseline for undamaged type I-II cement.

A series of gas flow measurements were made at a confining stress of 13.8 MPa. The data are given in Fig. 2.2.22 as the interpreted permeability as a function of the inverse of the mean pore pressure (a so-called Klinkenberg plot). The variation of the gas permeability with pore pressure is due to gas slip, where the gas molecules collide with the walls of the pore structure. This behavior becomes important in low permeability media where the pore size is on the order of the mean free path of the gas molecule. The intercept of a straight-line fit through these data is the intrinsic permeability.

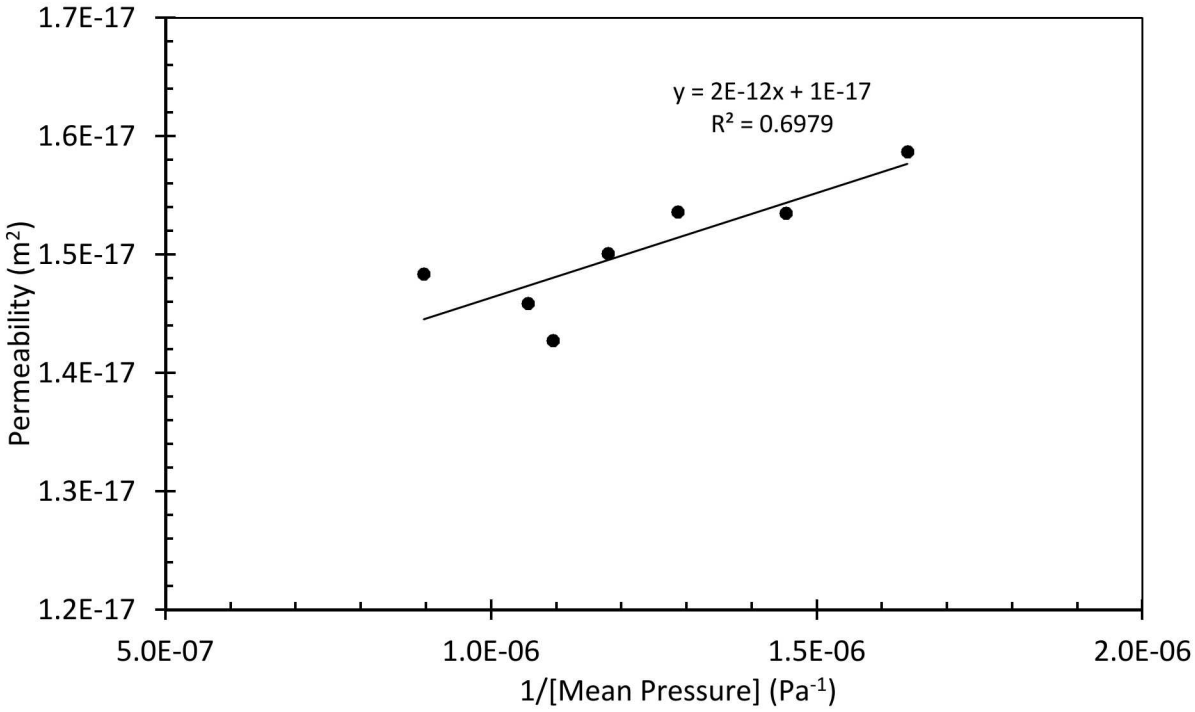

Fig 2.2.22: Klinkenberg plot for sample ICZ01.

From the best fit of a straight line to these data shown in the figure, the interpreted gas permeability for this figure is 1.3×10^{-17} m^2, and the gas slippage factor is 137 kPa. This result allows us to account for gas slip when estimating gas flow through intact cement. In contrast to these results for intact cement, the flow path size in the fractured cement samples are much larger and there is no appreciable gas slip.

A subsequent test with silicone oil was unsuccessful due to clogging of tubing with rubbery material. It is speculated that the epoxy coating on the sample had not fully cured for this sample, and some was displaced into the downstream tubing.

2.2.1.8. Sample C10

Similar to C12 (Section 2.2.1.6), the objective of the testing on sample C10 was to determine the transition from linear to non-linear flow as a function of confining stress. As shown in Table 2.2.7, after increasing the confining stress up to 13.79 MPa (2000 psi), the pressure was reduced back to 0.086 MPa (125 ppsi) in steps to investigate the effect of hysteresis on the permeability, hydraulic aperture and transition flow. It should be mentioned that some measurements with back pressure at different confining stresses were made, though the results are not shown here since due to the very low transition flow values, it was not possible to get a linear flow through the sample with back pressure.

Table 2.2.7 Gas flow measurements made on sample C10.

TEST No.	Confining stress	Back Pressure	Effective stress
1	0.86 MPa (125 psi)	0	0.86 MPa (125 psi)
2	3.45 MPa (500 psi)	0	3.45 MPa (500 psi)
3	6.89 MPa (1000 psi)	0	6.89 MPa (1000 psi)
4	10.34 MPa (1500 psi)	0	10.34 MPa (1500 psi)
5	13.79 MPa (2000 psi)	0	13.79 MPa (2000 psi)
6	10.34 MPa (1500 psi)	0	10.34 MPa (1500 psi)
7	6.89 MPa (1000 psi)	0	6.89 MPa (1000 psi)
8	3.45 MPa (500 psi)	0	3.45 MPa (500 psi)
9	0.86 MPa (125 psi)	0	0.86 MPa (125 psi)

After correcting for non-linear flow, the hydraulic aperture interpreted from the from measurements, including correcting for non-linear flow, is shown as a function of confining stress at different loading and unloading stages in Fig. 2.2.18. These results indicate that the hydraulic aperture and permeability of the sample decreases as the confining stress is increased. During subsequent unloading, the change in the hydraulic aperture is less than it was during loading. This result is likely due to plastic deformation of the asperities of the fracture during loading.

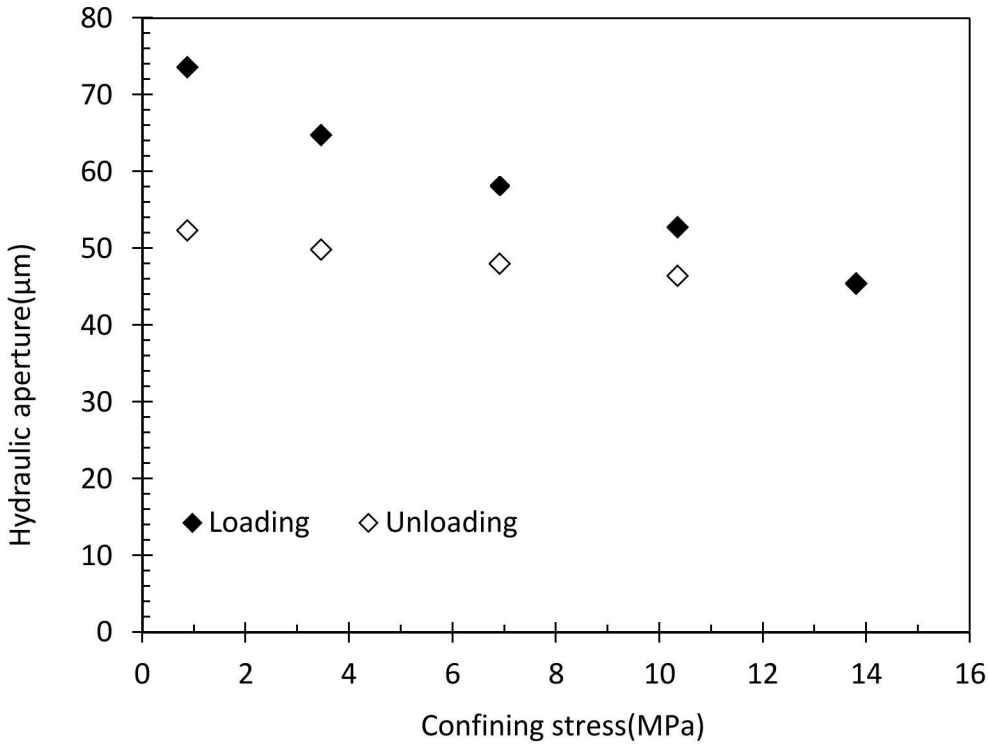

Fig 2.2.23: Hydraulic aperture determined from gas flow measurements as a function of confining stress for sample C10 at loading and unloading stages.

2.2.1.9. Sample C13

Similar to C12 (Section 2.2.1.7) and C10 (Section 2.2.1.8), gas flow measurements were made on this sample to determine the transition from linear to non-linear flow as a function of confining stress. Also, the hysteresis effect - the difference between flow behavior observed as stress on the sample is increased compared to that as stress is decreased - was investigated by unloading the sample to 0.86 MPa (125 ppsi), after first increasing confining stress up to 13.79 MPa (2000 ppsi) (Table 2.2.8).

Table 2.2.8 Gas flow measurements made on sample C13.

TEST No.	Confining stress	Back Pressure	Effective stress
1	0.86 MPa (125 psi)	0	0.86 MPa (125 psi)
2	3.45 MPa (500 psi)	0	3.45 MPa (500 psi)

3	6.89 MPa (1000 psi)	0	6.89 MPa (1000 psi)
4	10.34 MPa (1500 psi)	0	10.34 MPa (1500 psi)
5	13.79 MPa (2000 psi)	0	13.79 MPa (2000 psi)
6	10.34 MPa (1500 psi)	0	10.34 MPa (1500 psi)
7	6.89 MPa (1000 psi)	0	6.89 MPa (1000 psi)
8	3.45 MPa (500 psi)	0	3.45 MPa (500 psi)
9	0.86 MPa (125 psi)	0	0.86 MPa (125 psi)

The hydraulic aperture corrected for non-linear flow versus confining stress is plotted in Figure 2.2.24. The decrease in hydraulic aperture with confining stress as well as the effect of hysteresis can be seen in the figure.

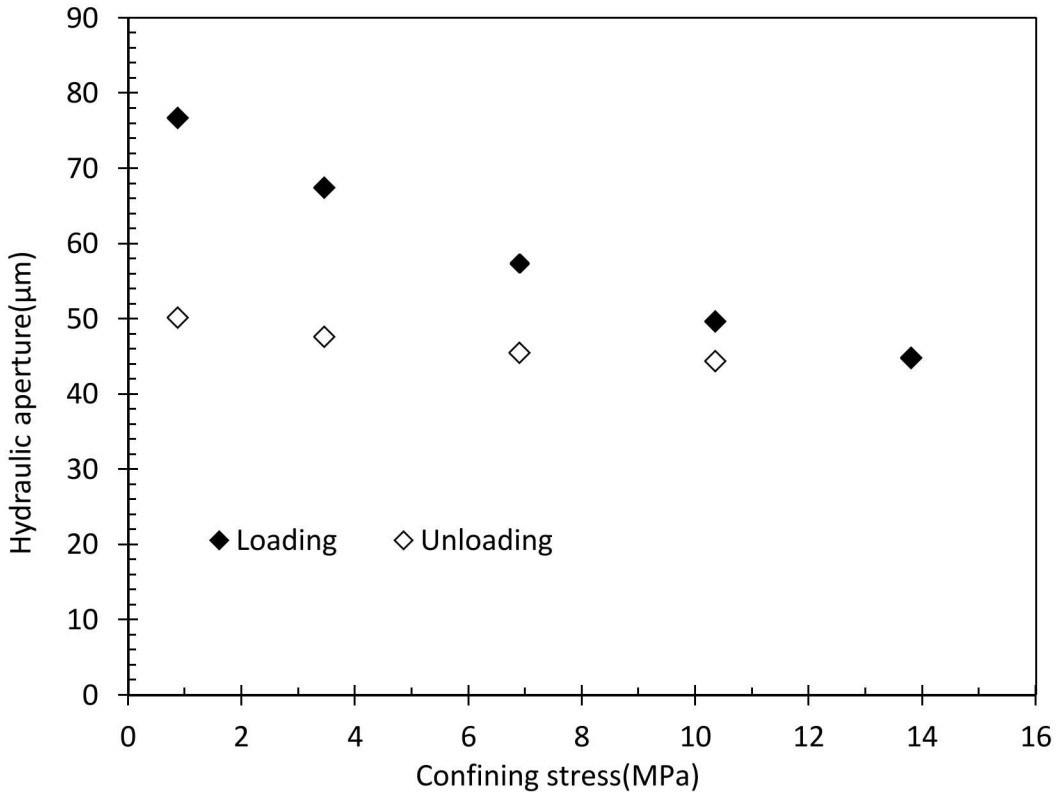

Fig 2.2.24: Hydraulic aperture determined from gas flow measurements as a function of confining stress for sample C13 at loading and unloading stages.

Also, the non-linear coefficient (β) ,described in Section 2.1.3.1, developed at each confining stress is given as a function of confining stress in Fig. 2.2.25 at loading and unloading stages.

These results indicate that the non-linear coefficient is not a constant and is affected by the magnitude and history of stress applied to the fracture. The hysteresis effect observed here is consistent with the results of Tiss and Evans (1989) on consolidated porous media.

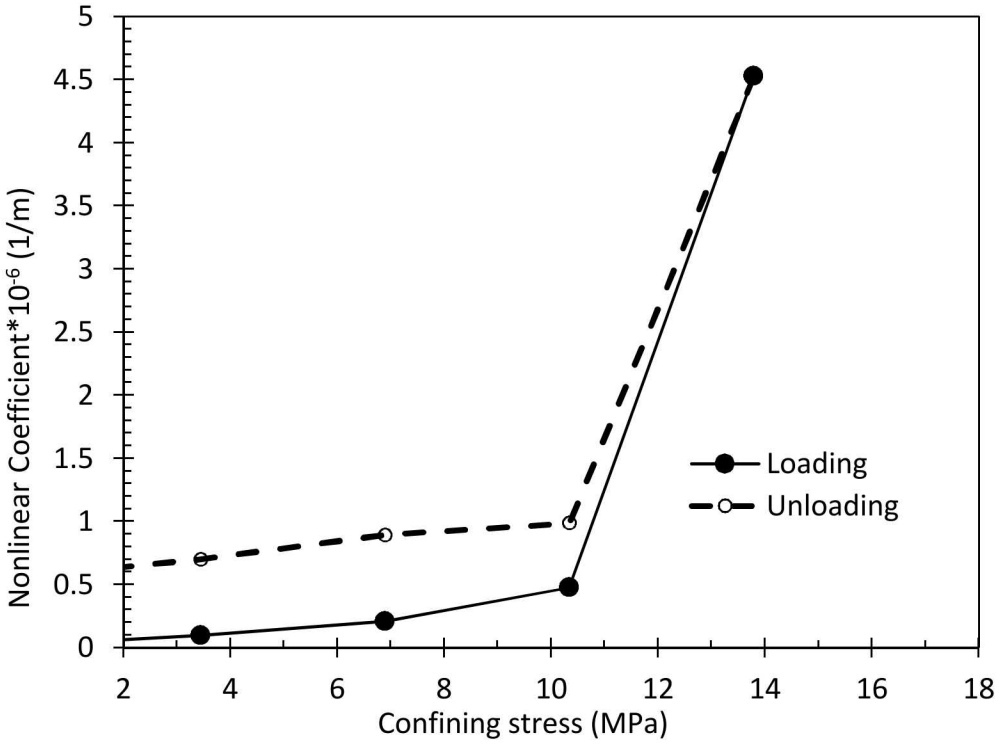

Fig 2.2.25: Nonlinear coefficient β as a function of the confining stress.

2.2.2. Flow through cement-steel interface (microannulus)

2.2.2.1. Sample CS01

Sample CS01 was tested first with gas, then silicone oil, and finally with gas again. The initial gas flow tests are summarized in Table 2.2.9 below. These tests included measurements at the same effective stress (confining stress – pore pressure).

Table 2.2.9 Initial gas flow tests conducted on CS01.

Test No.	Confining stress(Gauge)	Back Pressure (Gauge)	Effective stress
1	13.79 MPa (2000 psi)	1.03 MPa (150 psi)	12.76 MPa (1850 psi)
2	13.79 MPa (2000 psi)	4.14 MPa (600 psi)	9.65 MPa (1400 psi)
3	16.89 MPa (2450 psi)	4.14 MPa (600 psi)	12.76 MPa (1850 psi)
4	13.79 MPa (2000 psi)	6.89 MPa (1000 psi)	6.90 MPa (1000 psi)

5	19.65 MPa (2850 psi)	6.89 MPa (1000 psi)	12.76 MPa (1850 psi)

Results from the initial gas flow tests are given in Fig. 2.2.26 as hydraulic aperture as a function of the effective stress during each of the tests. Interpreted as permeability, they are in the 10^{-15} m^2 range, in line with that which was expected for a relatively open fracture. The data do not exhibit a clear trend of hydraulic aperture with effective stress.

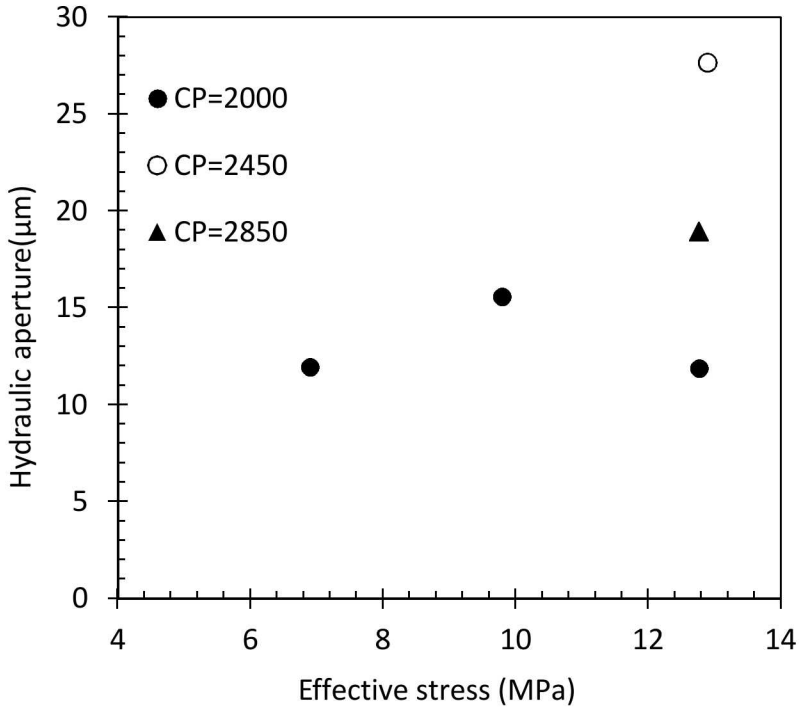

Fig 2.2.26: Results from series of gas flow measurements made on CS01. Results are given as hydraulic aperture vs. effective stress (confining stress – pore pressure).

Silicone oil tests were conducted at 4 different flow rates and consequently slightly different pore pressures. Outflow collected during this test confirmed steady flow for each test. Results are given in Fig. 2.2.27. The hydraulic aperture does not vary significantly with oil pore pressure. The values are similar to those found in the initial gas testing.

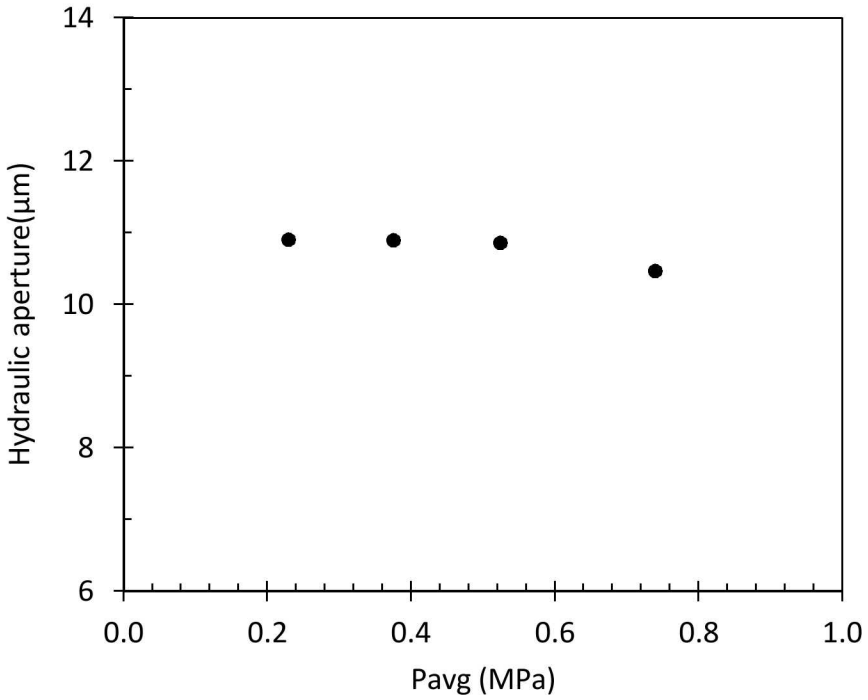

Fig 2.2.27: Results from silicone oil measurements made on CS01. Results are given as hydraulic aperture vs. average oil pore pressure during tests.

Following the oil measurements, the gas displacement pressure of 0.83 MPa (120 psi) was measured. This value corresponds to an aperture much less than 1 μm. No gas flow measurements were made after the gas displacement pressure was achieved.

The average hydraulic aperture from the initial gas flow tests and the silicone oil tests are given in Fig. 2.2.28. The hydraulic aperture from the initial gas tests are somewhat larger than that from the subsequent oil test.

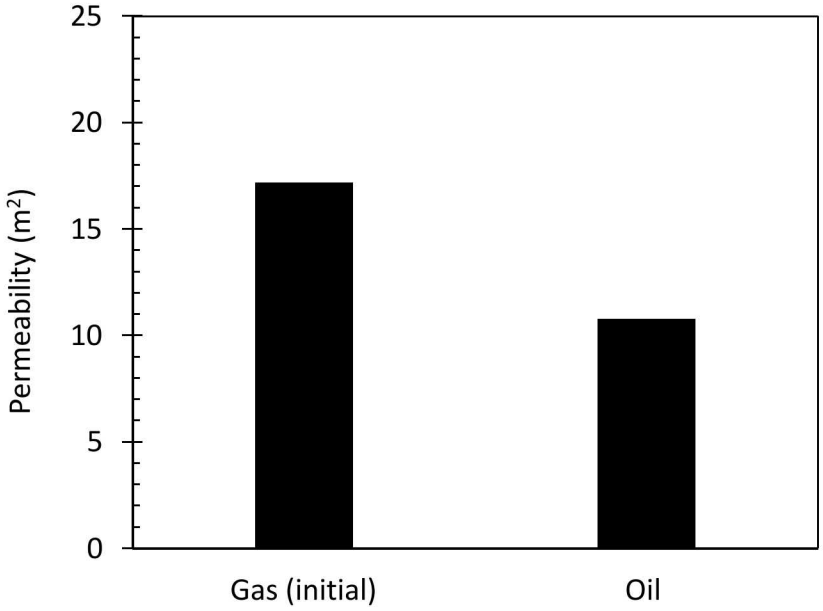

Fig 2.2.28: Comparison of average hydraulic aperture measured with gas and silicone oil for CS01.

There was concern that the steel-cement contact in the sample was tighter than desired. Consequently, following this test, the sample preparation procedure was changed with the intention of producing samples with rougher cement-steel contacts. This sample was produced by casting the steel plate within the cement, and then de-bonding after full curing. Subsequent sample were produced by casting and curing the cement, creating a tensile split, gluing the steel plate to one side and reassembling the sample.

2.2.2.2. Sample CS02

Sample CS02 was tested first with gas, then silicone oil, then with crude oil, and finally with gas again. The initial gas flow tests are summarized in Table 2.2.10 below. These tests included measurements at the same effective stress (confining stress – pore pressure).

Table 2.2.10 Initial gas flow tests conducted on CS02.

Test No.	Confining stress	Back Pressure	Effective stress
1	13.79 MPa (2000 psi)	0	13.79 MPa (2000 psi)
2	13.79 MPa (2000 psi)	1.03 MPa (150 psi)	12.76 MPa (1850 psi)

3	13.79 MPa (2000 psi)	4.14 MPa (600 psi)	9.65 MPa (1400 psi)
4	16.89 MPa (2450 psi)	4.14 MPa (600 psi)	12.76 MPa (1850 psi)
5	13.79 MPa (2000 psi)	6.89 MPa (1000 psi)	6.90 MPa (1000 psi)
6	19.65 MPa (2850 psi)	6.89 MPa (1000 psi)	12.76 MPa (1850 psi)

Fifteen individual steady-state gas flow measurements were made as part of test 1. These tests were conducted over a very wide range of flow rates and are given in Fig. 2.2.29. These data demonstrate flow conditions that did not include non-linear flow (solid squares), a transitional behavior (open circles), and flow that include non-linear flow and could be fit to a straight line with a non-zero slope (solid circles). The criterion for flow rate to achieve simple linear flow was estimated as 4.7 SCCS. This result implies that for any flow rate in the cemented annulus greater than about 5 SCCS, the flow will deviate from strictly linear (Darcy) flow. Under these conditions, not accounting for non-linear flow when interpreting cemented annulus pressure build-up or flow rates if the cemented annulus is vented at the surface will result in underestimating the actual permeability of the cemented annulus.

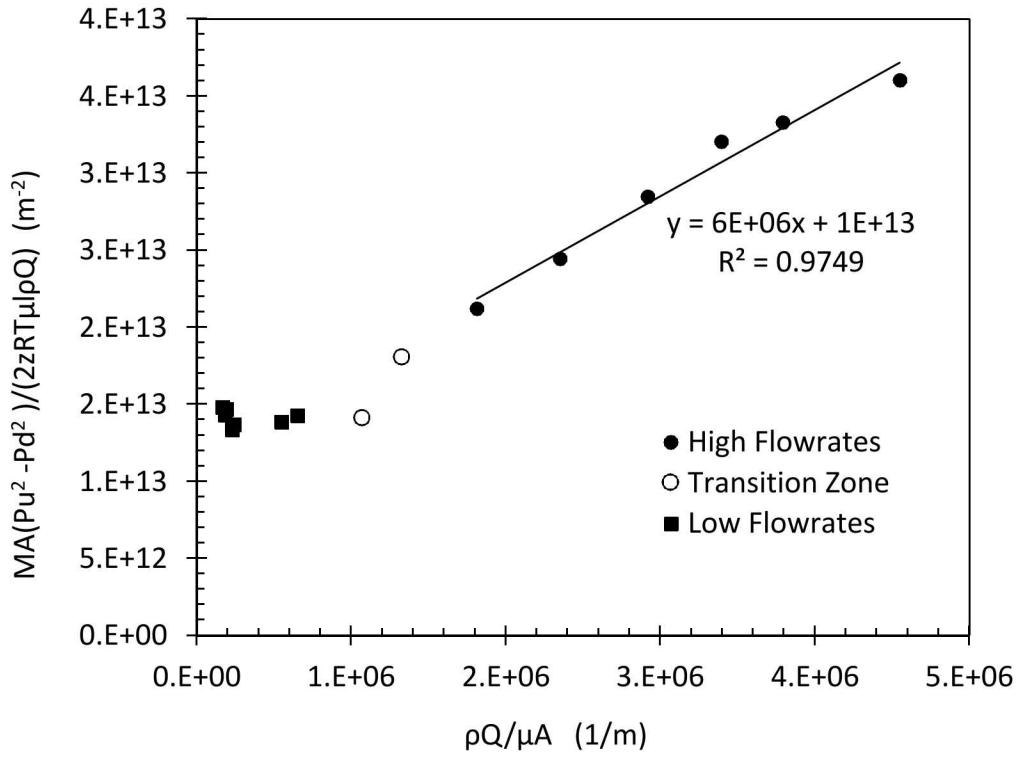

Fig 2.2.29: Forchheimer data from test number 1 of gas flow measurements made on CS02.

Results from all of the initial gas flow tests are summarized in Fig. 2.2.30 as hydraulic aperture as a function of the effective stress during each of the tests. The data made at the same effective stress but different confining and pore pressures agree very well. One measurement (test no. 1) was considerably greater than the remaining gas tests. The reason for the decrease in flow may be due to displacement of the glue used to affix the steel plate to one of the cement surfaces; subsequently we would discover this material did not fully and completely set and thus could be squeezed out of the sample and into pore spaces and the permeameter.

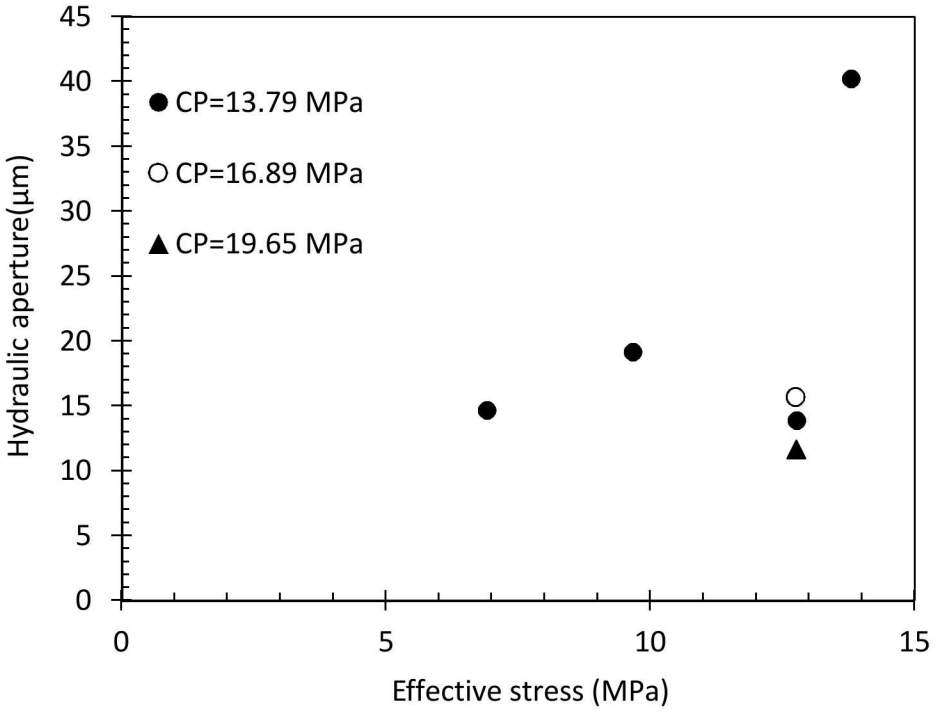

Fig 2.2.30: Results from series of gas flow measurements made on CS02. Results are given as hydraulic aperture vs. effective stress (confining stress – pore pressure).

Silicone oil was next introduced into the sample. After waiting for 3 hours, there was no arrival of silicone oil at the outflow. Because we expected oil to be produced well before this time based on the gas test results and previous measurements, the silicone oil test was discontinued.

SPR-supplied crude oil was next introduced to the sample. The pressure to maintain a modest flow rate (2 ml/min) continually increased with time up to 2.6 MPa (377 psi), and then dropped over the course of a few minutes to 1.1 MPa (159 psi). Subsequently, first silicone oil and then crude oil were produced at the downstream. This response was consistent with the pressure rising to overcome blockage in the sample and/or the permeameter lines.

Crude oil tests were conducted at 6 upstream pressures in order to determine if increasing the pore pressure further props open the fracture (Fig. 2.2.31). Outflow collected during this test confirmed steady flow for each test. The hydraulic aperture increases with increasing pore pressure. The values in the same ranges those found in the initial gas testing.

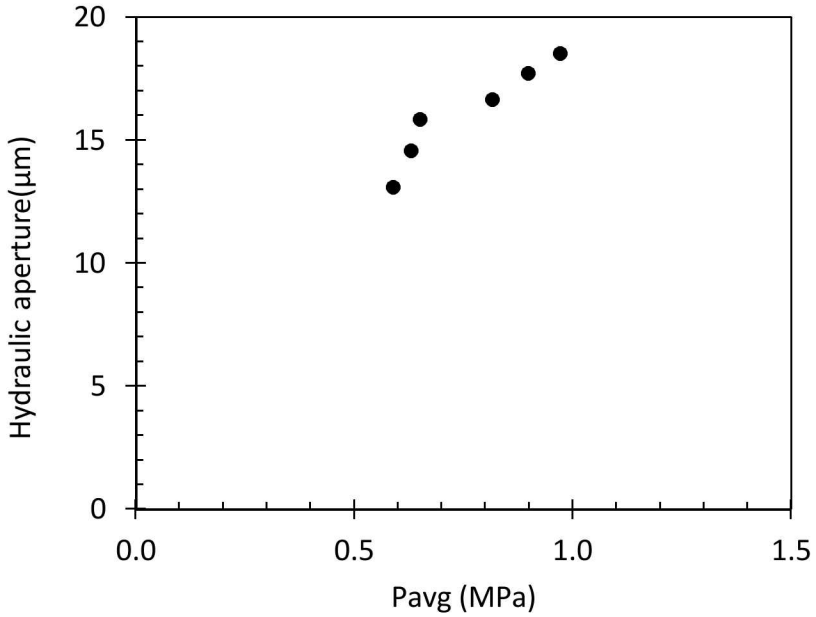

Fig 2.2.31: Results from crude oil measurements made on CS02. Results are given as hydraulic aperture vs. average oil pore pressure during tests.

Following the oil measurements, the gas displacement pressure of 2.8 MPa (406 psi) was measured. This large value could be in response to blockage with the sample or permeameter. Final gas flow measurements are given in Fig. 2.2.32 along with average values from the initial gas and crude oil tests.

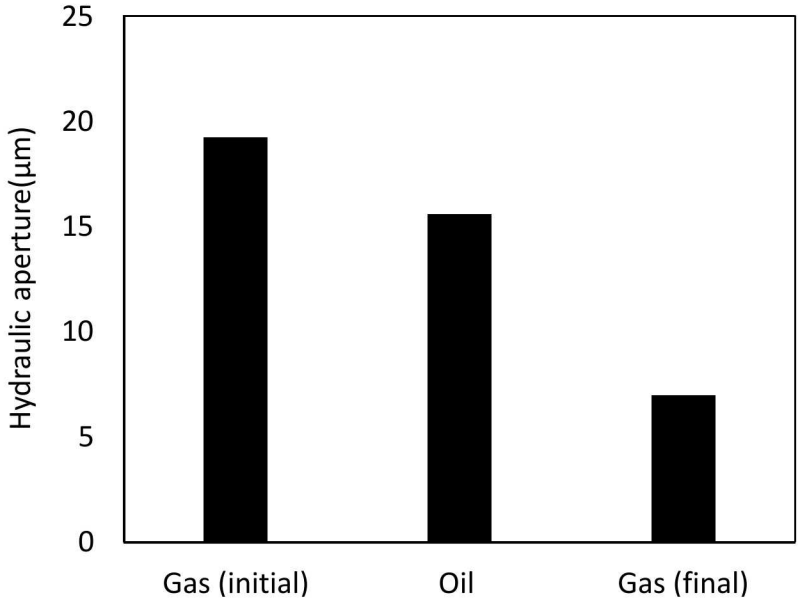

Fig 2.2.32: Comparison of average hydraulic aperture measured with initial gas, crude oil and after gas displacement for CS02.

Fig. 2.2.33 is a photograph of the collection cylinder during the crude oil and subsequent gas displacement and flow tests. The outflow from the specimens enters the cylinder through a tube from the right side in the photograph. Crude oil accumulates in the bottom of the graduated cylinder. Gas in the headspace above the oil leaves the graduated cylinder through a tube and passes through a flow meter before being vented to the atmosphere. The figure provides an indication of how "dirty" the crude oil is. In Fig. 2.2.34, photographs of the top of sample CS02 is shown before and after testing. Staining and accumulation of waxy deposits from the crude oil is visible on the surface of the sample.

Fig 2.2.33: Photograph of outflow collection graduated cylinder for crude oil and subsequent gas displacement tests.

Fig 2.2.34: Pre-test (left) and post-test (right) photographs of the top of sample CS02 showing staining and accumulation of waxy deposits from crude oil.

From inspection of the silicone oil that was displaced and subsequent investigation, we found that the glue backing the cement plate was soluble in silicone oil. Upon disassembly of the permeameter, we found considerable deposits and blockage of lines with what appeared to be the glue. In addition, there were waxy or greasy deposits in the measurement system from testing with the crude oil. The interpretation of the crude oil measurements and subsequent gas measurements

did not account for the likely, but unknown, effects of blockage and should therefore be considered with caution. Future testing will be directed at measuring crude oil flow without blockage. The crude oil contained an appreciable volatile content. This was readily detected by odor, and also by the reduction in volume with time of the crude oil that was collected as effluent.

2.2.2.3. Sample CS04

Sample CS04 was tested with the following sequence: gas, silicone oil, gas, silicone oil, and finally with gas again. The purpose of the test was to determine if gas flow after oil flow had to overcome a displacement pressure and to determine with gas and silicone oil produced the same results.

The first gas test was attempted at 13.8MPa confining stress and indicated that very little flow was moving through the sample. Subsequently, the confining stress was reduced to 3.45 MPa and a gas flow test was conducted. Flow tests were made at progressively reduced confining stresses (Table 2.2.11). These flow tests indicated a hydraulic aperture of about 20 μm. We then completely removed the confining stress, and then reapplied the confining stress to 0.86 MPa. Flow testing under these conditions revealed a hydraulic aperture of about 50 μm, which is more in line with the expectations of a relatively large flow path in this sample. We attribute the very different hydraulic aperture values at the same confining stress to extreme hysteresis in the hydraulic aperture response.

Table 2.2.11 Initial gas flow tests conducted on CS04.

TEST NO.	Confining stress	Back Pressure	Effective stress
1	3.45 MPa (500 psi)	0	3.45 MPa (500 psi)
2	2.59 MPa (375 psi)	0	2.59 MPa (375 psi)
3	1.72 MPa (250 psi)	0	1.72 MPa (250 psi)
4	0.86 MPa (125 psi)	0	0.86 MPa (125 psi)
5 (after releasing confining stress and re-loading)	0.86 MPa (125 psi)	0	0.86 MPa (125 psi)

Results from the gas flow measurements are given as hydraulic aperture in Fig. 2.2.35.

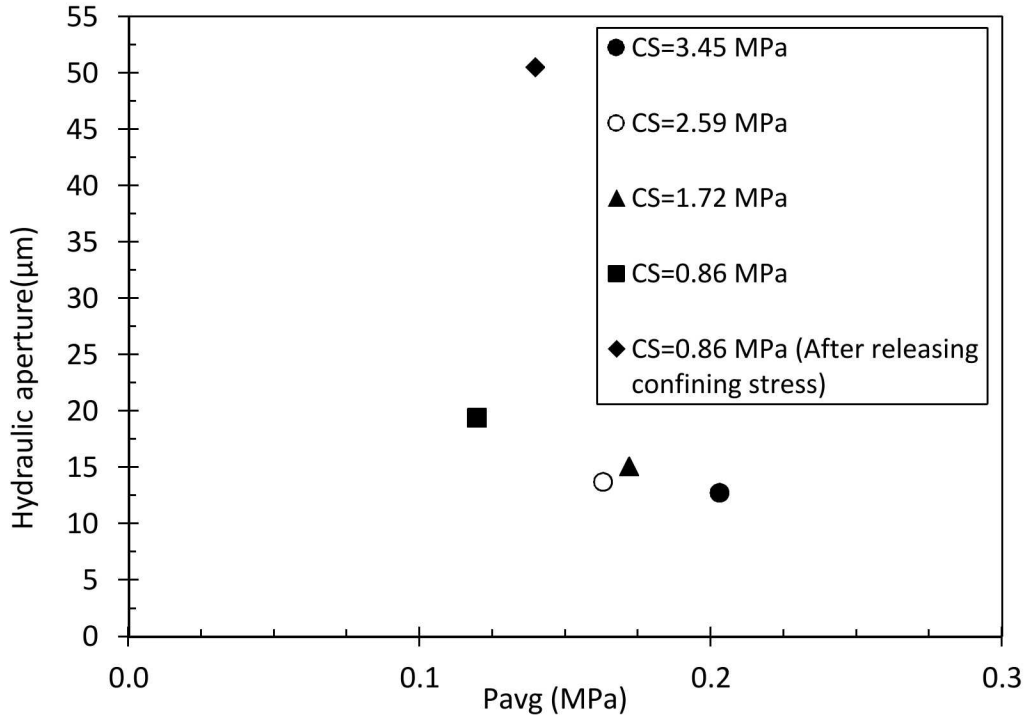

Fig 2.2.35: Hydraulic aperture as a function of average gas pressure for initial series of gas flow measurements on sample CS04.

Silicone oil was next introduced into the sample under a confining stress of 0.86 MPa. Steady flow through the sample was confirmed by confirming that the effluent collection rate was equal to the imposed upstream flow rate. Hydraulic apertures interpreted from the silicone oil testing are in the range of 46.8 to 51.1 μm (Fig. 2.2.36). This is in a good agreement with gas test results after the sample had been unloaded and reloaded.

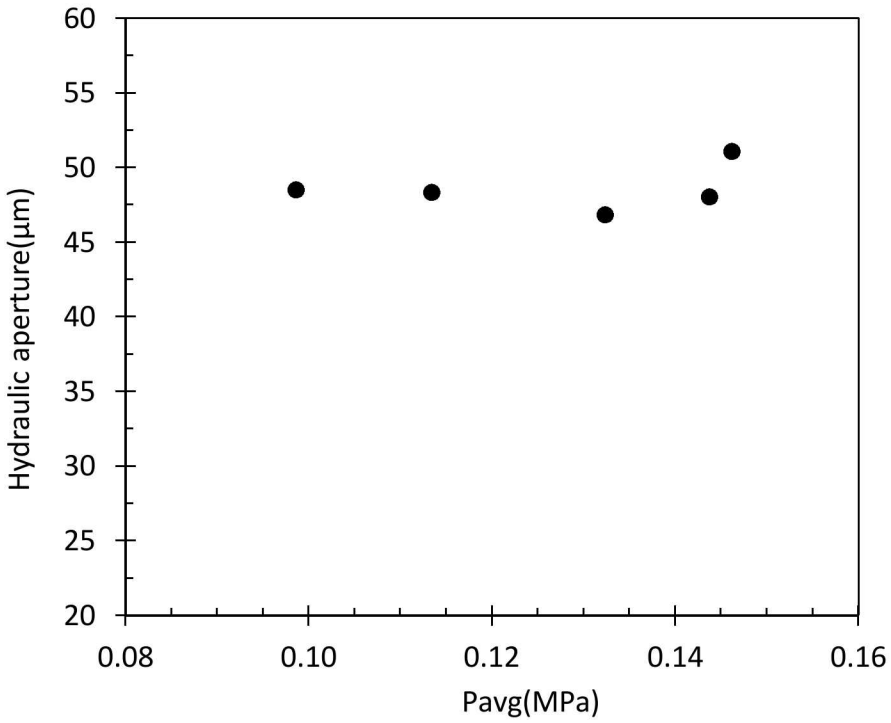

Fig 2.2.36: Results from first silicone oil measurements made on CS04. Results are given as hydraulic aperture vs. average oil pore pressure during tests.

The first gas displacement test displaced gas and oil simultaneously at 10 kPa (1.5 psi), which corresponds to an aperture size of about 4 μm. We note that this value is much lower than the hydraulic aperture for this sample. After the gas displacement pressure was reached, the flow rate was measured and the gas pressure was progressively increased. In response, oil continued to be produced and the gas flow rate was periodically measured. Results from these measurements are shown in Fig. 2.2.37. After 180 kPa (25 psi), no additional oil was produced.

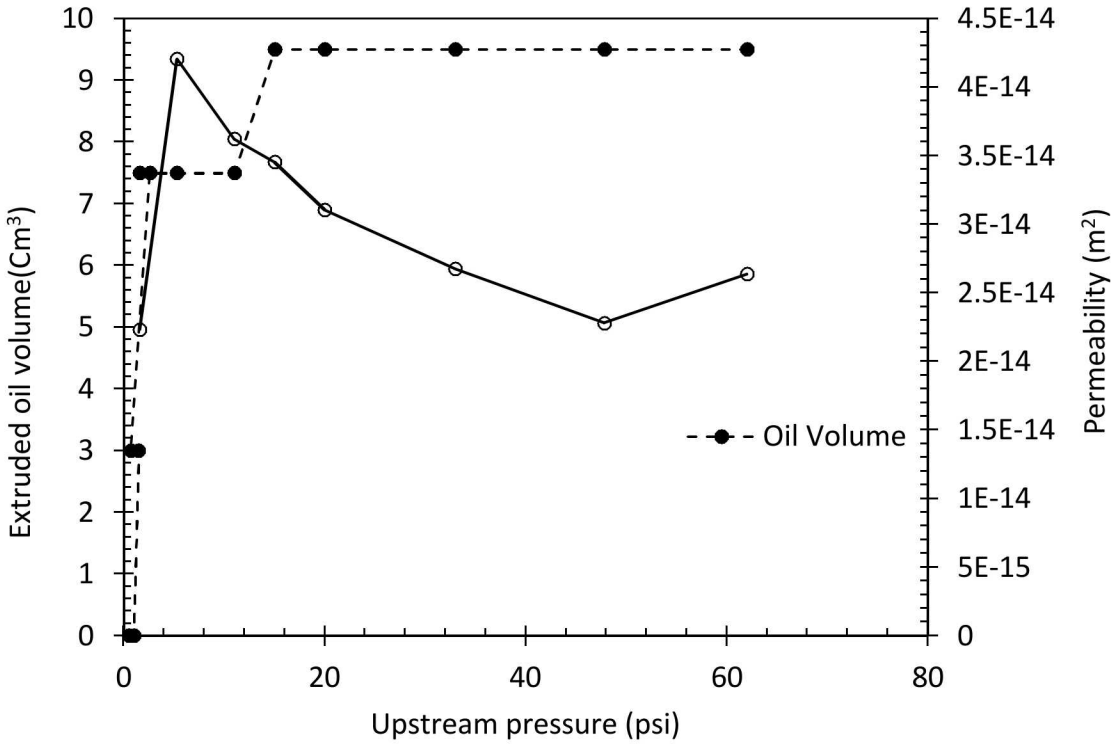

Fig 2.2.37: Gas displacement phase permeabilities and volume of oil collected at downstream at different upstream pressures for gas displacement measurements on sample CS04.

A second series of measurement were then made with silicone oil. Hydraulic apertures from these tests were in the range of 47.8 to 51.5 μm. This is in a good agreement with gas test results as well as the first oil test.

A second gas displacement test was conducted on this sample. Gas and oil were simultaneously produced at about 80 kPa (12 psi), which is greater than the first gas displacement test on this sample.

The average hydraulic aperture from the initial gas flow tests and the subsequent silicone oil and gas tests are given in Fig. 2.2.38. The final hydraulic aperture from the final gas flow tests are less than the previous measurements, possibly due to residual oil in the specimen reducing the gas-accessible pore spaces.

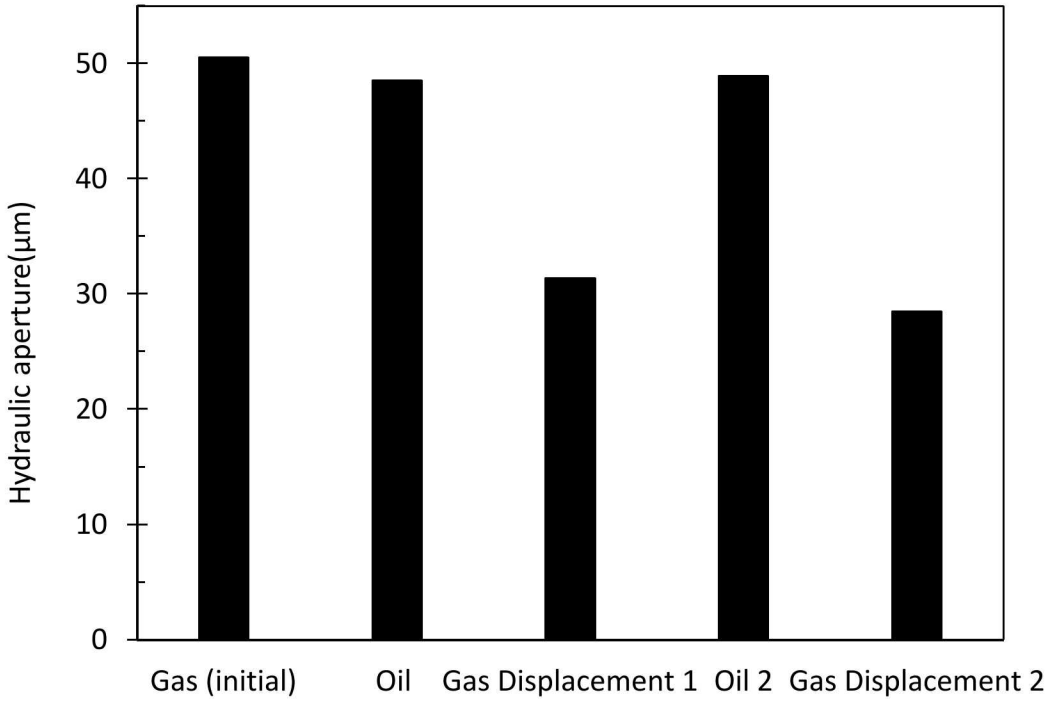

Fig 2.2.38: Comparison of average hydraulic aperture measured with initial gas and subsequent silicone oil and gas displacement tests for CS04.

2.2.2.4. Sample CSC02

The main objective of these set of test is to study the significance of cement- corroded steel interface as potential cemented annulus leakage path. Sample CSC02 was tested first with gas, then silicone oil, and finally with gas again.

The initial gas flow measurements were made at a series of confining stress as indicated in Table 2.2.12.

Table 2.2.12 Conditions for initial gas flow measurements on sample CSC02.

TEST NO.	Confining stress(Gauge)	Back Pressure (Gauge)	Effective stress
1	17.24 MPa (2500 psi)	0	17.24 MPa (2500 psi)
2	13.79 MPa (2000 psi)	0	13.79 MPa (2000 psi)
3	6.90 MPa (1000 psi)	0	6.90 MPa (1000 psi)
4	3.45 MPa (500 psi)	0	3.45 MPa (500 psi)
5	1.72 MPa (250 psi)	0	1.72 MPa (250 psi)

The gas flow measurements were corrected for non-linear flow. In Fig. 2.2.39, the hydraulic aperture as a function of effective stress is given. There is a clear trend of decreasing hydraulic aperture with confining stress. The corresponding decrease in permeability is from $5x10^{-13}$ to $6x10^{-15}$ m^2.

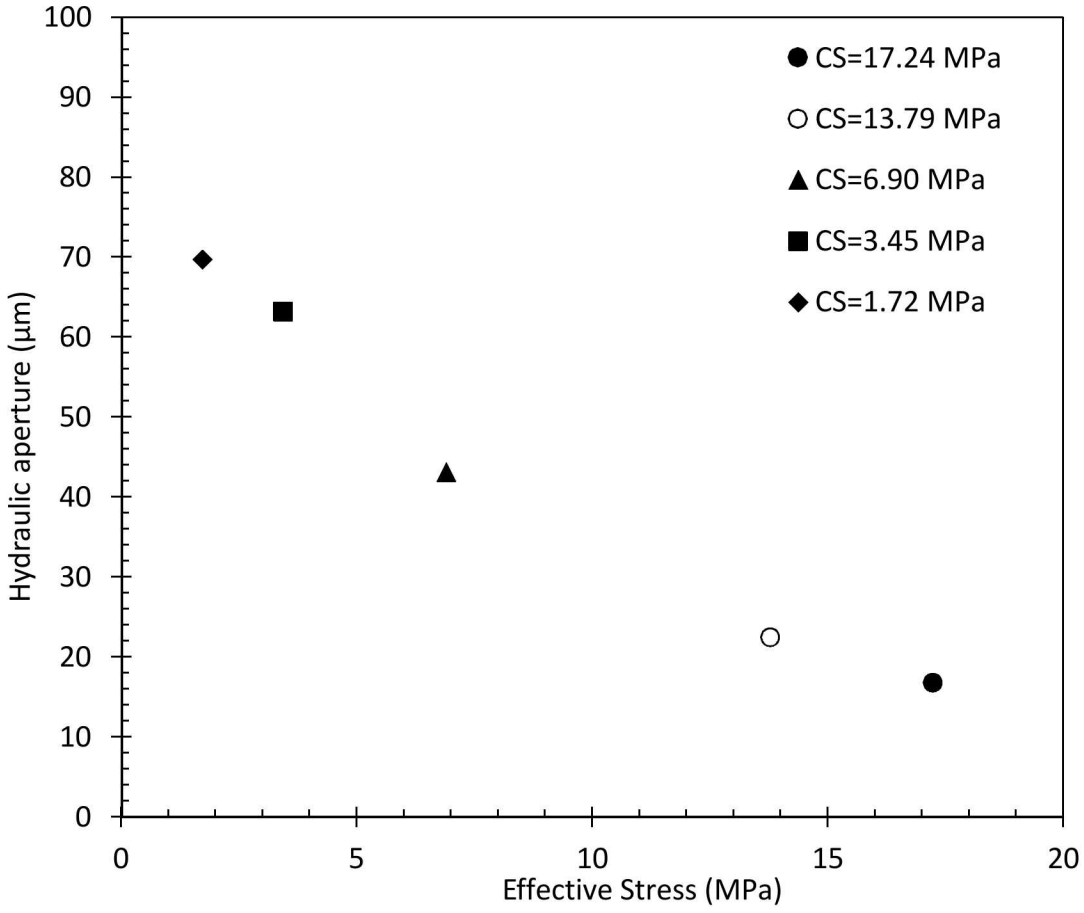

Fig 2.2.39: Hydraulic apertures derived from gas flow measurements on CSC02.

Tests with silicone oil were conducted at a confining stress of 13.8 MPa. Hydraulic apertures interpreted from these tests are shown in Fig. 2.2.40 as a function of the average pore pressure. The hydraulic aperture is smaller than that from the initial gas testing under comparable conditions.

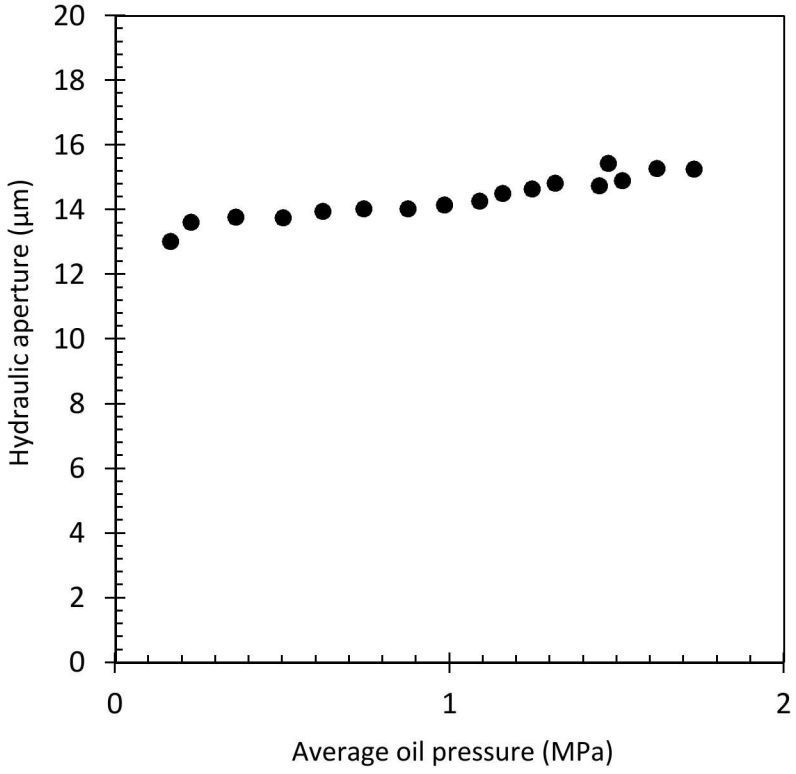

Fig 2.2.40: Hydraulic aperture vs average pore pressure for tests on CSC02 using silicone oil.

Gas flow testing was conducted after testing with silicone oil. The gas displacement pressure was about 10 kPa (1.5 psi). After the gas displacement pressure was reached, the flow rate was measured and the gas pressure was progressively increased. In response, oil continued to be produced and the gas flow rate was periodically measured. Results from these measurements are shown in Fig. 2.2.41. After 75 kPa (10.7 psi), no additional oil was produced. Gas flow measurements continued to 1.0 MPa.

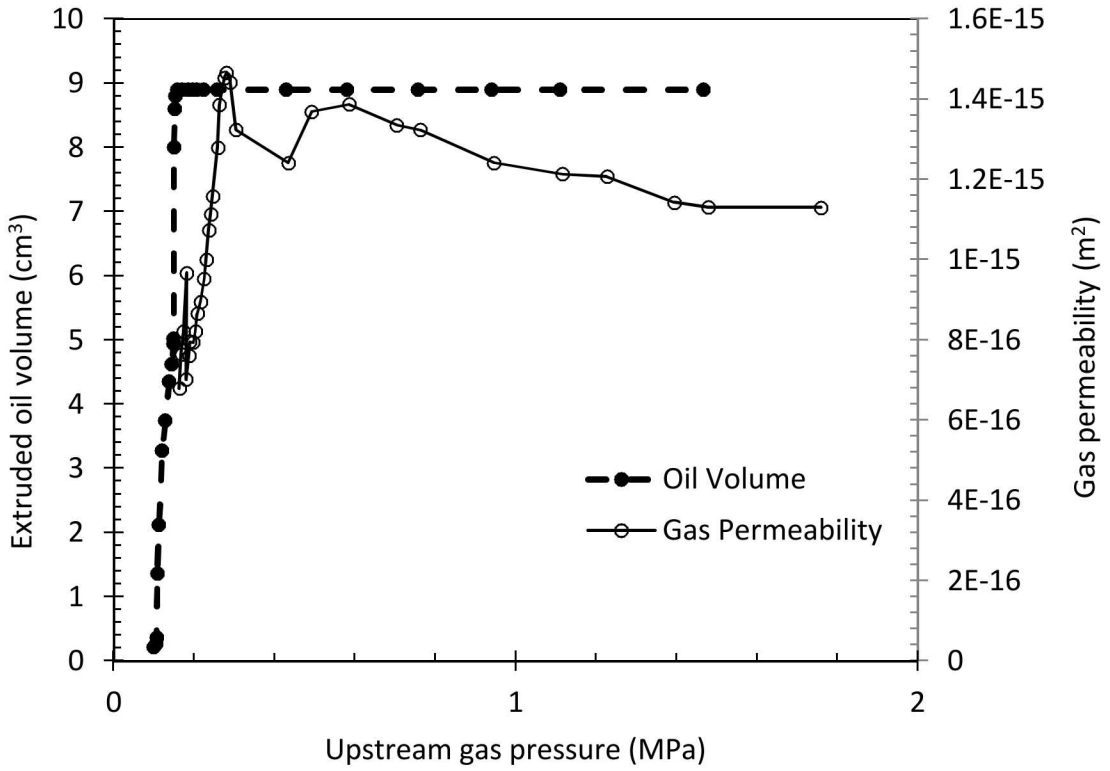

Fig 2.2.41: Silicone oil collected from downstream and gas permeability during gas displacement testing of sample CSC02.

A summary of the initial gas, oil and gas displacement test results in terms of hydraulic aperture is given in Fig. 2.2.42. All data in this figure was obtained at a confining stress of 13.8MPa.

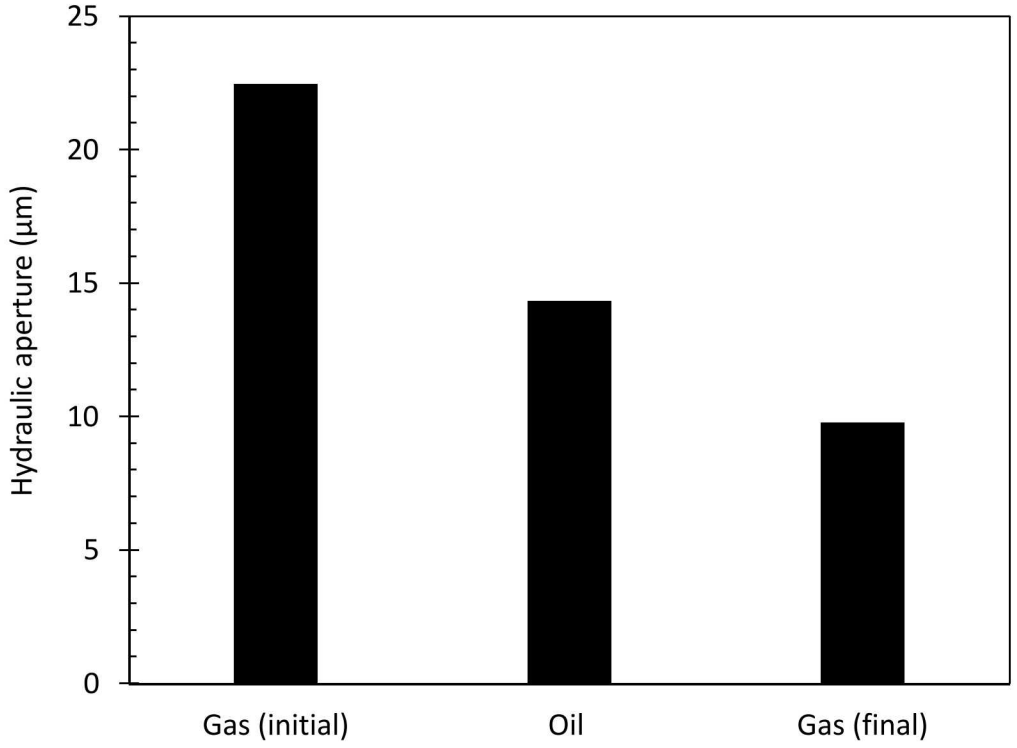

Fig 2.2.42: Comparison of average hydraulic aperture measured with initial gas, subsequent silicone oil and gas displacement tests for CSC02.

2.2.2.5. Sample CSC03

The main objective is to study the significance of corrosion product itself as potential cemented annulus leakage path. Sample CSC03 was tested only Nitrogen with gas. The initial gas flow measurements were made at a series of confining stresss as indicated in Table 2.2.13.

Table 2.2.13 Conditions for initial gas flow measurements on sample CSC03.

TEST NO.	Confining stress	Back Pressure	Effective stress
1	13.79 MPa (2000 psi)	0	13.79 MPa (2000 psi)
2	10.34 MPa (1000 psi)	0	10.34 MPa (1500 psi)
3	6.90 MPa (1000 psi)	0	6.90 MPa (1000 psi)

More than twenty-five individual steady-state gas flow measurements were made for each test. Results from the initial gas flow tests are given in Fig. 2.2.43 as hydraulic aperture as a function of the effective stress during each of the tests. Interpreted as permeability, they are in the 10^{-15} m^2

– 10^{-17} m^2 range, in line with that which was significant for flow through corrosion product alone. There is a clear trend of decreasing hydraulic aperture with confining stress. The corresponding decrease in permeability is from $6x10^{-15}$ to $4x10^{-17}$ m^2.

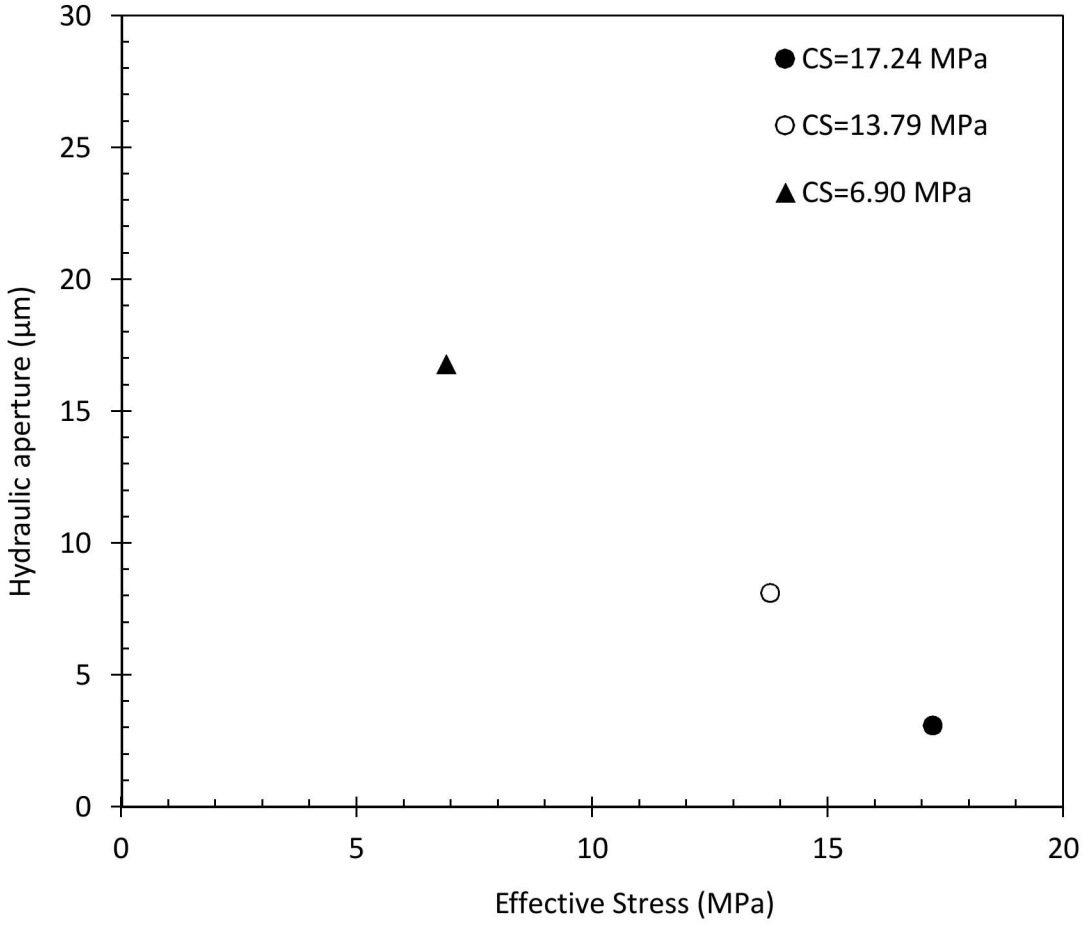

Fig 2.2.43: Results from series of gas flow measurements made on CSC03. Results are given as hydraulic aperture vs. effective stress (confining stress – pore pressure).

2.2.3. Observations of flow paths

2.2.3.1. Sample C05

A merge of 6 microphotographs of sample C05 is given in Fig. 2.2.44. From the merged photographs, the mechanical aperture along the fracture was measured using image analyses techniques and is given in Fig. 2.2.45 The average mechanical aperture of this fracture was 92 µm, and the percent of contact along the fracture was only .02%.

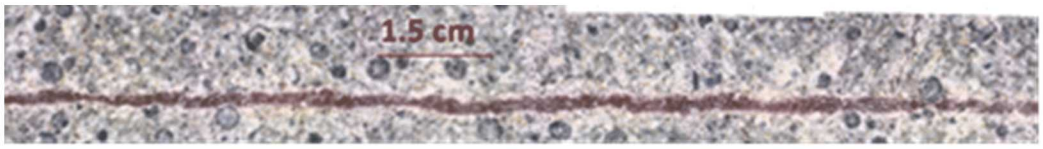

Fig 2.2.44: Example of automated merge done using automated photomerge in Photoshop.

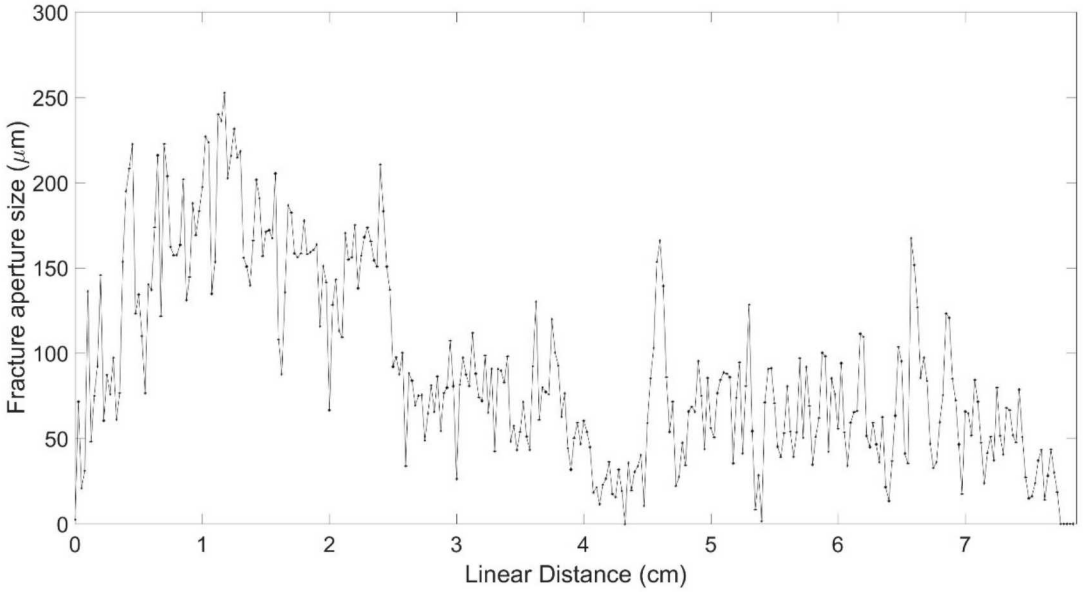

Fig 2.2.45: Fracture aperture distribution along the epoxy impregnated fracture in sample C05.

The gas permeability measurement on this sample conducted under the same stress conditions as the epoxy injection yielded a hydraulic radius of 152 μm. This value is larger than the average mechanical aperture from the single cross-section.

3. ANALYSIS AND INTERPRETATION OF THE RESULTS

The initial gas flow tests yield hydraulic apertures that ranged from about 20 to > 100 μm, which corresponds to effective cemented annulus permeabilities of about 10^{-14} to 10^{-12} m^2, respectively. The size of the flow paths in the samples we tested, as defined by the hydraulic aperture, are consistent with those estimated by others from field measurements of leaky wells (e.g., Checkai et al., 2013). This implies that the results of these measurements are relevant to flawed or damaged cements that may be present in some SPR wells. The intact cement sample had a gas permeability of $1x10^{-17}$ m^2. Thus, the flawed specimens typically had permeabilities that were many orders of magnitude greater than that of the intact cement, and flow was principally through the fractures and interfaces. One sample with a cement fracture had a permeability comparable to intact cement

possessed a very smooth fracture, and under a confining stress of 13.8 MPa apparently mated back together.

Gas flow testing through the flawed specimens indicated that many tests experienced non-linear flow, that is, the flow rate and the gradient were not linearly related as would be expected for purely viscous (Darcy) flow. Non-linear gas flow occurs in the cement specimens because the flaws are very conductive and allow large flow rates; the contribution of non-linear flow increases with the flow rate. Interpreting flow data with Darcy's law when there is an appreciable nonlinear flow component will result in significantly underestimating the permeability. By conducting flow tests under a range of pressures, a correction for non-linear flow can be developed, and the correct permeability and hydraulic aperture can be determined. Thus, for every gas permeability or hydraulic aperture that we report, we conducted at least 6 gas flow measurements.

Below some critical flow rate, non-linear flow was negligible and permeability can be measured with a single test. We conducted measurements to identify the transition between linear and non-linear flow. The preliminary results suggest that the critical flow rate for gas flow is on the order of about 5 SCCS. In addition, an analysis of the Reynolds number under different flow conditions to identify the transition from linear to non-linear was consistent with the results of others. However, a test on a different cement fracture suggested a much lower critical flow rate (about 0.5 SCCS). Thus, determining the transition between linear and non-linear flow will be a subject of continued investigation.

The flow tests using oil often resulted in slightly smaller hydraulic aperture than the initial gas tests. One possible reason for this result is some gas may move through pores in the cement adjacent to the flaws that are too small to permit entry of oil.

Gas flow measurements were conducted on many specimens after the oil flow measurements. The gas pressures required to initiate gas flow through the oil saturated flaws (referred to as the gas displacement pressure) were generally considerably greater than those expected for the probable aperture size, in part due to difficulties in controlling and measuring pressures below about 10 kPa as well as detecting the small volume of oil that would be produced initially. As the pressure was increased above the displacement pressure, more oil was produced from the sample and continuous gas flow through the specimen was detected and measured. The gas permeability progressively increased as more oil was removed with increasing pressure. The final gas permeability, or hydraulic aperture, was less than that from either the initial gas or subsequent oil test. It is believed that residual oil in the flow paths are responsible for the decreased gas permeability.

The single test with crude oil was problematic in that waxy deposits from the oil clogged the tubing system of the permeameter. The crude oil was screened prior to use to remove solids, but the waxy material was either too small to be removed by the screen, or its solubility with pressure resulted in deposits accumulating on the downstream side of the specimen. This result suggests that solids from the crude oil may be deposited with flow paths within cemented annulus systems, and reduce the permeability of the system.

The corroded steel specimens were found to be permeable. This permeability is believed to be attributable to the corrosion product itself, and not a separate discrete flow path along the interface between the cement and corroded steel. The permeability of this sample was more sensitive to confining stress than tests on other steel-cement interface samples.

The general trend was that the larger the hydraulic aperture, the more sensitive it was to changes in the applied confining stresses and fluid (pore) pressures. Increased confining stresses tended to reduce the hydraulic aperture and increased fluid pressures tended to increase the hydraulic aperture. In some samples, there was a significant difference in the change in hydraulic aperture depending on whether the sample was being loaded or unloaded (that is, hysteresis in the hydraulic aperture response to confining stress). In one test on a cement-corroded steel sample, the permeability was reduced 2 orders of magnitude as the confining stress was increased from 1.7 to 17.2 MPa. These results suggest corrosion product is very soft, so that it deforms and becomes less permeable as stress is increased. Taken together, these results suggest that different flow paths through cement systems (fractures, cement-steel interfaces, corroded steel) will respond differently to changing stresses and fluid pressures acting on the cement.

Microphotographs of a section of a cement fracture that had been impregnated with epoxy resin indicate that that the cement fracture as largely continuous across the sample, that is, very little contact between fracture surfaces. The aperture varies along the fracture and is far from a constant value. The average mechanical aperture and the hydraulic aperture interpreted from gas flow measurements are reasonably consistent.

With respect to the objective of identifying whether gas and oil flow deviate from one another, we found systematic differences in gas and oil flow through the flawed cement samples. Hydraulic apertures (or permeabilities) interpreted from tests on the same sample were different depending on whether gas or oil was used as the test fluid. The differences include:

1. Most of the gas flow measurements included a significant component of non-linear flow. In contrast, because the difference in oil properties compared to those of gas, oil flow measurements were completely within the linear range. Thus, the fundamental equations that describe gas and oil flow are different; linear flow is described by Darcy's law and non-linear flow is described by Forchheimer's law. The gas flow measurements were corrected for non-linear flow so that parameters for linear flow (i.e., hydraulic aperture) were obtained from these measurements and could be directly compared to the parameters determined from oil flow measurements.
2. When we compare hydraulic apertures (or permeabilities) interpreted from flow measurements first made with gas and then oil, we found modest differences between the gas and oil values. In six of the seven tests in which oil flow measurement followed gas flow measurements, the hydraulic aperture interpreted from the oil test was slightly lower (typically about 5 microns) less than that interpreted from the initial gas flow measurement. One possible reasons for this result is gas may move through pores in the cement adjacent to the flaws that are too small to permit entry of oil.
3. When gas flow measurements are made <u>after</u> oil flow measurements, there are significant effects.
    a. The gas pressure has to overcome the displacement pressure in order to begin to displace oil in the fracture. This effect was difficult to measure in these experiments, but it is expected that the smaller the size of the flow path filled with oil, the greater the gas pressure will need to be to displace the oil.
    b. On the gas begins to displace oil, both gas and oil flows within the flow path. Under these conditions the resulting flow rate of gas and oil will be different from one another and depend on how much of each fluid type is present.

c. Once the gas pressure reaches a certain value, no more oil is displaced from the flaw and only gas moves through the flaw. The interpreted hydraulic aperture (or permeability) from the measured gas flow under these conditions is significantly less that interpreted from the initial gas and oil flow measurements. This result is consistent with residual oil remaining in the flaw and limiting the open space for gas to move through.

4. With crude oil, it is possible that flow paths within the flaw can become blocked or plugged from solids within the crude oil. These solids may re-mobilize or dissolve in crude oil under increased pressure. Gas flow would likely be reduced compared to oil flow due to this blockage. We suspect but could confirm that this may have occurred in the single test we conducted with crude oil.
5. Gas flow measurements on an intact cement sample included gas slip, often referred to as the Klinkenberg effect. This phenomenon occurs in low permeability media at relatively low gas pressures, and results in a greater effective permeability of a medium to gas compared to a liquid. We did not observe significant gas slip during measurements of gas flow in fractured samples.

4. IMPLICATIONS FOR SPR

4.1. Simulations of gas and oil flow through cemented annulus

The response of the cemented annulus pressure at the surface depends in large part on the nature of the flow paths through the cement and the fluid(s) moving through the cement. Flow through the cemented annulus could be through discrete flow paths such as fractures or microannuli, or through the matrix of the wellbore cement. Although the vertical distance traveled in the cemented annulus is the same in these two cases, flow concentrated through a fracture will travel much faster compared to matrix flow, and a more rapid response at the surface would be expected. Because flow rates and pressure changes are a function of fluid properties, we expect a difference in the response at the surface depending on if nitrogen or crude oil if the flowing fluid. In addition, boundary conditions are important to the response at the surface. In particular, the volume and the compressibility of the fluid in the open volume at the surface (between the top of the cement and vent to atmosphere) will greatly affect observed pressure changes at the surface.

To provide some insight into the response at the wellhead to different conditions and properties, we conducted some simple calculations that used observations and knowledge derived from the experimental results described previously. In these simulations, we use hydraulic apertures (or permeabilities) for fractures that are consistent with the values we measured. These calculations simulate one-dimensional flow of either nitrogen or crude oil from depth to the surface. These calculations are not intended to match a particular SCP response as they include numerous simplifying assumptions, including single-phase flow, constant crude oil compressibility, no gas solubility in crude oil, and constant permeability or hydraulic aperture of the flow path. Nonetheless, these calculations can provide some useful trends of approximate responses that may be expected.

The simulations were conducted using MatLab script employing an explicit solution to finite difference equations for one-dimensional, single-phase gas and oil flow. A schematic illustration of the modeled problem is shown in Fig 4.1.1. The simulations assume a wellbore geometry of 0.32 m diameter casing cemented in a 0.5 m diameter wellbore. The wellbore was assumed to be extend a vertical length of 644 m between the casing shoe and the surface. When fracture flow was assumed, an effective permeability is calculated from the hydraulic aperture using the cubic law and assuming the fracture is at the contact between the casing and the cement, i.e., a microannulus. The upper boundary condition was a fixed volume at the surface, allowing pressure build-up. This volume was arbitrarily fixed at 0.1 m^3. When gas flow was simulated, the entire system was assumed to be gas saturated, including the fixed volume at the surface. The density of the gas was not considered in these simulations, and the initial condition was atmospheric gas pressure throughout. The constant pressure lower boundary condition was fixed at 15 MPa for the gas simulations. In the case of oil flow, the entire system was initially oil saturated; the exception is that some calculations included some amount of gas in the surface volume. The density of the oil was considered in the simulations, and the initial condition was equilibrium with the surface at atmospheric pressure. The bottom boundary condition was a total hydraulic potential of 15 MPa.

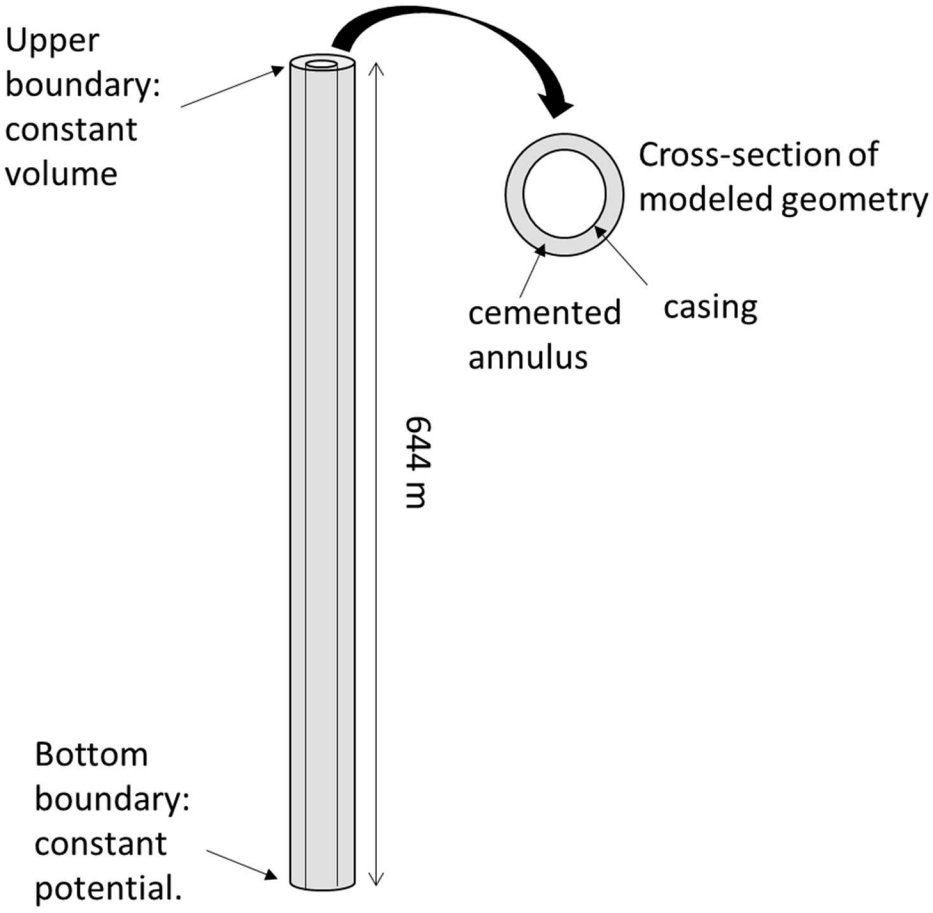

Fig 4.1.1: Schematic of simulation problem geometry for gas and oil flow from depth to surface. Flow is through cemented annulus, either through the cement matrix or a fracture. The schematic is not to scale.

4.1.1. Comparison of fracture and matrix flow

Fractures, including microannuli and corroded casing, provide a direct path through the cemented annulus. In the case of fractured cement, we expect that the cemented annulus pressure at the surface would respond much faster to a pressure at depth than if flow is through the matrix of the cement. We conducted simulations to investigate the expected difference in the cemented annulus pressure response for fracture flow and matrix flow. The results of the simulations highlight the dramatic impact a single fracture, with a size on the order of those measured in the experiments described herein, can have on the cemented annulus pressure build-up.

For simulations of fracture flow, the hydraulic aperture of the fracture was assumed to be 50 μm, which corresponds to an effective permeability of the cemented annulus of about $1x10^{-13}$ m^2. The calculated porosity of the fracture was about 0.05%. These values are consistent with the values we interpreted from measurements on various cement flaws. For matrix flow, we assumed a permeability $1x10^{-13}$ m^2, which is the same as that of the fracture. However, the porosity of the cement matrix was taken as 30%. The assumed permeability of the cement matrix is much greater

than that we measured, but we assumed it was equivalent to that of fracture so that the only difference in the two simulations is the effect of porosity and storage of gas and oil during flow.

In Fig 4.1.2 and Fig 4.1.3, fracture and matrix flow are compared for gas and oil flow, respectively. The gas moving through the fracture first arrives within 15 minutes at the surface in contrast to an arrival time of about 6 days for flow through the matrix. The difference for the arrival time and the subsequent cemented annulus pressure build-up between fracture and matrix flow is a consequence of the amount of storage along the flow path due to the differences in porosities for these two cases. Fractures have a relatively very small amount of fluid storage compared to the matrix and is therefore able to transmit fluid much faster compared to matrix flow even though the effective permeability of the two systems is equivalent. Similarly, oil moving through the fracture arrives within 10 minutes at the surface in contrast to an arrival time of about 2 days for flow through the matrix.

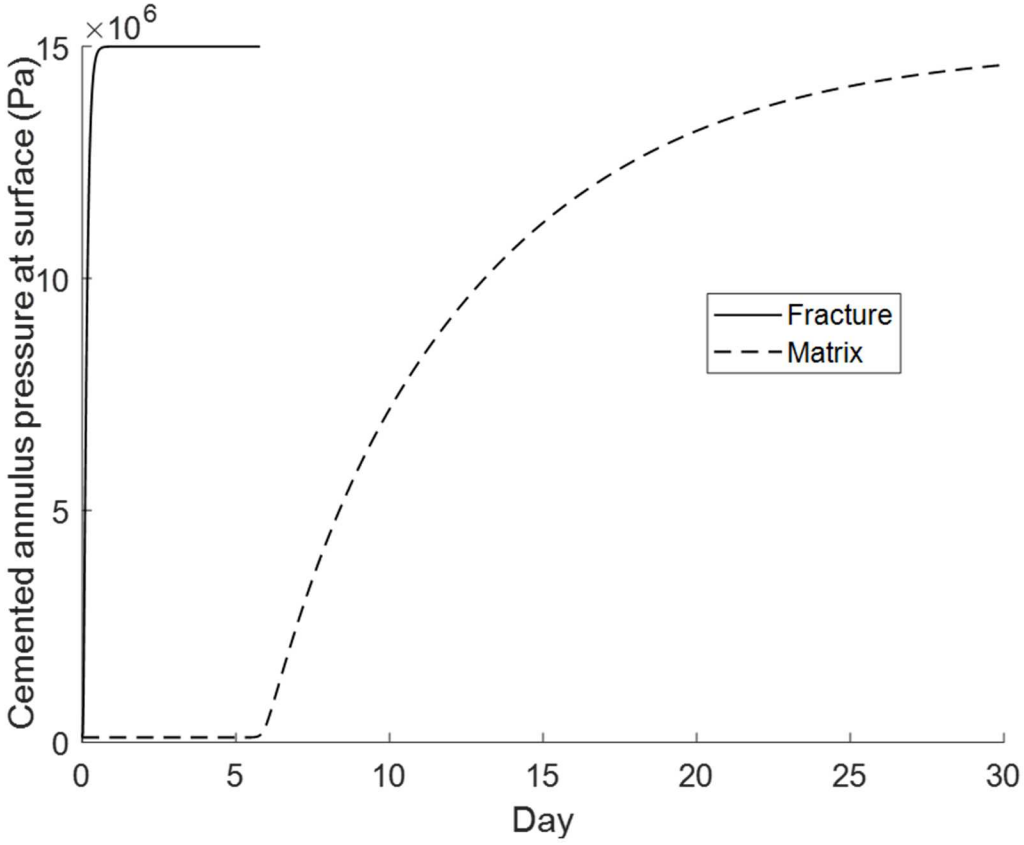

Fig 4.1.2: Wellhead pressure for gas flow through cement. The fracture had a hydraulic aperture of 50 μm and the matrix had a permeability of 1x10-13 m2; the matrix had an assumed permeability of 1x10-13 m2.

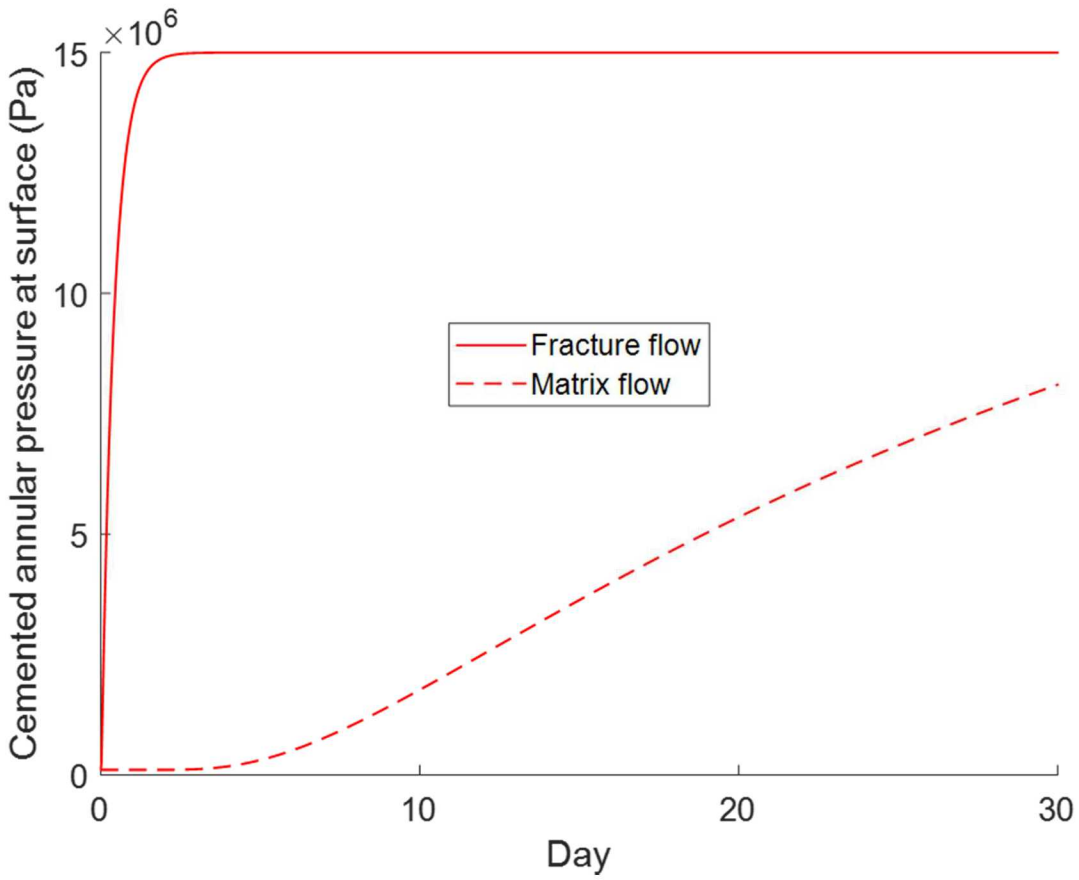

Fig 4.1.3: Wellhead pressure for oil flow through cement. The fracture had a hydraulic aperture of 50 μm and the matrix had a permeability of $1x10^{-13}$ m^2; the matrix had an assumed permeability of $1x10^{-13}$ m^2.

In Table 4.1.1, the amount of gas that flows into the surface volume to reach equilibrium is given for both fracture and matrix flow, along with the amount of gas required to flow from the constant pressure source.

The volume required for achieving equilibrium is equal in the two cases (fracture and matrix flow) as the surface volume is fixed. In contrast, the amount of gas that flows from the constant pressure source is dramatically different for fracture and matrix flow due to the amount of porosity along the flow path. Similar results were obtained for oil flow through a fracture and a matrix and are given in the table.

Table 4.1.1: Volumetric flows to reach equilibrium in fractured and matrix systems with equivalent permeabilities.

	Nitrogen flow (standard m^3)		Oil flow (m^3)	
	Into surface volume to reach equilibrium	From constant pressure source at depth	Into surface volume to reach equilibrium	From constant pressure source at depth
Fracture	15	22	.0013	.0017
Matrix	15	3077	.0013	.257

4.1.2. Comparison of nitrogen and crude oil flow through fractures

Flow rates and pressure changes depend not only on the properties of the medium (e.g., hydraulic aperture of fractured cement) but also on the properties of the fluids themselves. We conducted a series of simulations to investigate the role that the cement fracture size and fluid properties have on cemented annulus pressure build-up and flow rates. The assumed fracture size used in the simulations are consistent with those measured in the experiments described in this report.

In Fig 4.1.4, results for gas and oil flow through a 50 μm fracture are given. Although both gas and oil initially arrive at the surface within 15 minutes, a different pressure response with time is observed depending on the fluid type: the gas pressure build-up is faster than that of the oil. These results illustrate that the fluid type moving through a fracture significantly affects the measured rate (slope) of with time.

In Fig 4.1.5, results for gas and oil flow through a 10 μm fracture are given. It is noted that the 10 μm fracture corresponds to a much lower effective permeability of the cemented annulus ($8x10^{-16}$ m^2) compared to the 50 μm fracture ($1x10^{-13}$ m^2). Again, the gas pressure build-up rate is faster than that of the oil pressure build-up. When compared to the results given in Fig 4.1.4, it is seen that the response takes approximately 100 times longer with the smaller fracture. This result demonstrates that the cemented annulus pressure response to fracture flow is highly dependent on the size of the fracture as well as the fluid type.

The flow rates of gas and oil into the cemented annulus can be estimated from these simulations. We found the flow rates for the gas and oil in these fractured systems to be very different. We note that flow rates are not constant; as pressure builds up at the surface, the flow rate into the volume at the surface will decrease. In Table 4.1.2, the maximum nitrogen flow rate and the time it occurs is given for flow through the 10 μm and 50 μm fractures. Note that the flow rates for gas are given at standard conditions. The smaller fracture has significantly lower maximum flow rate and it occurs at a later time. Similar results are provided for oil flow in the table. The maximum oil flow rates are orders of magnitude less than those of the gas flow rates. These results highlight the large differences in flow rates through the fractures depending on whether gas or oil is flowing.

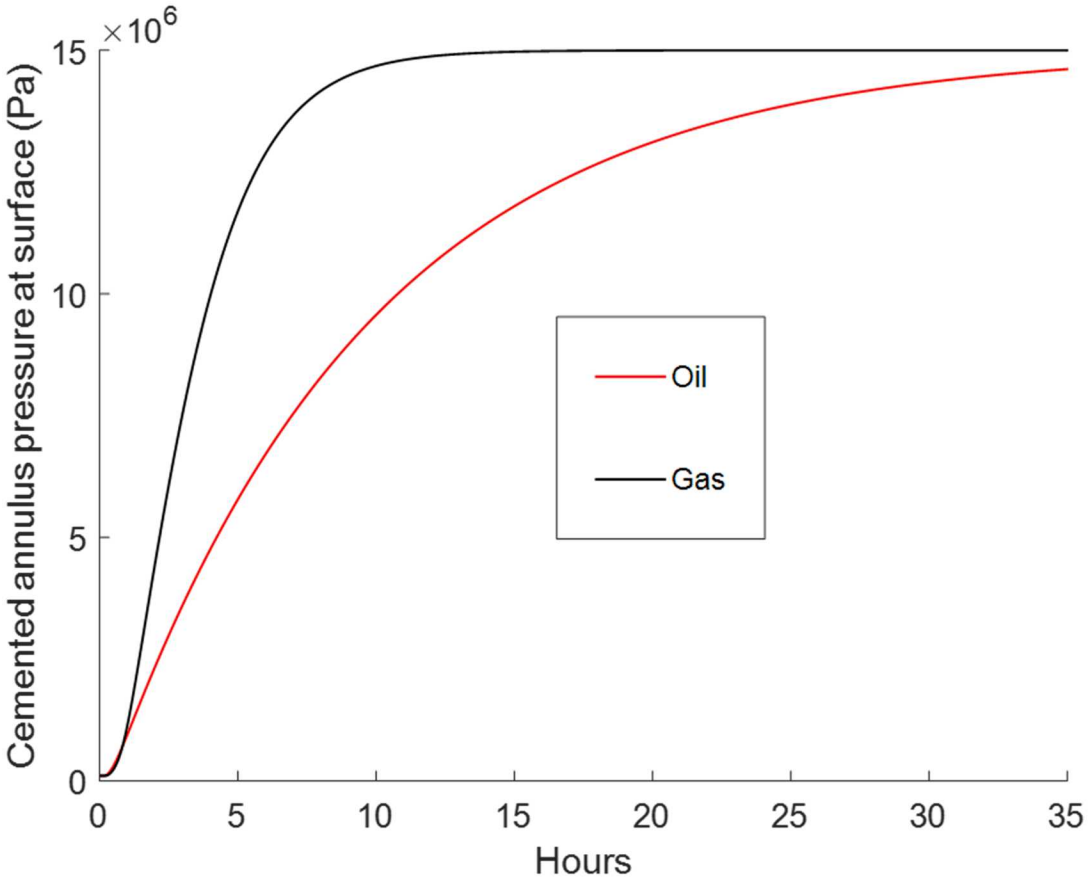

Fig 4.1.4: Comparison of cemented annulus pressure build-up for oil and gas flow through 50 μm fracture.

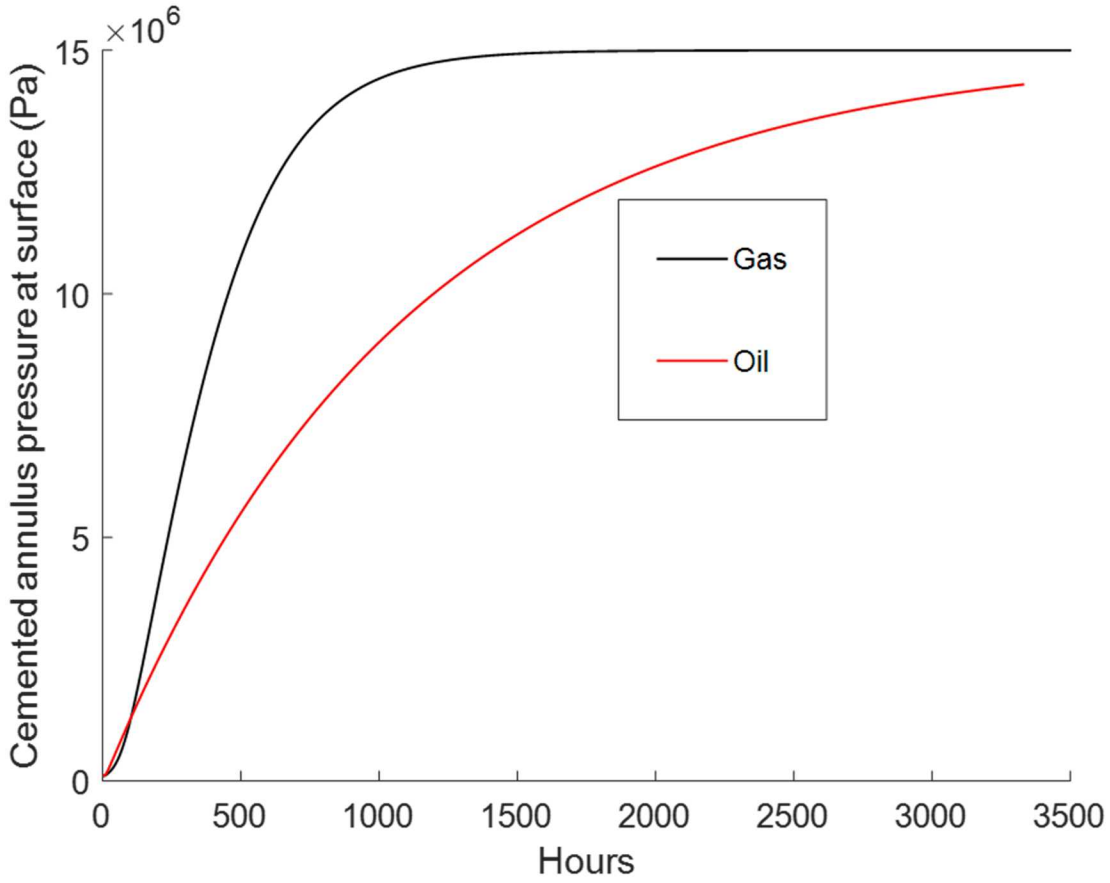

Fig 4.1.5: Comparison of cemented annulus pressure build-up for oil and gas flow through 10 µm fracture.

Table 4.1.2: Maximum nitrogen and oil flow rates during flow through 10 µm and 50 µm fractures.

Fracture size (µm)	Maximum nitrogen flow rate into volume above cemented annulus at surface		Maximum oil flow rate into volume above cemented annulus at surface	
	Flow rate (standard m^3/s)	Time maximum flow rate occurred (days)	Flow rate (m^3/s)	Time maximum flow rate occurred (days)
10	8e-6	8	4e-10	1.5
50	9e-2	0.1	4e-8	.05

4.1.3. Impact of residual oil in fracture on subsequent gas flow

The experimental results revealed that gas flow through a fractured specimen was reduced from its initial value after oil was introduced to the specimen. It is believed that this result is a consequence of residual oil left in the fracture and subsequent gas flowing only through the

remaining gas-filled portion of the fracture. Essentially, the hydraulic aperture of the fracture to gas is reduced depending on whether oil was previously present in the fracture. We conducted simulations to investigate the impact of residual oil on the gas pressure build-up.

In Fig 4.1.6, simulations of pressure build-up to gas flow were conducted with two different hydraulic apertures of the fracture: 50 and 30 μm. These two values are similar to the hydraulic apertures measured before and after oil was introduced to the fracture (see results for specimen CS04). These results illustrate the potential for residual oil along flow paths within the cemented annulus system to have a large impact on the cemented annulus pressure build-up in response to gas flow.

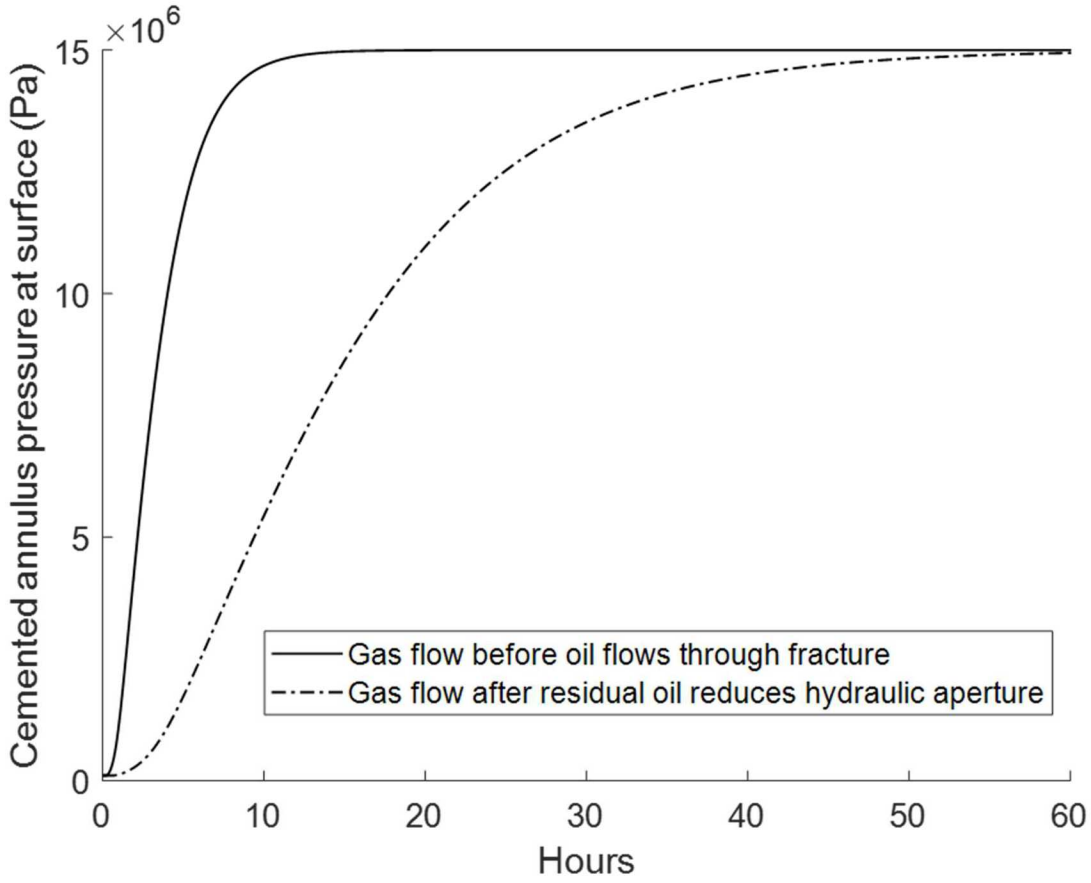

Fig 4.1.6: Comparison of cemented annulus pressure build-up for gas flow through 50 μm and 30 μm fracture representing condition before and after oil introduced into fracture, respectively.

4.1.4. Effect of fluid composition in surface volume

The cemented annulus pressure build-up in response to oil flow is sensitive to the amount and compressibility of the fluid assumed to occupy the open volume above the cemented annulus at the surface (herein referred to as the surface volume). Because of the differences in compressibility between oil and gas, even small amounts of gas in the surface volume may affect the pressure build-up response. The source of the gas could include gas ex-solved from crude oil or remnant gas not flushed from the surface volume. To investigate this effect, simulations were conducted with different amounts of gas initially in the surface volume.

Results are given in Fig 4.1.7 for 1% and 10% of the initial surface volume being occupied by gas along with results for a simulation with the entire volume filled with oil. As shown in the Figure, the rate of pressure build-up slows significantly when there is as little as 1% gas in the surface volume even though only oil is flowing in this simulation. These results illustrate the importance of the composition of the fluid during build-up tests and suggest that also capturing flow rate data would be helpful in understanding the flow system.

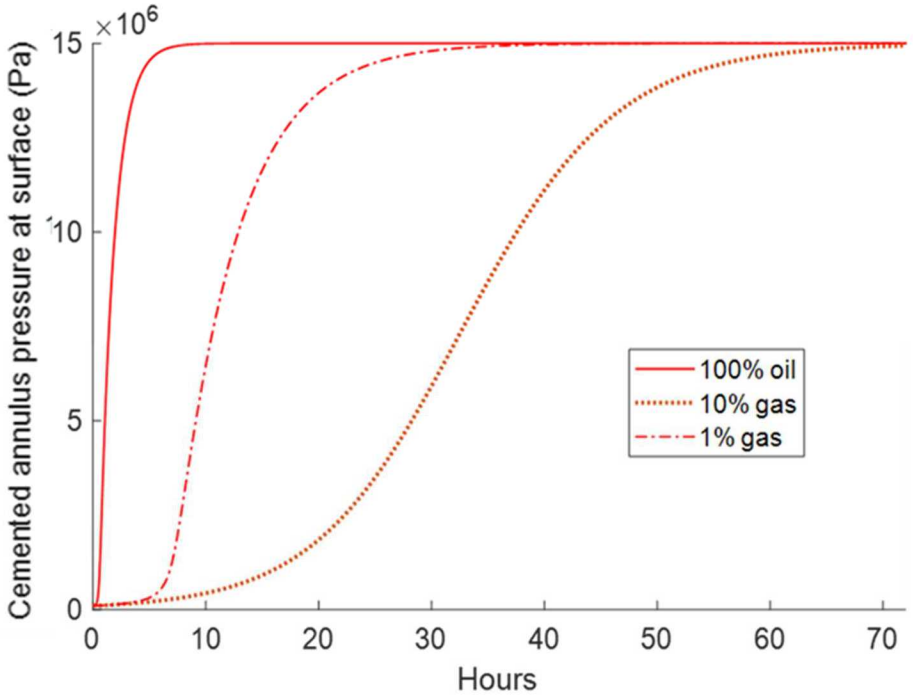

Fig 4.1.7: Comparison of cemented annulus pressure build-up for oil flow through 50 µm fracture into an oil-filled surface volume and surface volumes that initially contained 1 and 10% gas by volume.

4.1.5. The potential for non-linear flow

The simulations assume only linear or viscous flow that follows Darcy's law. For gas flow through cement flaws, we often observed non-linear flow. An important question is whether non-liner gas flow would be expected for the conditions of these simulations. We use the calculated flow rates to determine under which conditions non-linear flow might be expected. Based on measurements presented in this report, a volumetric flow rate of 5×10^{-4} standard m^3/s was used as a first-order estimate of the criterion for the transition to non-linear flow.

In Fig 4.1.8, flow rates from the constant pressure boundary at depth and into the surface volume are shown for flow through a 50 µm fracture. Also shown on the figure is the flow rate criterion for non-linear flow. Between these two boundaries, that is, along the fracture, flow rates will be between these two curves. The results from simulations suggest that much of the gas flow

occurred under conditions that will result in appreciable non-linear flow. Future simulations of gas flow through the cemented annulus should include non-linear flow. An impact of non-linear flow is that if pressure build-up or flow data at the surface are being used to estimate properties of the cemented annulus, the effective permeability will be substantially off (possibly by 100% or more) if non-linear flow is not accounted for. The flow of oil is below the non-linear flow criterion for these simulations.

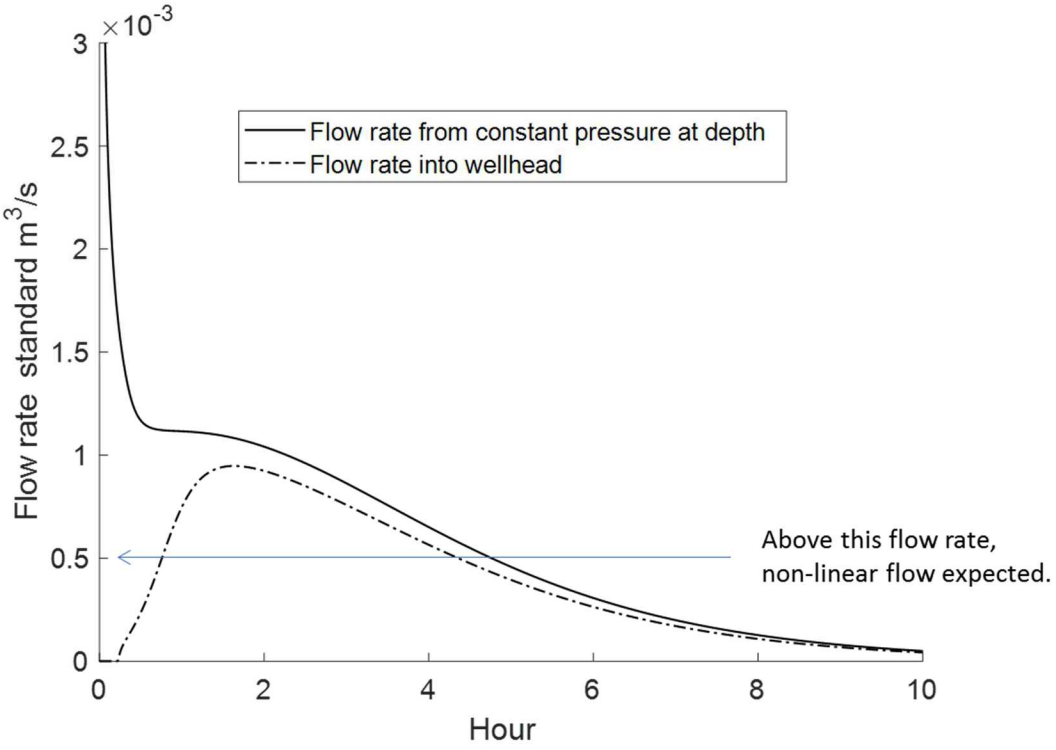

Fig 4.1.8: Flow rates at constant pressure source and at surface volume for gas flow through 50 μm fracture. The criterion for transition to non-linear flow is also shown. Results indicate that flow rates often exceed the criterion for non-linear flow.

5. CONCLUSIONS AND FUTURE PLANS

We have conducted gas and oil flow tests on cement specimens with flaws including cement fractures and interfaces along the cement-steel contact. Many specimens were tested initially with gas, followed by oil, and finally with gas again. Nitrogen was used as the gas, and silicone oil with properties similar to typical crude oil was used in most tests. One set of measurements were made with crude oil. Steel-cement specimens with corroded steel also tested. We also injected one fractured cement sample with epoxy to preserve the pore structure, sliced the sample and used image analysis techniques to measure the mechanical (actual) aperture along the fracture. An intact cement sample was also tested to provide a baseline response. For both gas and oil tests, we used the measured flow test data to interpret permeability and, assuming the cubic law for flow between parallel plates, the corresponding hydraulic aperture of the flaw. Larger hydraulic apertures correlate with higher flow rates and increased permeability.

The initial gas flow tests yield hydraulic apertures that ranged from about 20 to > 100 μm, which corresponds to permeabilities of about 10^{-14} to 10^{-12} m^2, respectively. The intact cement sample had a gas permeability of $1x10^{-17}$ m^2. Thus, the flawed specimens typically had permeabilities that were many orders of magnitude greater than that of the intact cement, and flow in the experiments was principally through the fractures and interfaces. The measured hydraulic apertures of flawed samples are consistent with a common range of values (5-100 μm) interpreted from field measurements for cement in leaky wells (Checkai et al.; 2013). Because the flows were large enough to permit rapid flow during measurements with gas, non-linear flow developed and had to be corrected for in order to obtain hydraulic apertures and permeabilities. Flow tests using silicone oil were consistent with the initial gas flow tests, but often resulted in slightly smaller hydraulic aperture than the initial gas tests. The single test with crude oil resulted in plugging of the experimental system with small solids from within the crude oil.

Gas flow was significantly reduced when gas flow measurements were made after oil flow measurements. Initially, the gas had to overcome a "displacement pressure" in order to begin to displace oil in the fracture. This effect was difficult to measure in these experiments, but it is expected that the smaller the size of the flow path filled with oil, the greater the gas pressure will be required to displace the oil. Once the gas began to displace oil, both gas and oil flows within the flow path. Under these conditions of two-phase flow, the resulting flow rate of gas and oil will be different from one another and depend on how much of each fluid type is present. After the gas pressure reached a certain value, no additional oil was displaced from the flaw and only gas moved through the flaw. The interpreted hydraulic aperture (or permeability) from the measured gas flow under these conditions was significantly less that interpreted from the initial gas and oil flow measurements. This result is consistent with residual oil remaining in the flaw and limiting the open space for gas to move through.

The measurements on cement-steel interfaces (often called microannuli) produced similar results and trends to those for fractured cement. Furthermore, we determined that corroded steel itself is permeable, and implies that corroded steel casing can be a continuous flow path in a cemented annulus system.

The larger the hydraulic aperture, the more sensitive it was to changes in the applied confining stresses and fluid (pore) pressures. Increased confining stresses tended to reduce the hydraulic aperture and increased fluid pressures tended to increase the hydraulic aperture. The cement-corroded steel samples were especially sensitive to changes in confining stress, consistent with the corrosion product being very compressible.

To provide insight into the response of the cemented annulus pressure to different conditions and properties, we conducted some simple calculations that used observations and knowledge derived from the experimental results described previously. In these simulations, we use hydraulic apertures (or permeabilities) for fractures that are consistent with the values we measured. These calculations simulate one-dimensional flow of either nitrogen or crude oil from depth to the surface through the cemented annulus. These calculations are not intended to match a particular well response as they include numerous simplifying assumptions, including single-phase flow, constant crude oil compressibility, no gas solubility in crude oil, and constant permeability or hydraulic aperture of the flow path. Nonetheless, these calculations can provide some useful trends of approximate responses that may be expected. The simulation results highlight that a single fracture, with a size on the order of those measured in the experiments described in this report, can have a dramatic impact on the cemented annulus pressure build-up. Further, the rate of pressure build-up will be different for gas and oil. Even a small amount of gas in the cemented annulus system will affect the pressure build-up response.

Areas of future investigation include:

- Linear to non-linear flow transition. We have measured the transition from linear to non-linear gas flow in two samples. Additional measurements are necessary to determine how to best describe the transition condition (possibilities include the flow rate, Reynolds number, Forchheimer number) so that these results can be used to estimate when non-linear flow will occur under field conditions.
- Flow through corrosion product. We have identified that corroded casing is permeable and can serve as a flow path along the outside of the casing. Additional tests will quantify the relationship between the permeability of the corroded casing and the degree of corrosion. Because casing can corrode under field conditions, quantifying the magnitude of the potential leakage along corroded casing is important.
- Flow response to changes in pore pressure. The trend we observed from limited measurements was that the larger hydraulic aperture was, the more sensitive to changes in fluid pressure it was. Additional measurements are needed to define this relationship over the range of fluid pressures expected in the field.
- Two-phase flow. Measurements of gas flow following oil flow indicate that after gas has displaced the oil, residual oil may remain in the flow paths and limit gas flow. Additional measurements will be focused on quantifying two-phase flow properties when both gas and oil are present. These parameters are required for understanding and modeling flow when both fluids are present as is likely the case for SPR facilities.
- Flow path plugging from solids in crude oil. It is likely that some reduction in flow along the fracture due to plugging of flow paths from solids in crude oil will occur. We observed plugging in our experimental system (fluid pressure lines) when testing with crude oil, but were not able to observe plugging along the flow path. Additional testing will be directed

at direct observation and quantification of plugging of flow paths from solid in crude oil. If significant plugging occurs, this would be another source of a large difference between gas and oil flow in flawed cements.

[Blank page following section.]

[Blank page following section.]

REFERENCES

1. ASTM C305-14, 2014, Standard Practice for Mechanical Mixing of Hydraulic Cement Paste and Mortars of Plastic Consistency.
2. Bettin, G. and D. L. Lord (2015) "Cemented Annuli Sustained Pressure Analysis for Big Hill and Bryan Mound Wells." Milestone FY15-1.4(g1), Geotechnology & Engineering Department. Sandia National Laboratories, Albuquerque, NM 87185-0750. U.S. Strategic Petroleum Reserve. 11-August-2015
3. Bettin, G. and D. B. Hart (2016). "Cemented Annuli Sustained Pressure Analysis for Bayou Choctaw and West Hackberry Wells." Milestone FY16-1.4(f1), Geotechnology & Engineering Department. Sandia National Laboratories, Albuquerque, NM 87185-0750. U.S. Strategic Petroleum Reserve. 18-May-2016
4. Bourgoyne, A.T Jr., Scott, S.L. and Manowski, W. (2000). “A Review of Sustained Casing Pressure Occurring on the OCS”, final report submitted to US Department of Interior Minerals Management Service, Washington, D.C.
5. Chekai, D., S. Bryant, and Q.Tao (2013). Towards a Frequency Distribution of Effective Permeabilities of Leaky Wellbores, Energy Procedia 37, pp. 5653-5660.
6. Farahani, M., Saki, M., Ghafouri, A., Khaz'ali, A.R., 2017, “Laboratory measurements of slippage and inertial factors in carbonate porous media: A case study”, Journal of Petroleum Science and Engineering
7. Forchheimer, P., 1901, Wasserbewegung durch Boden, Zeitz ver Deutch Ing., 45, 1782-1788.
8. Fox, R.W., McDonald, A.T., Pritchard, P.J., 2004. Introduction to Fluid Mechanics. Wiley, New
9. Rushing, J. A., et al., 2004, "Klinkenerg-corrected permeability measurements in tight gas sands: steady-state versus unsteady-state techniques." SPE annual technical conference and exhibition. Society of Petroleum Engineers.
10. Tiss, M. and Evans, R.D., 1989, Measurement and Analysis of non- Darcy flow coefficient in consolidated porous media. Journal of Petroleum Science and Engineering, 3, 19-33
11. Wang M, Chen YF, Ma GW, Zhou JQ , 2016, Influence of surface roughness on nonlinear flow behaviors in 3D self-affine rough fractures Lattice Boltzmann simulations. Adv. Water Resour. 96:373–388
12. Witherspoon, P.A., J. S. Wang,, K. Iwai, J.E.Gale. 1980, Validity of cubic law for fluid flow in a deformable rock fracture. Water Res. Res. 16 (6), 1016-1024.
13. York. Ma, H. and Ruth, D. W.: 1993, The microscopic analysis of high Forchheimer number flow in porous media, Transport Porous Media 13, 139–160.
14. Zeng, Z. and R. Grigg. 2006, A Criterion for Non-Darcy Flow in Porous Media, Transport in Porous Media, 63, 57-69.

DISTRIBUTION

[List external recipient names and full mailing addresses]

4 Lawrence Livermore National Laboratory
Attn: N. Dunipace (1)
P.O. Box 808, MS L-795
Livermore, CA 94551-0808

[List in order of lower to higher Mail Stop numbers.]

1	MSXXXX	Name of Person	Org. Number
1	MSXXXX	Name of Person	Org. Number

[The housekeeping entries are required for all SAND reports.]

1	MS0899	Technical Library	9536 (electronic copy)

For LDRD reports, add:

1	MS0359	D. Chavez, LDRD Office	1911

For CRADA reports add:

1	MS0115	OFA/NFE Agreements	10012

For Patent Caution reports, add:

1	MS0161	Legal Technology Transfer Center	11500


Sandia National Laboratories